



VAIVA ŠIAUČIŪNAITĖ

**APPLICATION
OF NONLINEAR
DYNAMICS METHODS
AND ALGORITHMS
IN CARDIAC SIGNAL
ANALYSIS**

DOCTORAL DISSERTATION

K a u n a s
2 0 2 2

KAUNAS UNIVERSITY OF TECHNOLOGY

VAIVA ŠIAUČIŪNAITĖ

APPLICATION OF NONLINEAR DYNAMICS
METHODS AND ALGORITHMS IN CARDIAC
SIGNAL ANALYSIS

Doctoral dissertation
Natural Sciences, Informatics (N 009)

Kaunas, 2022

This doctoral dissertation was prepared at Kaunas University of Technology, Faculty of Mathematics and Natural Sciences, Department of Mathematical Modelling during the period of 2017–2021.

The doctoral right has been granted to Kaunas University of Technology together with Vytautas Magnus University and Vilnius Gediminas Technical University.

Scientific Supervisor

Prof. Habil. Dr. Minvydas RAGULSKIS (Kaunas University of Technology, Natural Sciences, Informatics, N 009).

Scientific Advisor

Prof. Habil. Dr. Alfonsas VAINORAS (Lithuanian Health Science University, Biomedicine, Medicine, M 001).

Edited by: English language editor Brigita Brasienė (Publishing House *Technologija*), Lithuanian language editor Violeta Meiliūnaitė (Publishing House *Technologija*).

Dissertation Defence Board of Informatics Science Field:

Prof. Habil. Dr. Rimantas BARAUSKAS (Kaunas University of Technology, Natural Sciences, Informatics, N 009) – **chairperson**;

Prof. Dr. Srečko GAJOVIC (University of Zagreb, Croatia, Biomedicine, Medicine, M 001);

Prof. Dr. Arvydas MARTINKĖNAS (University of Klaipėda, Natural Sciences, Informatics, N 009);

Prof. Dr. Daiva PETRUŠEVIČIENĖ (Lithuanian University of Health Sciences, Biomedicine, Nursing M 005);

Assoc. Prof. Dr. Kristina POŠKUVIENĖ (Kaunas University of Technology, Natural Sciences, Informatics, N 009).

The official defence of the dissertation will be held at 1 p.m. on 30 August, 2022 at the public meeting of Dissertation Defence Board of Informatics Science Field in M7 Hall at The Campus Library of Kaunas University of Technology.

Address: Studentu 48–M7, 51367 Kaunas, Lithuania.

Tel. no. (+370) 37 300 042; e-mail doktorantura@ktu.lt

Doctoral dissertation was sent on 29 July, 2022.

The doctoral dissertation is available on the internet <http://ktu.edu> and at the library of Kaunas University of Technology (K. Donelaičio St. 20, 44239 Kaunas, Lithuania), Vytautas Magnus University (K. Donelaičio St. 52, 44244 Kaunas, Lithuania) and Vilnius Gediminas Technical University (Saulėtekio AV. 14, 10223 Vilnius, Lithuania).

© V. Šiaučiūnaitė, 2022

KAUNO TECHNOLOGIJOS UNIVERSITETAS

VAIVA ŠIAUČIŪNAITĖ

NETIESINĖS DINAMIKOS METODŲ IR
ALGORITMŲ TAIKYMAS KARDIOSIGNALŲ
ANALIZĖJE

Daktaro disertacija
Gamtos mokslai, informatika (N 009)

Kaunas, 2022

Disertacija rengta 2017–2021 metais Kauno technologijos universiteto Matematikos ir gamtos mokslų fakultete, Matematinio modeliavimo katedroje.

Doktorantūros teisė Kauno technologijos universitetui suteikta kartu su Vytauto Didžiojo universitetu ir Vilniaus Gedimino technikos universitetu.

Mokslinis vadovas:

Prof. habil. dr. Minvydas RAGULSKIS (Kauno technologijos universitetas, fiziniai mokslai, informatika, N 009).

Mokslinis konsultantas:

Prof. habil. dr. Alfonsas VAINORAS (Lietuvos sveikatos mokslų universitetas, biomedicinos mokslai, medicina, M 001).

Redagavo: anglų kalbos redaktorė Brigita Brasienė (leidykla „Technologija“), lietuvių kalbos redaktorė Violeta Meiliūnaitė (leidykla „Technologija“)

Informatikos mokslo krypties disertacijos gynimo taryba:

Prof. habil. dr. Rimantas BARAUSKAS (Kauno technologijos universitetas, fiziniai mokslai, Informatika, N 009) – **pirmininkas**;

Prof. dr. Srečko GAJOVIČ (Zagrebo universitetas, Kroatija, biomedicinos mokslai, medicina, M 001);

Prof. dr. Arvydas MARTINKĖNAS (Klaipėdos universitetas, fiziniai mokslai, informatika, N 009);

Prof. dr. Daiva PETRUŠEVIČIENĖ (Lietuvos sveikatos mokslų universitetas, biomedicinos mokslai, slauga, M 005);

Doc. dr. Kristina POŠKUVIENĖ (Kauno technologijos universitetas, fiziniai mokslai, informatika, N 009).

Disertacija bus ginama viešame Informatikos mokslo krypties disertacijos gynimo tarybos posėdyje 2022 m. rugpjūčio 30 d. 13 val. Kauno technologijos universiteto Studentų miestelio bibliotekoje, salėje M7.

Adresas: Studentų g. 48–M7, 51367 Kaunas, Lietuva.

Tel. (+370) 37 300 042; el. paštas doktorantura@ktu.lt

Disertacija išsiųsta 2022 m. liepos 29 d.

Su disertacija galima susipažinti interneto svetainėje <http://ktu.edu> ir Kauno technologijos universiteto bibliotekoje (K. Donelaičio g. 20, Kaunas LT-44239), Vytauto Didžiojo universiteto bibliotekoje (K. Donelaičio g. 52, Kaunas LT-44244 ir Vilniaus Gedimino technikos universiteto bibliotekoje (Saulėtekio al. 14, Vilnius LT-10223).

TABLE OF CONTENTS

LIST OF TABLES	6
LIST OF FIGURES	7
LIST OF ABBREVIATIONS AND TERMS.....	
INTRODUCTION.....	9
I. DYNAMICS OF COMPLEX AND CHAOTIC SYSTEMS.....	12
1.1. Introduction to the theory of chaos.....	13
1.2. Models of chaos in medicine	16
1.3. Human as a complex system	16
1.4. Heart as a complex system	18
1.5. Overview of the electrocardiography	20
II. SCALAR TIME SERIES ANALYSIS TECHNIQUES FOR THE ASSESSMENT OF COMPLEX SYSTEMS	24
2.1. Time series analysis for complex systems.....	25
2.1.1. The weighted moving average.....	28
2.1.2. Effects induced by the additive noise	29
2.2. Attractor embedding: Uniform and non-uniform	30
2.2.1. Uniform embedding.....	31
2.2.2. Non-uniform embedding	31
2.3. Permutation entropy	32
2.4. Second order Lagrange matrix of differences	34
2.5. Synchronization determination algorithms.....	39
2.5.1. Identical synchronization.....	40
2.5.2. Generalized synchronization	41
2.5.3. Phase synchronization	41
2.5.4. Anticipated and lag synchronization	42
2.5.5. Amplitude envelope synchronization	42
III. ALGORITHMS AND APPLICATIONS IN THE CARDIAC SIGNAL ANALYSIS	44
3.1. The algorithm for the detection of anaerobic threshold.....	44
3.2. The algorithm for the detection of ischemic heart episodes	53
3.3. Synchronization of human heart rhythms with the Earth's time-varying magnetic field.....	62
3.4. Visualization of complex processes in the cardiovascular system during the electrical auricular vagus nerve stimulation.....	72
IV. CONCLUSIONS	85
REFERENCES	86
SUMMARY.....	99
CURRICULUM VITAE	122
LIST OF PUBLICATIONS AND CONFERENCES	123
ACKNOWLEDGEMENTS	125

LIST OF TABLES

Table 1. Six different elements of time series x and y mapped in the Lagrange matrix of differences	355
Table 2. The results of repeated measures.....	67
Table 3. The results of the correlation coefficient statistical significance test	68
Table 4. The description of subjects participating in the experiment.....	76

LIST OF FIGURES

Fig. 1. A sample solution in the Lorenz attractor	144
Fig. 2. Schematic distribution of the phenomena obtained from the grids of connected iterative models	15
Fig. 3. Model of a human, as a part of a complex system	17
Fig. 4. The electrical system of the heart.....	19
Fig. 5. The main components of the ECG	221
Fig. 6. Reconstruction scheme of the measurement process and dynamic system attractor.....	266
Fig. 7. Phase plane of the optimal time delay during the load.....	37
Fig. 8. Phase plane of the optimal RR-JT algebraic relationship after the load.	38
Fig. 9. RR and JT interval series phase plane.....	39
Fig. 10. Visualization of the transit through the AnT for person 1.....	48
Fig. 11. Visualization of the transit through the AnT for person 2.....	51
Fig. 12. Visualization of the transit through the AnT for person 3.....	52
Fig. 13. The dynamics of the JT/ST relationship during the load and the recovery processes for person 1	566
Fig. 14. The dynamics of the JT/ST relationship during the load and the recovery processes for person 2	577
Fig. 15. The dynamics of the JT/ST relationship during the load and the recovery processes for person 3	588
Fig. 16. The dynamics of the JT/ST relationship during the load and the recovery processes for person 4.	59
Fig. 17. The dynamics of the JT/ST relationship during the load and the recovery processes for person 5.	60
Fig. 18. The dynamics of the JT/ST relationship during the load and the recovery processes for person 6	61
Fig. 19. LMF-HRV correlations by day and group on average.....	69
Fig. 20. Averaged LMF-HRV correlation by day and group.	70
Fig. 21. The auricle's natural sensory innervation contrasts its artificial stimulation.	73
Fig. 22. Baroreceptor control loops in the context of the model of integral evaluation	76
Fig. 23. The time protocol of the experiment	77
Fig. 24. The location of four needle electrodes	77
Fig. 25. The transit through the stimulation and placebo for Subject 1	80
Fig. 26. The transit through the stimulation and placebo for Subject 2.....	81
Fig. 27. The transit through the stimulation and placebo for Subject 3.....	82
Fig. 28. The transit through the stimulation and placebo for Subject 4.....	83

LIST OF ABBREVIATIONS AND TERMS

ABP – arterial blood pressure
ANS – autonomic nervous system
AnT – anaerobic threshold
aVN – auricular vagus nerve
aVNS – auricular vagus nerve stimulation
CHD – coronary heart disease
CNS – central nervous system
ECG – electrocardiogram
HLI – heart lock-in
HR – heart rate
HRV – heart rate variability
IBI – inter-beat-interval
LMF – local magnetic field
LRS – linear recurrence sequence
LT – lactate threshold
MA – moving average
PE – permutation entropy
RMSE – root mean square error
SVD – singular value decomposition
VN – vagus nerve
WMA – weighted moving average

INTRODUCTION

Relevance of the topic

From a systemic point of view, human body is a complex system or, more precisely, a complex set of complex systems. One of the most developed complex systems in human body is the cardiovascular system, which plays a major role in the living organisms, as it provides the necessary substances, accumulates their reserves to support vital functions, and at the same time, removes the accumulated metabolic by-products. It consists of subsystems that are interacting together to perform the vital tasks (such as optimizing arterial and pulmonary circulation) and fighting with each other for resources, such as maintaining cerebral blood flow in a person with heavy bleeding. These regulatory mechanisms operate rhythmically, continually adjusting the cardiovascular variables that can be seen on the electrocardiogram (ECG) recordings. These mechanisms that work simultaneously on different time scales and can vary the relationships of variables create the dynamic complexity of cardiovascular variables (Porta et al., 2009).

The analysis of human physiological systems remains a very ambitious task. The complexity of the problem often encourages the use of new mathematical methods to analyze the processes that take place in space and time. The nature of a complex system is defined by the dimensional and temporal organization (Biggiero, 2001). The changes in the models of interrelationship and variability have precious information about the state of the system as a whole (Seely, Christou, 2000). It is possible to extract very useful information just by measuring the absolute value of a clinical parameter, like the heart rate (HR). Nevertheless, the evaluation of interrelationships between ECG characteristics provides additional beneficial clinical information that could be even more valuable than just the heart rate alone, especially when the heart rate is within the normal range (Que et al., 2001). In this dissertation, electrocardiography (ECG) analysis has been chosen because it is the main and most studied non-invasive technique used in the modern study of cardiovascular system functionality.

One of the major causes of death in the world is cardiovascular diseases. For this reason, the non-invasive assessments in cardiology like ECG recordings are essential. The ability to detect even minor electrocardiographic changes in a timely manner is very important for the clinical investigation. More than ten years ago, Lithuanian scientists proposed a methodology for studying the dynamics of parameter interconnections of the ECG signal. The proposed methodology, based on the structural analysis of matrices, has given good results in the study of electrocardiographic signal parameters and has been approved in many publications and projects. For the above-mentioned reasons, the concept of electrocardiographic signal research methodology based on the matrix analysis is further developed in this work. The characteristics that were evaluated in the previous studies are supplemented by descriptive estimates of the latest matrix structure. The aim is to determine how the shape (morphology) and complexity of the dynamic behavior between two signals are related to the physiological and pathological processes.

While the practical applications are the main determinants of significance, the specific second-order matrices structure is defined as the foundation of this work.

The object of investigation is the development and application of algorithms, based on the nonlinear algebraic relationships between the cardiac intervals.

The aim of investigation is to develop new algorithms and apply them for the analysis of electrocardiographic signal dynamics.

Objectives:

1. To analyse the interfaces of electrocardiography parameters;
2. To observe the dynamic processes and relationships of complex human body systems under changing conditions;
3. To develop new algorithms, biomarkers under different physiological conditions (e.g., during exercise);
4. To apply the electrocardiographic parameters relationships in order to monitor the effects external factors, i.e., magnetic field, vagus nerve stimulation;
5. To apply LaGrange matrixes of differences for the evaluation of dynamics of cardiac parameter relationships.

The novelty of the work and practical importance

In this work, the author analyzes the relationships between two different cardiac parameters, relationships of several relationships in the phase planes, and the relationships between the cardiac parameters and the two external factors (local magnetic field and vagus nerve stimulation). The author has proposed new algorithms that allow qualitatively observing and evaluating the relationships between cardiac intervals and are used to monitor and assess the state of human health.

Methods, software, and experimental tools

There have been created and deployed information reduction methods, algorithms for optimum reconstruction of attractors into delay phase planes, algebraic correlations between cardiac parameters, local magnetic field, and vagus nerve stimulation algorithms. MATLAB programming and numeric computing platform were used to create all programs and algorithms. The Kaunas-Load system was used to record cardiograms, the HeartMath Institute's magnetometer network was used to detect the local magnetic field, and the vagus nerve was stimulated by using a technique developed at the Technical University of Austria.

Provided for the defense

There were provided new estimates for the evaluation of the relationship between two signals based on the structural analysis of second-order matrices. These estimates enable the assessment of unique quality changes in the electrocardiographic signal, which is not possible using the classical ECG analysis methodology.

Approbation of the results

The thesis consists of 6 scientific articles, including 4 publications in the Institute of Scientific Information Database (ISI) with a citation index, three

publications printed by the international publishers. The remaining 2 publications have been published in other international databases.

The results of the dissertation have been presented at 3 international conferences: 9th International Workshop “Data Analysis Methods for Software Systems”, Earth's magnetic field, moon position, and phase influence on human cardiovascular system; 2018 IEEE International Symposium on Systems Engineering "Auricular vagus nerve stimulation affects fractality of the human body as resolved by advanced ECG"; Electrocardiological changes during auricular vagus nerve stimulation in humans; In King of Organs 2019, The 5th International Conference for Advanced Cardiac and Heart Transplant "Heart Sciences from Genes to Galaxies": March 24–27, 2019, Kingdom of Saudi Arabia: conference abstracts/organized by the Prince Sultan Heart Center in Al-Ahsa, in collaboration with the Cardiology Center at the Hospital La Salpetriere in Paris, European Heart Association and the Saudi Heart Association.

The size and structure of the dissertation

This doctoral dissertation consists of an introduction, 3 main chapters, conclusions, bibliography, and a list of publications. The volume of the dissertation is 126 pages. The dissertation contains 28 figures and 198 cited sources.

I. DYNAMICS OF COMPLEX AND CHAOTIC SYSTEMS

Over the years, the scientists have revealed a variety of complex physical properties, features, and concepts underlying the development, maintenance, and evolution of biological and social systems that are applicable to nearly every field. Much effort continues to be made in formulating the theory of complexity, formalizing its manifestations, and searching for new methodologies to assess it. Complexity is characterized by the following main features (Baranger et al., 2001; Vainoras et al., 2005):

- Complex systems comprise many nonlinear interacting components. Nonlinearity is a precondition for chaos, and practically, all nonlinear systems with three or more dimensions in their phase space are chaotic in at least part of their phase or parameter space.

- The elements of a complex system are interrelated.

- The structure of a complex system is determined by numerous scales. The upper multiscale system includes lower-level systems, but a system at each level is no less complex than at the higher level. Going deeper into the system does not become simpler. When the complexity does not decrease and the phenomena are investigated on the scales of different detail, this feature of a complex system is called fractality (the self-similarity). From the perspective of chaotic dynamics, there are always certain kinds of similarities that are embedded into each other. The chaos theory defines fractals as similar structures duplicating different scales of generalization.

- A complex system can exhibit an abrupt change in its behavior. Sudden changes occur when one attractor switches to another, which can be caused by changes in a smaller multiscale system. Certain behaviors that are characteristic to a particular scale can be sudden and cannot be adequately assessed, understood by examining each scale, each component on that scale separately. Each component may as well include a complex system, only on a smaller scale. Adaptive complex systems are able to change themselves, self-adapt to the environmental conditions. However, by adapting, they can change and influence the environment as well.

- Complexity involves intermittent changes of processes between the chaos and non-chaos. Usually, complexity emerges on the edge of chaos. The chaotic dynamics of the system are defined by the attractors of various natures and properties.

- Complexity describes the changes in system behavior from cooperation to competition and includes interaction between different scales. Cooperation (synergetic) on a smaller scale diminishes competition on a scale of n (scale $n-1$).

- The management of a complex system is distributed among its constituent elements that interact synergistically across all control functions (Bar-Yam, 2002; Vainoras et al., 2005).

The term "complex systems analysis" refers to a scientific technique that explores how interconnections of the system's components lead to collective behaviors as well as how the system communicates with its surroundings and creates interactions (Bar-Yam, 2002). In its broadest meaning, a system is a collection of elements that form a cohesive whole through their connections, relationships, or

reliance. The entities from outside the system are then incorporated into the environment of the system. These frameworks and behaviors are separate from the characteristics of the system's components and show how the system communicates with its environment or how its components behave. According to the concept of behavior, the study of systems typically deals with the processes that occur throughout time. Nonlinear behavior is common in the complex systems. Nonlinearity is a term used in mathematics and physics to describe the processes in which a change in the input size does not result from the change of the output size. Depending on the present conditions of the system or its input settings, such systems can produce significantly larger or lower than proportionate output changes, or even not measurable outcome at all, in response to a given input change. Nonlinear differential equations with one or more nonlinear terms are of particular importance to the complex systems. Chaos, a mathematical phenomenon, can be produced by certain dynamical systems that are nonlinear, such as the Lorenz system (Eq. 1, 2, 3):

$$\frac{dX}{dt} = \sigma(Y - X), \quad (1)$$

$$\frac{dY}{dt} = X(r - Z) - Y, \quad (2)$$

$$\frac{dZ}{dt} = XY - bZ; \quad (3)$$

where $\sigma = \frac{V}{K}$ is the prandtl number (ration between the momentum diffusion, V , and the heat diffusion, K), $r = \frac{Ra}{R_c}$ is the Rayleigh number over the critical Rayleigh number (a measure of heat into the system), and $b = \frac{4}{(1+a^2)}$ gives the size of the region to be approximated. All the parameters are taken to be positive.

This relates to the complex systems as well as the risky reliance on initial conditions and the "butterfly effect" (Fig. 1) that can arise in them. In such a system, even minor changes in the original conditions can result in significantly different outcomes. As a result, it can be extremely difficult to numerically modeling the chaotic behavior, as even little rounding errors might cause the model to provide false results at a later stage of computation. Likewise, if a complex system goes back to the former state regarding the same stimulus, it can behave differently, making the extrapolation from experience difficult (Peitgen et al., 2006).

In the perspective of determinist chaos, chaotic behavior is the result of a small number of non-linear interactions. The term "complexity" refers to the ability of a large number of complicated and dynamic sets of relationships to generate some basic behavioral patterns (Cilliers, 1998).

1.1. Introduction to the theory of chaos

The theory of chaos began to take shape as early as in the 1960s. In 1961, E. Lorenz observed the so-called "butterfly effect" (Fig. 1) in the weather forecast calculations.

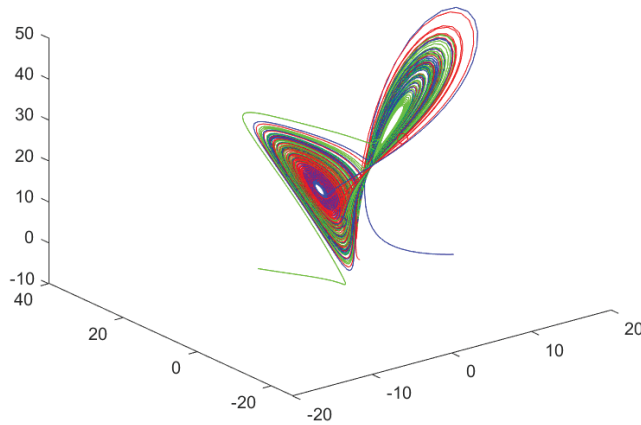


Fig. 1. A sample solution in the Lorenz attractor

In order to reduce the cost of computing time, Lorenz came up with the idea to use part of the data from a previous study. A later review of the obtained figures revealed that completely new results were obtained, although the calculations were analogous to those performed previously. Upon further examination, he noted that the figures he had entered were slightly rounded.

It was concluded that a long-term weather forecast is not possible because the worst changes in initial conditions cause huge deviations over the time. Although Lorenz's discovery was accidental, it was the beginning of a science of chaos (Ofulla, 2013).

Another pioneer of the theory of chaos was Feigenbaum. He discovered a law inherent in all chaotic systems, i.e., a constant that describes the ratio of scales between the adjacent points of doubling of a period. Richard J. Cohen with fellow physicians have observed that the period doubling bifurcations are associated with an impending heart attack. This discovery as a theory of chaos made an integral part of cardiovascular science (Karagueuzian et al., 2013).

The simplest models of chaotic behavior are chaotic iterative models. The application of iterative models to neuronal dynamics is reviewed in a detailed study by Ibarz et al. (2011). Although from the very first works of Hodgkins and Huxley (1952), in which the change of the membrane potential of biological neurons and the ion dynamics are determined by differential equations, the discrete iterations of these systems were developed in parallel models. The study of Ibarz et al. (2011) pointed out that the models of nonlinear iterations are well suited to describe the biological neurons and their network, where several advantages of the following neuronal models have been identified:

1. Models based on iterative relations are characterized by computational efficiency.
2. Models based on iterative relationships are simple and flexible. By changing only a few parameters, it is possible to obtain models those with different dynamic properties.

3. Iterative models are based on certain mathematical methods and paradigms, which allow the expansion of possibilities of modeling.

A few more examples can be mentioned when the models described by the iterative equations are more acceptable than the mathematical ones described by differential equations, especially if the primary objective of the research is a qualitative study of the solutions of these systems. The computational efficiency of discrete iterative model solutions is higher, and the errors of the results are smaller than the solutions described by the differential equations.

The list of chaotic iterative models is long. One way of classification is the space dimension of models (Fig. 2). Among the most discussed one-dimensional chaotic iterative models, the following can be mentioned: logistic, Chebyshev map, Bernoulli shift map, Liebovitch map, tent map, intermittency map, Gaussian map, sinusoidal map, sine map, Circle map. Although the variety of one-dimensional chaotic iterative models is large, the logistical and circular iterations are most widely used in biomedicine models. Circular iterative models are commonly used to simulate ECG signals, and various complexity-estimating measurements are compared with the measures of the already established logistic iterative model (Zanin et al., 2012; Zaylaa et al., 2015).

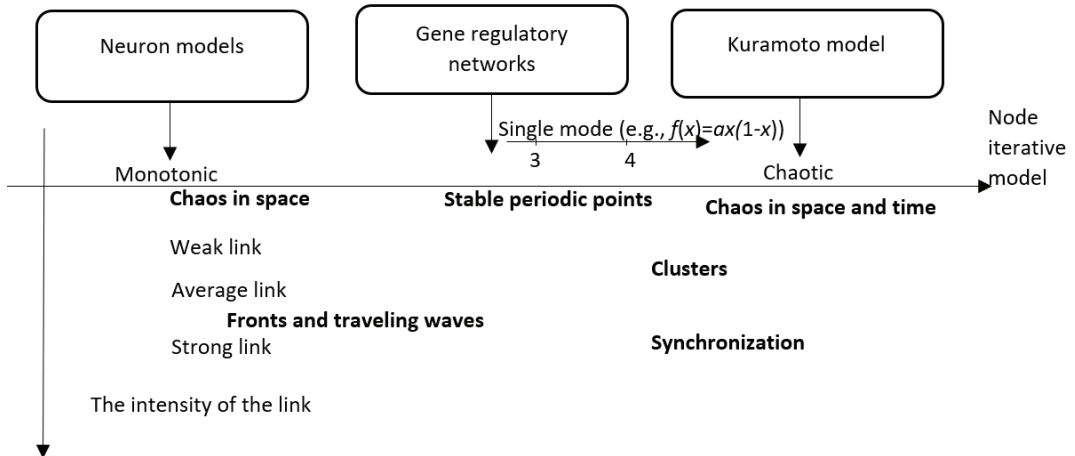


Fig. 2. Schematic distribution of the phenomena obtained from the grids of connected iterative models (Chazottes et al., 2005)

Chaotic behavior causes a system to create chaotic order in equilibrium, which differs from what is often referred to as 'order'. As they approach chaos, dynamic systems deviate from equilibrium (Hazewinkel, 2012). Chaotic systems are a subcategory of complex systems, distinguished by their lack of historical dependability. Many genuinely complex systems are stable even throughout the extended but finite time periods. However, while maintaining structural credibility, they do have the capacity for fundamental qualitative reform of sorts. Metamorphosis is far more than a term for such changes.

1.2. Models of chaos in medicine

A long time ago, medicine was dominated by empirical and phenomenological diagnostic methods. However, these methods can neither assess the holism and complexity of the human body, nor the synergies and fractal characteristics of the interacting living systems in the human body (Sidorenko et al., 2006). The development of a holistic approach to the human body has been greatly influenced by the development of mathematical models (Ursino et al., 1998; Marmarelis et al., 1978; Goldberger et al., 1998), which examine the complexity of the body's reactions in detail. The research methods that are applying the chaos theory are quite widely used in the biological sciences: Liapunov's exponent (Hu et al., 2009; Yaragani et al., 2009), "recurrence plots" (Freitas et al., 2009), bifurcation diagrams (Sun et al., 2005). The nonlinear analytical methods such as fractal dimensions (Vainoras et al., 2005; Schmitt et al., 2007) and Hankel matrices (Šliupaitė et al., 2009) are used to assess the complexity of human body functions. Entropy in systems processes is evaluated by the approximate entropy (Pikkujamsa et al., 2001; Beckers et al., 2001), sample entropy (Botting et al., 2009), multistage entropy (Costa et al., 2005), Lempel-Ziv entropy (Aboy et al., 2005).

Despite having a well-defined underlying order, chaos is a dynamic process that tends to be unpredictable. It appears to be the prevailing order in systems that are sensitive to the minor causes and disturbances, and single systems can flip among the ordered and chaotic dynamics. These usually are the structures that emerge as a consequence of collective action, such as solitary cells joining to form a coordinated tissue (Spurlin, Nelson, 2017). The fractal geometries can be used to approximate the chaotic systems in specific cases. The structures with infinitely iterated self-similar patterns are known as fractals. They are scaled according to a set of principles and have properties that are maintained over multiple levels of observation. The fractal dimension parameter can quantify a type of organization in complex systems. Fractals are a type of geometry that defines chaos in general. As a result, it is necessary to combine chaos with fractals to model intricate and non-linear dynamical systems like those found in nature (Theiler, 1990; Tulppo et al., 2002).

1.3. Human as a complex system

Consider designing a model of all the chemical reactions that take place within a cell. Thousands of variables will be undoubtedly defined by thousands of differential equations in this approach. It is reasonable to assume that the consequent dynamics will be chaotic if these many differential equations will be written down in the correct general form, but the parameters will be chosen at random. Despite occasional bursts of interest in the prospect of chaos in biological systems, this type of generic behavior of massive dynamical systems is not what defines life. However, it is not appropriate to declare that everything works, because every parameter has been adjusted to the exact right value; these parameters, in particular, are dependent on details that are out of the cell's control, such as temperature or nutrient concentration in the environment (Biggiero, 2001). More particularly, a cell's dynamic is determined by how many copies of each protein it produces, and one must either assume that everything works

regardless of how many copies are produced or that the cell has ways of controlling this number precisely. Either answer would be interesting. The balance between the robustness and fine tuning is a challenge that arises at many levels of biological organization (Bialek et al., 2012).

In the 16th century, Vesalius named the constituents of the human body systems with exceptional features. These systems cover the whole human organism in different fractal levels and are called holistic: body level: skeletal and musculoskeletal system (P), cardiovascular system (supply (S)), and nervous system (regulatory (R)); heart level: R_H – the heart's regulating system, P_H – the heart's periphery, S_H – the supplying system to the heart that acts on the function of each cell in the body and responds to the needs of each cell, integrating the functionality of all elements into a unified functionality of the organism. In addition to these three systems, the respiratory (L) system was mentioned (Fig. 3). The sum of a system's features cannot define and explain all of its properties. However, the system determines how its components function. Each arrow represents dynamics, organization, and control between separate subsystems. The identification of those interactions is one of the prime objectives of this dissertation.

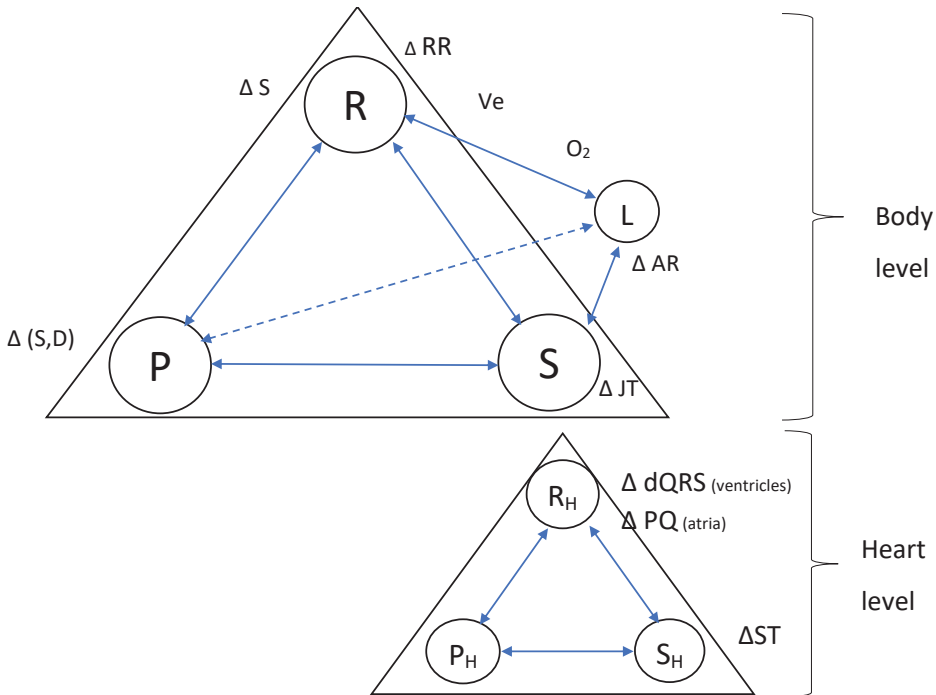


Fig. 3. Model of a human as a part of a complex system (adapted from Vainoras et al., 1996)

The connections between several systems of the human body and the functions they perform can be described in several ways. Compiling Figure 3 model, the parameters that were selected were measured non-invasively: S, D – systolic, diastolic

arterial blood pressures, RR – a time period between two heartbeats, JT – time interval in the electrocardiogram from point J to the end of the T wave, ST – segment amplitude, dQRS – duration of QRS complex, PQ – time interval in the ECG from the beginning of the P wave to the beginning of Q wave (Fig. 5), Ve – inhaled air volume per minute, O₂ – the volume of oxygen consumed per minute, AR – amplitude of the R tooth, Δ – the change of a certain parameter. As the environment or its effects change, the human body is able to adapt. As the body adapts, all three systems change together (not necessarily in the same way). The totality of holistic systems in the human body and their functions and interactions is an excellent example of a complex system (Poderys et al., 2015; Vainoras et al., 2002).

The body adjusts to the changes in the environment and its effects: all three systems react together (to varying degree and shape), and the body's overall response is always a result of combined response of all three systems. The totality of holistic systems determines the complexity of the system both structurally and functionally.

In assessing the whole body, it is appropriate to keep in mind the complexity of the reactions of individual systems (Skinner et al., 2008). There are many and varied models for assessing the functional state of the body in literature, which seek to include the assessments of many body functions (Goshvarpour, 2012; Ubeyli, 2009; Mishra et al., 2010; Porta et al., 2013; Aktaruzzaman et al., 2014; Graff et al., 2015).

The current literature is rich in a variety of scientific articles including the modeling of individual cell groups in the body. However, the task of modeling the functional state of the entire human body is still too complex for contemporary science. Therefore, an attempt is made to study the characteristics of certain systems, their complexity, dynamics, and adaptive changes and seek to form unified, combined conclusions based on the obtained results. Because human body systems can be explored as different subsystems (e.g., molecules, cells, tissues, organs, systems), it is necessary to analyze the physiological data at several levels, i.e., to assess their complexity and dynamical relationships.

1.4. Heart as a complex system

Heart is one biological example of a complex system. Both experimental trials and modeling tasks explore the occurrence of chaos in the heart muscle. The heart demonstrates the fractal structure in both aspects, i.e., the dimension and time. Heart muscle is multilayered and has a fractal feature based on fibers. Fractal self-similarity occurs at ranges from nm to μm and cm, from the molecular scale microfilament to the striated cell and tissue dimensions. Tubular actin and myosin filaments make myofibrils, which then build myocytes, which then form heart muscle fibers. The function of heart tissue requires this highly ordered hierarchical architecture (synchronized contraction). The electrical activity of the heart is endogenously varying as well: from the sinoatrial node to cardiomyocytes and the entire organ (Sharma, 2009; Mandel et al., 2012). Both electrocardiography and photoplethysmography readings can be used to determine the heart rate and heart rate variability (HRV), which are two different but related characteristics (Goncalves et al., 2016; Elgendi, 2012). Heart rate, which measures the pace at which the heart

pumps blood, is calculated by counting how many times the heart contracts in one minute. As a result, heart rate variations are more common during the activity than at rest, even when other factors are taken into consideration. HRV is used to characterize the variability of time intervals between the beats, since the duration of succeeding beat-to-beat intervals varies over the time. It has been shown that a normal HRV is a chaotic deterministic system (Lombardi, 2000), and it has been investigated by using fractal and multifractal analysis (Lin, Sharif, 2010). The variations in HRV have been linked to the pathophysiology, as their fractal aspects have. This was used as a predictive and diagnostic guideline that reduced the variability and is a marker for disease and increased risk (Malik, 1995; Cripps, 1991; Ahmad, 2009).

The physiology of the heart is linked to the electrical activity. It entails nonlinear reaction-diffusion processes and serves as an activation stimulus for the dynamics of the heart and ultimately, blood ventricular flow. The relationship is reciprocal, as the circulatory system regulates cardiac dynamics and relying on the individual's physiopathology, may cause an overload. Throughout a heartbeat, the bioelectric activity of the heart is a very complex process indeed (Quarteroni et al., 2006). The sinoatrial node (SN), which is positioned between the vena cava superior and inferior in the right atrium, is responsible for the rhythmic cardiac activity (Bleeker et al., 1980; Brooks, Lu, 1972). The SN consists of three main parts: 1) the upper, located medially from the right atrium of the right atrium (crista terminalis), where there is usually a pacemaker, 2) lower, through which the heart rhythm (HR) guidance passes, regulated by the autonomic nervous system, particularly adrenaline; 3) an intermediate region (Fig. 4).

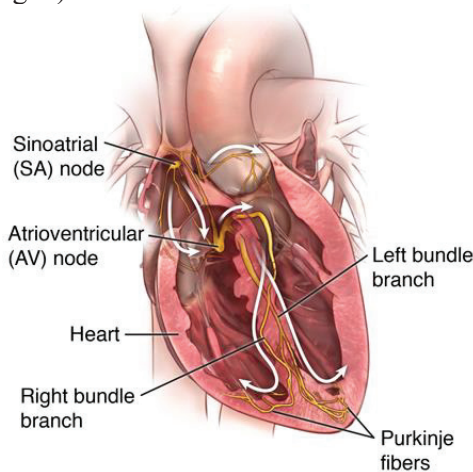


Fig. 4. The electrical system of the heart (<https://www.hopkinsmedicine.org/>)

The sino-atrial node acts as a pacemaker: a front-like fluctuation of the transmembrane potential v spreads first in the atria and then in the heart with a very fast transition from the resting value v_r to the plateau value v_p .

For cardiac cells, v_r and v_p are around 90 mV and 10 mV, respectively. This is the phase of excitation or depolarization, which is accompanied by a constant potential interval (refractory period) and a slower restoration to the initial state (repolarization). The position x and the local condition of the heart, in general, may change the temporal profile of the transmembrane potential v ; the full bioelectric cycle in the human heart lasts about 300 milliseconds (Quarteroni et al., 2006). The changes in the actions of the adrenergic and cholinergic systems influence the heart rate in response to the changes in internal and external environmental factors. Acetylcholine (a mediator of the parasympathetic nervous system) acts by hyperpolarizing the cell and slowing down diastolic depolarization, resulting in a decrease in the heart rate (DiFrancesco, 2005). This effect is achieved by increasing the outflow of K^+ current, as specific channels open in the outer part of the membrane. Catecholamines (mediators of the sympathetic nervous system) increase the heart rate by increasing diastolic depolarization, decreasing the resting potential and the magnitude of critical depolarization, increasing the slow Na^+ / Ca^{++} current and the outgoing K^+ current. The magnitude of the resting potential, temperature, and chemicals that change the conductivity of ions, particularly adrenaline (Adr) and acetylcholine (Ach), all influence the heart rate (HR). The main pacemaker center is activated at the earliest; the impulses propagate to the atria through the posterior atrium of the right atrium (crista terminalis), then pass through the atria to the atrioventricular and ventricular conduction system. The effects of sinus node cells can be combined in three ways: electrical coupling associated with the phases, phase shift, and the mutual influence on the cell-cell. SN cells work alone if they are enzymatically separated. According to the concept of phase dependence, the synchronization of their activities is a process that takes place due to their influence on each other, which develops the dominant area of the "pacemaker center" that organizes the activities of other cells. Phase-dependent effects have physiological significance. They change the fundamental frequency of the pacemaker: if the pulse rises in the early phase, the heart rate slows down; if in the late phase of the cycle, the heart rate increases (Michaels et al., 1986).

1.5. Overview of the electrocardiography

Electrocardiography is a process of producing an electrocardiogram (ECG), which is a graph of voltage versus time of the electrical activity of the heart using electrodes that are placed on the skin (Iaizzo, 2010). This activity is associated with the electrical activity of the heart fibers; therefore, electrocardiography is an important tool in assessing cardiac work. Electrocardiography is a method of recording the number of heart cells with a special device (an electrocardiograph). The electrocardiogram (ECG) is a curve of the total electric field potential generated, according to the peculiarities of which the activity of the heart is decided (Walker et al., 1990). Electrocardiographic signals have been studied for more than a century. British physiologist Augustus D. Waller described the first human ECG in 1887. Augustus D. Waller used B. Lippman in 1873 to record the electrocardiogram with a developed capillary electrometer. Nevertheless, the pioneer of electrocardiography is considered to be W. Einthoven, who recorded the first electrocardiogram in 1902,

using a more sensitive string galvanometer. In 1924, W. Einthoven was awarded with the Nobel Prize for the invention and development of electrocardiography. Since 1940, electrocardiography has become a common method of cardiac diagnosis. The electrocardiogram records the electrical excitation cycles of the heart. It begins in the sinus node on the right atrium of the sino-atria. Sinus node pulses cause atrial contraction, which is characterized by a P-wave ECG signal (Fig. 5). Further, the impulses propagate from the atrial fibers to the atrium ventricular a node that controls the transmission of this impulse from the atria to the ventricles. Hiso and Purkinje fibers (Fig. 4) transmit a nerve impulse to the part of the lower and outer ventricle. Ventricular contraction generates a QRS complex of ECG signal (Fig. 5). At 150 ms, the ventricles repolarize, resulting in a T wave.

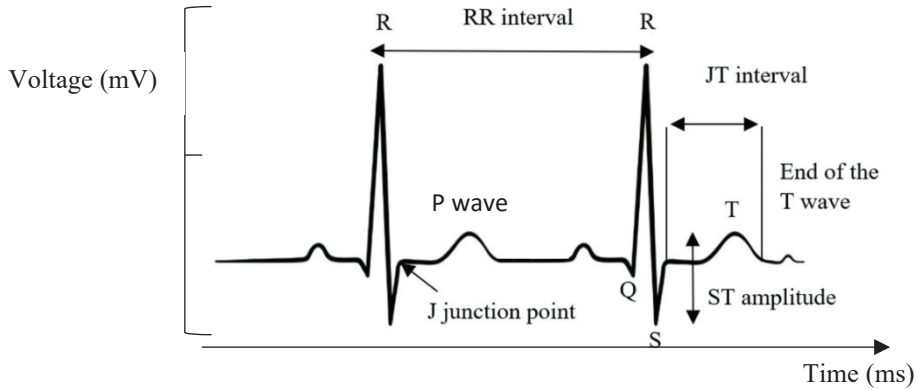


Fig. 5. The main components of the ECG

The linked models of differential equations are often used to generate cardiac signals; however, in order to simplify the calculations, it is possible to discretize time, i.e., apply the linked iteration models. Kirichov's standard bound iteration model was used to develop a heart model (Gidea et al., 2011). A grid of linked iterative models describes a neural impulse transmission model of the heart cell. The applications of chaos started at the time same time as the external stimuli has been used to normalize the activity of the heart in people with arrhythmias. Chaos synchronization in cardiac cells was discussed by Qu et al. (2014).

Much effort has been made to study the dynamics of ECG parameters and develop the methods for their evaluation (Pikkujamsa et al., 2001). More than two decades ago, the first research publications in cardiology, using nonlinear methods of analysis, appeared. Using chaos theory, the success of the treatment in patients who suffered a myocardial infarction was assessed by looking at the variations in the QT interval (Yaragani et al., 2002; Rautaharju et al., 2004). There are several works in which heart rhythm characteristics are examined by using various nonlinear methods of analysis (Sun et al., 2005). The RR interval is analyzed by comparing the efficiency of linear and nonlinear methods (Pikkujamsa et al., 2001; Schumaster, 2004). The complexity of heart rate is different between men and women, with men having lower rates than women. A number of articles examine the changes in RR interval

complexity in various cardiovascular diseases (Chen et al., 2007) by evaluating their prognosis (Skinner et al., 2008). The parameter's ST/HR was analyzed as a function of age (Beckers et al., 2006). A group of researchers from Finland (Pikkujamsa et al., 2001) examined the amplitudes of RR by using the calculation of approximate entropy and short-term fractal components.

Within an organism, an appropriate amount of RR interval fluctuations indicates healthy function as well as innate self-regulatory capacity, flexibility, or resilience (McCraty et al., 2009; Segerstrom, Nes, 2007). JT interval is linked to the metabolic rate in the myocardium (when the heart activity is the highest, JT interval is the shortest, and vice versa). The JT interval is a measurement of how long the ventricular repolarization lasts. The JT range is divided into the JT_a interval (from the point J to the peak of the T wave) and the JT_e interval (from the point J to the peak of the T wave; from the T wave peak to the end of T wave). JT interval is linked to the metabolic changes in the heart (Vainoras et al., 1996). The alterations of repolarization are extremely linked to the metabolic changes in the body. In specific cardiac regions, ECG leads with a shorter JT interval demonstrate that repolarization occurs earlier, and the metabolic changes occur faster. Longer dJT (duration of JT interval) is connected with slower repolarization and metabolic responses (Gargasas et al., 1998). QRS duration parameter, which is related to interventricular synchronization features, could be connected to the heart intrinsic regulatory system. The QRS complex is a part of the regulatory system of the heart, which reflects the spreading of depolarization in the ventricle and synchronization of depolarization spreading between the ventricles. The wider QRS complex shows slower conduction in the heart ventricle. The duration of QRS complex can range in normal conditions from 80 to 120 ms. This index is sensitive to the sympathetic and parasympathetic nervous system tonus alterations. During sympathetic activation like during load, in a healthy heart, the shortening of this parameter could be observed. It prolongs in some heart pathologies, like ischemic heart disease.

Chapter conclusions

The majority of methods that are used by clinicians are based on the evaluation of separate parameters, like the heart rate, blood pressure, or the length of a single cardiac interval. Analyzing the interrelationship of ECG features offers additional clinical information that is often more insightful than evaluating one feature (Que et al., 2001). More advanced contemporary studies evaluate the acceptable ranges of variation for a single cardiac interval during the physical exercise. Some recent studies do propose confidence intervals for the variation of a single cardiac interval at different heart rates (Malik et al., 2021).

The topic of interest is new techniques and algorithms for the evaluation of subtle variations of algebraic relationships between different cardiac intervals during different environmental and physical conditions. These techniques should be able to track individual reactions of the patient in real time. The goal is to create algorithms that are capable to provide a unique insight into the complex dynamical and self-organization processes that are taking place in a patient's cardiovascular system. The

ability to track these complex dynamical processes in a cardiovascular system can build the ground for the development of personalized health evaluation and treatment protocols.

II. SCALAR TIME SERIES ANALYSIS TECHNIQUES FOR THE ASSESSMENT OF COMPLEX SYSTEMS

Nonlinear interactions and complicated fluctuations are common in complex systems. In order to recover the dynamics of a system from a time series of only a few observed variables, it is critical to identify and analyze the connections between c and the random fluctuations (Gao et al., 2007).

Theoretically and computationally, it is very difficult to derive the explicit time-evolution equations for complex systems with a large number of degrees of freedom interacting on different time scales. In order to simulate the behavior of complex systems, several time series analysis and stochastic modeling approaches have been created based on the observed time series by splitting the system's activity between the observed macroscopic and hidden microscopic scales. The present perception of the mathematical structure of a complex system has significant flaws. As the model becomes more complicated, it is important to understand the mathematical structure of the constituent processes and how they interact with other parts of the model. A secondary objective of the analysis of fundamental mathematics is to invent new ways of posing issues to develop approaches that are more suited to the changing systems or architectures.

In order to convert a complex system mathematical model into a computational model there can be used a discrete representation of the system. Managing with system complexity correctly would force the use of a computational model that describes the underlying numerical solution of the problem. In this integrated setting, the discrete representation could incorporate uncertainty characterization, a model for integrating data with simulation, or an overall optimization method. The mathematical formulations that change the problem's structure are typically more challenging than the normal generic formulations and require far more advanced computational procedures. Moreover, the methodologies for merging algorithms from diverse disciplines need to be enhanced for these models to function together. The techniques need to be created to specify and monitor the instability in the algorithmic components as well as how they are interacting in the overall model. The computational models of complex systems that use the underlying mathematical structure of the system might lead to the need for solving linear and nonlinear equation systems that the structure represents (Bartocci, Lió, 2016). The techniques of linear and nonlinear solvers will be put to the test in these types of systems. Another important aspect of the solution process is the development of customized solution methods that make use of these systems particular structures. The methodologies based on more generic approaches are expected to degrade significantly in performance, especially in the transition to new designs that prioritize minimum data movement.

This holistic mindset involves a systematic consideration of all components of the solution process, rather than a method that is proceeding from the conceptualization to the approximation and to the algorithm.

The following are some of the most important study directions in multidimensional mathematics that mix various approaches to tackle complex systems:

- multiscale/multiphysics systems with stochastic and deterministic models: algorithms and methodological analysis;
- methodical techniques to building quantifiable fidelity surrogate or reduced-order models for the optimization, uncertainty quantification, and decision making;
- resolving model uncertainties with limited knowledge on parameter distributions, while addressing nonlinearities and unusual structures and evaluating alternate models of uncertainty and risk;
- algorithms and analysis for stochastic optimization that address model uncertainties with limited information on parameter distributions, considering alternative models of uncertainty and risk while addressing nonlinearities and special structures;
- strategies for propagating uncertainty across the scales and components of a multiphysics model in a multiscale model;
- system identification, control, and model uncertainty bounds by using improved data assimilation and model/data fusion methodologies (Alexander, 2012).

2.1. Time series analysis for complex systems

Although the analysis of time series is an extremely broad field of mathematics and statistics, in this work, the author will focus on some algebraic transformations of time series, i.e., the time delay embedding and the transformations of LaGrange matrices.

A time series is a collection of information gathered over the time: a week, a month, a quarter, or a year. The time series can be used to implement current decisions or implement plans based on the long-term forecasts. Time series analysis allows choosing a model in order to utilize in the time series prediction, such as building a time series producing model and utilizing that model to forecast the last time series values in the future. The goal of the time series analysis is to find a model that represents the data best and then use that model to extrapolate the time series most recent values into the future. The moving average model, exponential smoothing models, random walk and trend models, and models based on neural and fuzzy logic networks are the most prevalent time series prediction models.

In order to anticipate chaotic time series, the phase space must first be reconstructed (Tao et al., 2007). Data is commonly gathered by examining dynamics in the form of "time series", in which sequence values are taken at regular intervals, for example, such time series were utilized by Packard (Packard, 1980; Takens, 1980) to rebuild the time delay space of the finite measurement of the time evolution of the selected system by using the time delay approach. The topological properties and geometric structure of the reconstructed time delay space and the original dynamics are exactly the same (Ning et al., 2010). Scalar time series dynamics $\{x(t), t = 1, 2, \dots, N\}$ is integrated into the delay space of the d -th dimension where the time slots

are. Depending on the time delay technique, the delay space is expressed in (Packard, 1980):

$$X(t) = (x(t), x(t - \tau), \dots, x(t - (d - 1)\tau)); \quad (4)$$

where $t = (d - 1)\tau + 1, \dots, N$, τ is the time delay, d is the embedding dimension. In the dimension of the delay in the space, the initial characteristics and the regularity of the dynamics can be defined according to the trajectory of the d -th dimension reconstruction points. The dimension of time delay and reconstruction are important parameters in the reconstruction of space (Kim et al., 1999).

Fig. 6 shows the process of reconstruction of the delay space, starting from the measured process. In the most general form, the reconstruction of the delay space vector can be described by a d -dimensional vector: $y(t) = \Psi[\bar{x}(t)]$, where $\bar{x}(t) = \{x(t), x(t - \tau), \dots, x[t - (d - 1)\tau]\}$ is the delay vector at time t , and $\Psi: \mathbb{R}^d \rightarrow \mathbb{R}^n$ is a further reconstruction that considers the possibility of a more general reconstruction (Mayra et al., 2006). The upper graph on the left in Figure 6 is the actual system. If it is possible to measure the values of only one system variable (the lower graph in Fig. 6 on the left), its reconstruction practically replicates the dynamics of the system itself (comparing the two graphs on the right).

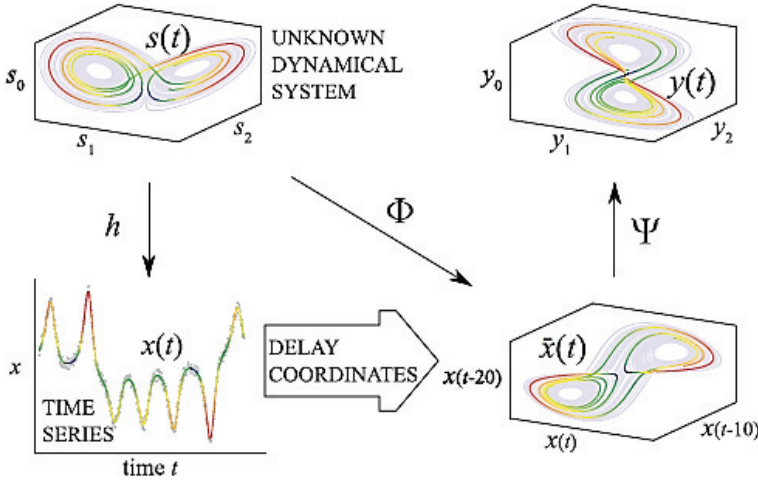


Fig. 6. Reconstruction scheme of the measurement process and dynamic system attractor (Uzal et al., 2011)

The prediction of time series is a difficult topic in a variety of fields. Most time series in the real world are chaotic and nonlinear. Many theoretical and practical problems use complex chaotic systems, including signal processing, social economics, and bioinformatics (Shen et al., 2013). There are two sorts of time series prediction approaches, i.e., long-term and short-term time series prediction techniques. Long-term time series prediction approaches, in general, try to build a process model and then use it to extrapolate previous behavior into relatively

extensive time frames in the future. Short-term time series prediction techniques have the same fundamental goal, i.e., to create a model of a process and project it into the future. Sadly, because the amount of supplied data is so limited, the application of approaches for developing a large time series model for a short time series is usually challenging.

It is known that no single predictor will outmatch all other forecasters. Various strategies for forecasting short-time series are still being developed: Ragulskis et al. (2011), Palivonaite and Ragulskis (2014), or Easton et al. (2014), to name a few, provide some typical examples of such innovations. Chen (2011) uses an intriguing blend of naive and other prediction models to forecast tourism demand. In the case of short-time series estimation, the naive technique may be the best option. The need for better or more advanced time series forecasting techniques has led to the development of a variety of other techniques, like the Hybrid Monte Carlo algorithm (Dong-xiao et al., 2012), wavelet-based time series decomposition (Jia et al., 2014), a linear combination of forecasters (Firmino et al., 2014), and the reconstruction of near-optimal algebraic skeletons (Palivonaite, Ragulskis, 2014). It was stated in Zhang et al. (2013) that to capture nonlinear relationships, the stochastic features of a real-world sequence require more complex methods than statistical techniques. In order for certain forecasting approaches to be effectively implemented, the data as well needs to be preprocessed (Wang et al., 2014).

The efficacy of short time series predictors can be improved as well by decomposing the original time series into a finite number of separate primitives, each of which can be predicted independently (Wang et al., 2014). Jia et al. (2014) outlined the importance of preprocessing track irregularity data and used the weighted moving average to preprocess the original time series to discover certain weight variables that lead to the best decomposition of the series. An equation of the form is a linear homogeneous recurrence relation of order n with constant coefficients:

$$x_j = \alpha_{n-1}x_{j-1} + \alpha_{n-2}x_{j-2} + \dots + \alpha_0x_{j-n}; \quad (5)$$

where coefficients $\alpha_k, k = 0, 1, \dots, n-1$ are constants. A linear satisfies linear recurrence sequence (LRS), which is the one that satisfies this form of relation. The initial values $x_k, k = 0, 1, \dots, n-1$ determine the evolution of this LRS (Kurakin, 1995; Kurakin, 2001; Park, Elden, 2003). The auxiliary polynomial to (5) reads as follows:

$$P(\rho) = \rho^n - \alpha_{n-1}\rho^{n-1} - \alpha_{n-2}\rho^{n-2} - \dots - \alpha_0; \quad (6)$$

where n roots describe the sequence satisfying the recurrence. If the roots $\rho_1, \rho_2, \dots, \rho_n$ are all different, then the recurrence forms:

$$x_j = \mu_1\rho_1^j + \mu_2\rho_2^j + \dots + \mu_n\rho_n^j; \quad (7)$$

where the coefficients $\mu_1, \mu_2, \dots, \mu_n$ are determined in order to fit the initial conditions of the recurrence. It is important to note that if just LRS is real, all roots are either real or complex to conjugate. If certain roots do, the recurrence is as follows:

$$x_j = \sum_{k=1}^r \sum_{l=0}^{n_k-1} \mu_{kl} \binom{j}{l} \rho_k^{j-1}; \quad (8)$$

where r is the number of distinct roots, n_k is the multiplicity index of the k -th root; $n_1 + n_2 + \dots + n_r = n$.

The algorithm for the reconstruction of the model of LRS from a sequence $\{x_j\}_{j=0}^{+\infty}$ is more complex if the order of LRS is not known beforehand. Hankel transform of $\{x_j\}_{j=0}^{+\infty}$ yields the sequence $\{h_j\}_{j=0}^{+\infty}$, where $h_j = \det H_j$, and

$\begin{bmatrix} x_0 & x_1 & \dots & x_n \\ x_1 & x_2 & \dots & x_{n+1} \\ \dots & \dots & \dots & \dots \\ x_{n-1} & x_n & \dots & x_{2n-1} \\ x_n & x_{n+1} & \dots & x_{2n} \end{bmatrix}$ is Hankel catalecticant matrix (matrix dimensions are $((j+1) \times (j+1))$). If there exists such $n \geq 1$ that $h_{n-1} \neq 0$ but $h_k = 0$ for all $k \geq n$, then $\{x_j\}_{j=0}^{+\infty}$ is LRS, its order is n , and the auxiliary equation now reads as follows:

$$\begin{vmatrix} x_0 & x_1 & \dots & x_n \\ x_1 & x_2 & \dots & x_{n+1} \\ \dots & \dots & \dots & \dots \\ x_{n-1} & x_n & \dots & x_{2n-1} \\ 1 & \rho & \dots & \rho^n \end{vmatrix} = 0. \quad (9)$$

There can only be considered the case, as stated earlier, when the roots of (9) are all distinct. $H = USV^T$ is the result of a singular value decomposition (SVD) of a real matrix H , where U comprises orthonormal eigenvectors of $H^T H$, and S is a diagonal matrix, which elements are sorted square roots of eigenvalues of $H^T H$.

2.1.1. The weighted moving average

A moving average is a type of finite impulse response filter that is used in statistics to analyze the data points by calculating a series of averages of different subsets of the entire data set. Simple, cumulative, and weighted forms are some of the variations (Yunfeng et al., 2001). The first element of the moving average is obtained by taking the average of the initial fixed subset of the number series, given a series of numbers and a fixed subset size. The subset is then modified by "shifting forward", which means excluding the first number in the series and including the number after the original subset in the series. This generates a new subset of numbers that are averaged. This procedure is repeated for the entire data set (Pandey, Giri, 2016).

A weighted average is an average that uses multiplying factors to assign different weights to data at various positions in the sample window. The weighted moving average is defined mathematically as the convolution of data with a fixed weighting function.

The initial sequence $\{x_j\}_{j=0}^{+\infty}$ is transformed into a sequence by using the moving average (MA) approach:

$$\{y_j\}_{j=0}^{+\infty} = \left\{ \frac{1}{L} \sum_{s=0}^{L-1} x_{s+j} \right\}_{j=0}^{+\infty}. \quad (10)$$

The width of the observation window is denoted as L . Signal smoothing is a typical implementation of MA methods in time series forecasting applications (Manikandan, Soman, 2012).

In comparison to $MA(L)$, the method of a weighted moving average, $WMA(L)$ differs in that the weight coefficients w_s are not identical.

$$\{y_j\}_{j=0}^{+\infty} = \left\{ \sum_{s=0}^{L-1} w_{L-s} x_{s+j} \right\}_{j=0}^{+\infty} \quad (11)$$

If it is considered that $\{x_j\}_{j=0}^{+\infty}$ is an LRS. $WMA(L)$ clearly transforms as LRS into an LRS as shown by Equations 8 and 11:

$$y_j = \sum_{s=0}^{L-1} w_{L-s} \sum_{k=1}^r \sum_{l=0}^{n_{k-1}} \mu_{kl} \binom{s+j}{l} \rho_k^{s+j-1} = \sum_{k=1}^m \sum_{l=0}^{n_{k-1}} \mu_{kl} j^l \rho_k^j. \quad (12)$$

A specific combination of weight coefficients w , k , and roots ρ_k can lead to a situation in which some of the expressions μ_{kt} become equal to zero. In these cases, the adjusted order of the LRS may be lower than the order of the original sequence. It is worth noting that the expressions μ_{kt} are independent of j . WMA can help to filter out the properties needed for the analysis of complex systems (Landauskas et al., 2017).

2.1.2. Effects induced by the additive noise

Several types of noise inevitably contaminate ECG recordings that are obtained through this process. The primary sources of this noise are the electrical activities of other body muscles, baseline shift due to the respiration, and poor contact between electrodes and equipment or electronic devices (Mozaffary, Tinati, 2005). Many diseases require a clean and clear ECG signal for screening and diagnosis. The author of the dissertation has employed the moving average filtering, including WMA to obtain a denoised ECG.

An H -rank is clearly not present in a random sequence, if the rank of a sequence $Hr(x_k + \varepsilon_k; k \in Z_0 = +\infty)$ (Trefethen, 1997). The suggested forecasting method, as previously stated, focuses on establishing the underlying skeletal algebraic progression that is contaminated in real-world time series by inherent noise. According to Trefethen (1999), the pseudospectrum of a square matrix is precisely described. Similar statements, concerning the pseudo H -rank, could explain the impact of additive noise on the algebraic relationships that govern the evolution of sequences. The spectrum of a square matrix A , denoted as $\Lambda(A)$, is the set of $z \in \mathbb{C}$ where the resolvent $(zI - A)^{-1}$ does not exist or is unbounded (I is the identity matrix). For each $\varepsilon > 0$, the ε -pseudospectrum of A is defined by (13):

$$\Lambda(A) = \{z \in \mathbb{C} : z \in \Lambda(A + E) \text{ for some } E \text{ with } \|E\| \leq \varepsilon\}. \quad (13)$$

The H -spectrum of the base fragment of the algebraic progression at the set of attributes roots was determined in the same way that the spectrum of a square matrix

was constructed (Landauskas et al., 2017). The subset on the complex plane containing all the possible positions of characteristic roots of the perturbed original sequence is ρ_k of the pseudospectrum:

$$P_\varepsilon(x_0, x_1, \dots, x_{2m-1}) = \left\{ z \in \mathbb{C} : z \in P((x_0 + \varepsilon_0), (x_1 + \varepsilon_1), \dots, (x_{2m-1} + \varepsilon_{2m-1})) \text{ for some } \varepsilon_0, \varepsilon_1, \dots, \varepsilon_{2m-1} \right\} \\ \left\{ \begin{array}{l} \text{with } \|\varepsilon_0, \varepsilon_1, \dots, \varepsilon_{2m-1}\|_2 \leq \varepsilon; \varepsilon_k \in \mathbb{R}; k = 1, 2, \dots, 2m-1 \end{array} \right\} \quad (14)$$

The Hankel matrix was perturbed, but instead, the elements of the foundation piece of algebraic progression are disrupted. Furthermore, the contradiction caused by the nonexistence of the H -rank of the additively contaminated algebraic progression was prevented. The element x_{2m} was not specified or changed. The equation can be used to solve this element: $d^{(m+1)} = 0$. As a result, the perturbed sequence's H -rank stays the same as the unperturbed sequence's H -rank (Landauskas et al., 2017). Another distinction is that in the classical formulation of the pseudospectrum, the disturbing matrix E comprises complex numbers, whereas in this case, the disturbing vector, which only contains real numbers, was used. The fact that real-time sequences were only extrapolated clarifies this, as stated previously.

The coefficients of the n roots of the polynomial of degree n are continuously dependent on them (Tyrtysnikov, 1997). The polynomial coefficients are proper adjuncts to the determinant in (9), but:

$$\det(A + \varepsilon E) - \det(A) = \det(A) \operatorname{tr}(A^{-1}E)\varepsilon + O(\varepsilon^2). \quad (15)$$

The following properties apply for a minor perturbation of the base fragment of the algebraic progression in the specified computing setup:

- It has no effect on the sequence's H -rank;
- The ε - H - pseudospectrum converges continuously to the H - pseudospectrum as $\varepsilon \rightarrow 0$;
- Since all components of the perturbed base element of the algebraic progression are real, all roots of the affected features polynomial are either real values or complex conjugate numbers.

In other words, removing corrections $\varepsilon_0, \varepsilon_1, \dots, \varepsilon_{2m-1}$ from the real-world time series is a well-posed task (Palivonaite, Ragulskis, 2013).

2.2. Attractor embedding: Uniform and non-uniform

In the nonlinear analysis of time series to reflect the evolution of the system in the m -dimensional space, the reconstruction of the underlying system's dynamic behavior is required. The most often used method is Takens time-delay embedding theorem, which needs to estimate two parameters, i.e., the embedding, which optimizes the distribution of the time series without obscuring the underlying dynamics in the m -dimensional space, dimension m , and time lag τ (Takens, 1980). He embedded dimension m , indicating that it was twice plus one greater than the system's actual dimension. Since a prioritized knowledge of the system's properties cannot be obtained in most cases, it is preferable to use other methods to estimate the

embedding dimension, such as the coherence of embedded data points (Small, 2005). Because the theorem is for an ideal time series with an infinite quantity of data and no noise, it is mute on how to measure the time delay τ , because any T value might be true in the ideal case given above. Even though the uniform embedding technique has been widely used to recreate the attractors that perform well in a variety of pattern recognition tasks, there are still some issues with multiple periodicity analysis of nonstationary biosignals.

2.2.1. Uniform embedding

Usually, the subject of nonlinear analysis of time series is the reconstruction of system dynamics in a state space that is called m -dimensional space. The aim of the reconstruction is to find a closed subset of the state space, called the system attractor, which includes all possible system state vectors and their dynamics, if the system is dissipative. It is difficult to reconstruct one-to-one original attractor of the system from the underlying time series. However, the mentioned time-delay embedding theorem proposes a comparable attractor (Takens, 1980). The state vectors of a time series are defined by the equal reconstruction or embedding, $s = \{x[0], x[1], \dots, x[n]\}$ with length n , as follows:

$$\vec{x}[t] = \{x[t], x[t - \tau], \dots, x[t - d_w]\}; \quad (16)$$

where the value $d_w = (m - 1)\tau$ represents the embedding window, m is the embedding dimension or the least number of coordinates required to represent the time series in the state space without overlapping, and τ is the time delay affecting the shape and spread of the reconstructed attractor. Moreover, because the τ parameter remains unchanged, the resulting embedding is called uniform embedding within the entire reconstruction process.

2.2.2. Non-uniform embedding

In order to improve the classification of nonlinearities by using non-uniform embedding techniques, another enhancement could be accomplished. Such methods test the time *lag vector* $\vec{l} = (l_1, l_2, \dots, d_w)$ instead of using the scalar τ for the state space reconstruction. Then the equation follows:

$$\vec{x}[t] = \{x[t - l_1], x[t - l_2], \dots, x[t - d_w]\}. \quad (17)$$

Because the non-uniform embedding methods are computationally intensive, they are limited to small databases and applications like time series modeling and prediction. Furthermore, applying these algorithms to the pattern recognition problems involving big databases is challenging.

A time sequence can be defined by using a variety of well-known complexity metrics, such as Lempel-Ziv or Kolmogorov complexity. The chaotic properties of a time series can be assessed by measuring its maximum Lyapunov exponent. Dimensional estimation techniques can be used to determine the complexity of a time series. Noise typically contaminates the real-world time series and experimental knowledge.

Even though the uniform and non-uniform embedding could be a great method for the reconstruction of the attractor, the permutation entropy (PE) may give some better results, because it is arguably the most important method for calculating the complexity of a time sequence (Huke, 2007; Manabe, 2007).

The developed attractor embedding algorithm by Timofejeva (2017) was used in the synchronization of Human Heart Rhythms with the Earth's Time-Varying Magnetic Field research. The optimal time delay parameter is used as a geometric characteristic of the embedded attractor. Similarly, if the data series are smoothed by using the moving average algorithm (or WMA algorithm), the optimal time delay can be reconstructed for both overlapping and nonoverlapping observation windows. In order to determine the optimal time delay, a geometric method is used to detect the shape of the reconstructed attractor when it occupies the largest area in the two-dimensional phase plane (Timofejeva et al., 2017).

Because the nature of the magnetic field (ML) and heart variability time series is completely different, for the ML attractor, embedding is used as a feature extraction algorithm, but H -ranks are used for feature extraction from the HRV data sets.

2.3. Permutation entropy

Permutation entropy is based on the permutation patterns or the order relationship between the signal values (Li, 2018). It compares the order of surrounding relative values rather than distributing amplitudes according to the varied quantities (Zanin, 2012).

For nonlinear time series, permutation entropy (PE) was established as a complexity metric (Zunino et al., 2017). Consider the time series $\{x_i\}_{i=1}^N$, where N is the length of the series, and denote it as m -dimension state space reconstruction series:

$$X_j^{m,\tau} = \{x_j, x_{j+\tau}, \dots, x_{j+(m-1)\tau}\}; j = 1, 2, \dots, N - (m - 1)\tau; \quad (18)$$

where m denotes the embedding dimension and τ denotes the time delay. The real values of the vector $X_j^{m,\tau}$ are permuted in ascending order as follows:

$$x_{j+(k_1-1)\tau} \leq x_{j+(k_2-1)\tau} \leq \dots \leq x_{j+(k_m-1)\tau}. \quad (19)$$

When the equality occurs, such as $x_{j+(k_{l1}-1)\tau} = x_{j+(k_{l2}-1)\tau}$, the quantities x will be ordered according to the values of their corresponding k , namely, if $k_{l1} < k_{l2}$, let $x_{j+(k_{l1}-1)\tau} < x_{j+(k_{l2}-1)\tau}$, else $x_{j+(k_{l1}-1)\tau} > x_{j+(k_{l2}-1)\tau}$. Therefore, each $X_j^{m,\tau}$ has a position sequence as follows:

$$S_j = [k_1, k_2, \dots, k_m], j = 1, 2, \dots, N - (m - 1)\tau; \quad (20)$$

and there will be $m!$ possible position types. The frequency of sequences of the same position is calculated as follows:

$$P_v^{m,\tau} = \frac{Num(v)}{N-(m-1)\tau}, v = 1, 2, \dots, m!; \quad (21)$$

where in all possible position sequences, $Num(v)$ represents the number of each type, and the total number of position sequences is denoted by $N - (m - 1)\tau$. The order m PE is defined as follows:

$$H_{PE}(m) = -\sum_{v=1}^{m!} P_v^{m,\tau} \ln(P_v^{m,\tau}), 0 \leq H_{PE}(m) \leq \ln(m!); \quad (22)$$

where $H_{PE}(m)$ is the maximum value $\ln(m!)$ when $P_v^{m,\tau} = \frac{1}{m!}$. In order to have more convenience, $H_{PE}(m)$ is normalized by $\ln(m!)$ as follows:

$$h_{PE}(m) = \frac{H_{PE}(m)}{\ln(m!)} . \quad (23)$$

The phase PE can be computed according to the following algorithm.

Assume that a discrete time series $\{x_i\}_{i=1}^N$, where the analytic signal $z(i)$ of $x(i)$ is a complex function of time given as:

$$z(i) = x(i) + j\tilde{x}(i) = A(i)e^{j\theta(i)}; \quad (24)$$

where the function $\tilde{x}(i)$ is the Hilbert transformation of $x(i)$:

$$\tilde{x}(i) = \frac{1}{\pi} \int_{-\infty}^{\infty} \frac{x(t)}{i-t} dt. \quad (25)$$

Thus, the instantaneous phase series $\theta(i)$ of $x(i)$ is:

$$\theta(i) = \arctan \frac{\tilde{x}(i)}{x(i)}, i = 1, 2, \dots, N; \quad (26)$$

and $\theta(i)$ ranges from $-\pi$ to π . Hilbert transform $\tilde{x}(i)$ of $x(i)$ can be considered as the convolution of $x(i)$ and $\frac{1}{\pi i}$. The following steps of phase permutation entropy (PPE) are then aligned with the PE algorithm's processing. $\theta(i)$ is converted into an m -dimension state space reconstruction vector as follows:

$$\theta_j^{m,\tau} = [\theta(i)_j, \theta(i)_{j+\tau}, \dots, \theta(i)_{j+(m-1)\tau}], j = 1, 2, \dots, N - (m - 1)\tau. \quad (27)$$

Then, each sequence in the reconstructed vector $\theta_j^{m,\tau}$ is permuted in an increasing order to obtain a position vector and calculate the frequency $P_v^{m,\tau}$ of each possible position type. Then:

$$H_{PPE}(m) = -\sum_{v=1}^{m!} P_v^{m,\tau} \ln(P_v^{m,\tau}). \quad (28)$$

After normalization, it follows:

$$h_{PPE}(m) = \frac{H_{PPE}(m)}{\ln(m!)} . \quad (29)$$

Weighted PE can be computed according to the following algorithm.

The amplitude disparities between similar ordinal patterns are ignored by the permutation entropy; thus, the information regarding the signal's amplitude is lost. The ordinal pattern provides a mechanism to measure the complexity in PE. The weighted permutation entropy is obtained by incorporating the amplitude information

into a change (WPE). The weight value w_j is applied to each vector $x_j^{m,\tau}$. The weighted relative frequencies are as follows:

$$P_w(\pi_i^m) = \frac{\sum_{j: x_j^{m,\tau} \text{ has type } \pi_i^m} w_j}{\sum_{j \leq N-m+1} w_j}. \quad (30)$$

It should be noted that $\sum_i P_w(\pi_i^m) = 1$. The weight value w_j is the variance of each vector $x_j^{m,\tau}$ as:

$$w_j = \frac{1}{m} \sum_{k=1}^m [x_{j+(k-1)\tau} - \bar{X}_j^{m,\tau}]^2; \quad (31)$$

where $\bar{X}_j^{m,\tau}$ is the arithmetic mean:

$$\bar{X}_j^{m,\tau} = \frac{1}{m} \sum_{k=1}^m x_{j+(k-1)\tau}. \quad (32)$$

Then, WPE is computed as (when only $w_1 = w_2 = \dots = w_{N-m+1}$):

$$H_w(m) = - \sum_{v=1}^{m!} (P_v^{m,\tau})_w \ln((P_v^{m,\tau})_w). \quad (33)$$

It is necessary to evaluate both the effectiveness and accuracy of all the available algorithms in order to choose the most suitable algorithm for each particular problem. As with other conditions, the complexity of numerical algorithms, their stability and convergence are the primary aspects for the selection of a suitable problem-solving strategy. Determining the algorithm's complexity means finding the upper limits or calculating how many elementary operations, such as scalar additions and multiplications, are required to perform any algorithm, such as matrix multiplication.

The eigenvectors of a square matrix can be discovered by finding a sequence of vectors x_n that converge to one eigenvector as n approaches infinity (Householder, 1975). Both PE and phase PE and WPE can be smooth by using MA or WMA algorithms.

2.4. Second order Lagrange matrix of differences

If the time series is scalar, Lagrange variations at the nodal point of a scalar time for the determination of derivatives of variables can be used. The reconstructed derivatives from a scalar time series enhance the noise in the series. The local relationships defined by perfect Lagrange matrices (Ziaukas et al., 2017) can be represented by a scalar parameter. In general, selecting such a parameter is an ill-posed inverse issue of parameter recognition. The matrices of Lagrange differences are second order square matrices that include such elements. A perfect matrix of Lagrange differences is a second order square matrix with components that satisfy the following conditions:

1. The matrix elements are all unique.
2. On the major diagonal, zeroth order disparities are found.
3. On the secondary diagonal, first order discrepancies are found.
4. The x and y indexes can take one of three potential values: $i \in \{n - \delta, n, n + \delta\}$ where n is the current time moment and δ is the time lag; $\delta \in \mathbb{N}$.

5. The perfect matrix of Lagrange differences is lexicographically balanced with the same number of x and y symbols in all of the matrix expressions.

6. In terms of time, the perfect matrix of Lagrange differences is balanced: all elements of the matrix have the same number of indices with subscripts $-\delta$ and $+\delta$ in their expressions.

Example 1

$\begin{pmatrix} 0 & x_{n+\delta} - y_{n+\delta} \\ x_{n-\delta} - y_{n-\delta} & y_n \end{pmatrix}$ —not a perfect matrix: the null element is not allowed;
 $\begin{pmatrix} y_n & x_{n+\delta} - y_{n+\delta} \\ x_{n-\delta} - y_{n-\delta} & y_n \end{pmatrix}$ —not a perfect matrix: no lexicographical balancing;
 $\begin{pmatrix} x_n & x_{n+\delta} - y_{n+\delta} \\ x_{n+\delta} - y_{n+\delta} & y_n \end{pmatrix}$ —not a perfect matrix: no balancing in respect of time;
 $\begin{pmatrix} x_n & x_{n+\delta} - y_{n+\delta} \\ x_{n-\delta} - y_{n-\delta} & y_n \end{pmatrix}$ —this is a perfect matrix of Lagrange differences.

A natural query is the number of different perfect matrices of Lagrange differences. In general, as illustrated in Table 1, six different elements of time series x and y were expressed.

Table 1. Six different elements of time series x and y mapped in the Lagrange matrix of differences

$x_{n-\delta}$	x_n	$x_{n+\delta}$
$y_{n-\delta}$	y_n	$x_{n+\delta}$

The classification and interpretation of perfect matrices of Lagrange differences would be simplified by a graphical representation of these matrices. The primary diagonal contains zeroth order differences ($\pm x$ and $\pm y$); however, the indexes of these elements can differ.

This type of graphical representation of perfect matrices of Lagrange differences allows for easy categorization of all possible perfect matrices. There are only 18 different types of perfect Lagrange difference matrices. One of the most important characteristics of each square matrix is that its own values are unique. It is self-evident that the elements on the diagonal and anti-diagonal can be switched, and their signs moved without altering the whole absolute value of their own. This implies that every graphical representation of a matrix can be the product of variations in Lagrange of $2^4 = 16$ different perfect matrices in terms of the maximum absolute eigenvalue. Overall, 288 distinct perfect matrices of Lagrange variations yield 18 different representations (Ziaukas et al., 2017).

The ECG parameters can be investigated by defining the target function, according to which the matrix architecture will be optimized. That allows for an objective assessment which matrix is better or worse, according to a given criterion. The structure of the matrix itself can hold valuable information about the human cardiovascular system. It should be noted that the target function needs to be constructed individually to solve each application task. Moreover, in individual cases,

the choice of 18 different matrices may be too specific to detect subtle changes in cardio signals. Then, some of the restrictions should be relaxed. For example, the relaxation of the second and the third conditions would greatly increase the number of different matrices. Thus, the selection of the number of constraints, the selection of matrix representations into a scalar time series, the smoothing factors, the length of the observation window for the computation of the H -ranks, the selection of the parameters for the algorithms used for the reconstruction of embedded attractors, the types of PE (not to mention assigning sequences x and y to the specific ECG parameters) are important fitting elements that are specific to each individual application.

In Ziaukas et al., (2017), two ECG parameters of interest (RR and JT) were selected, registered, and denoted as vectors, i.e., $x = (x_1, x_2, \dots, x_n)$ and $y = (y_1, y_2, \dots, y_n)$. The link between RR and JT intervals during cycling ergometry was investigated by using perfect matrices of Lagrange differences. The construction of the load function, the implementation of internal and external smoothing, and the embedding of scalar parameter time series into the phase plane allowed to trace complicated dynamical processes in the cardiovascular system during the load and recovery. As it has already been previously mentioned, the load of the bicycle ergometry exercise increases every minute. However, the RR intervals do vary during the exercise. Several inter-beat intervals were recorded during the first minute (before the exercise was started), and the further minutes are different. The ECG parameters were recorded for 5 minutes further after the workout was completed. The target function was created, and the parameter denoting local interactions was defined by perfect Lagrange matrices that were as close as possible (Ziaukas et al., 2017).

The structural coefficient $str = \frac{\max|\lambda_k|}{\min|\lambda_k|}$, the maximum absolute eigenvalue of a perfect matrix of Lagrange differences $\max|\lambda_k|$, the minimal absolute eigenvalue $\min|\lambda|$, and the discriminant $disc = (a_{11} \ a_{22})^2 + 4a_{12}a_{21}$ were selected, and 1 second has been set as the time delay.

The scaled inverse values of the load are denoted as l_k ; $k = 1, 2, \dots, 1199$. The values of the specific parameter computed for the perfect matrix of Lagrange differences constructed from the RR (x -time series) and JT (y -time series) are now denoted as p_k ; $k = 1, 2, \dots, 1199$. The aim of the optimization problem is to select the most suitable parameter to minimize the RMSE (root mean square error) between l_k and p_k , where the parameter is minimized for a specified expression; the values of p_k are normalized into the interval $[0, 1]$ before starting the operation of the optimization.

The optimal parameter is computationally tuned by using ECG records from ten persons. The value N fluctuates because each person stopped the bicycle ergometry exercise at a different time. RSME (root square mean error) for all 18 has been averaged, instead of picking a single perfect Lagrange difference matrix (Ziaukas et al., 2017).

In this case, parameter $\delta = 1$ is fixed. Max $|\lambda|$ was chosen as the best parameter reflecting the local relationships provided by perfect Lagrange matrices.

The computational experiments are carried on with $\max |\lambda(L_{\delta,k}^{(s)})|$ where $L_{\delta,k}^{(s)}$ denotes the perfect matrix of Lagrange differences centered on the time moment k . The potential of moving average (MA) (Savitzky et al., 1964) to smooth coarse signals is widely established. The number of parameter values produced for perfect Lagrange differences matrices that are averaged is determined by the internal smoothing radius. The inner averaging is written as follows:

$$\frac{1}{\Delta} \sum_{\delta=1}^{\Delta} \max |\lambda(L_{\delta,k}^{(s)})|. \quad (34)$$

The standard MA is now used to smooth the reconstructed parameter values at different time periods k ; this smoothing procedure is referred to as external smoothing. Nonetheless, for MA, the averaging windows with odd widths (denoted as m) was considered because the averaging is symmetrically built around the temporal instant k . The reconstructed parameter value is denoted as $p_k(s, \Delta, m)$, where k is the time moment, Δ is the radius of internal smoothing, and m is the radius of the external smoothing. Then:

$$p_k(s, \Delta, m) = \frac{1}{(2m+1)\Delta} \sum_{j=k-m}^{k+m} \sum_{\delta=1}^{\Delta} \max |\lambda(L_{\delta,k}^{(s)})|. \quad (35)$$

The external averaging (with the absence of internal averaging) reads like this:

$$p_k(s, 1, m) = \frac{1}{(2m+1)} \sum_{j=k-m}^{k+m} \max |\lambda(L_{\delta,k}^{(s)})|. \quad (36)$$

In order to have a better representation of the attractors and assess their stability, the dynamical processes of Fig. 7 were visualized in the phase plane (Ragulskis et al., 2009). 4 RR intervals are used to compute the appropriate time delay. Time-delay embedding is used to describe temporary stabilization and subsequent loss of attractor stability in the phase plane (Sauer et al., 1991) (Fig. 7). Star type markers reflect the normalized loads at 1, 0.8, 0.6, 0.4, 0.2, and 0 in Fig. 12.

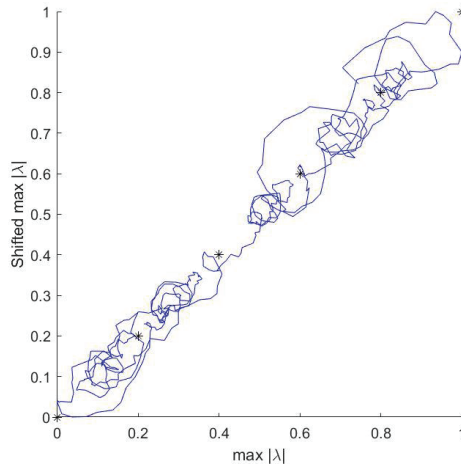


Fig. 7. Phase plane of the optimal time delay during the load; the time delay is $\tau=4$

The temporal stability of p_k around the 0.8 fixed-point attractor is expressed in Fig. 7. With a load of 0.8, the subject was able to complete the bicycle ergometry test for a longer time. However, the system is forced to reconstruct as the load increases. It takes a long time to get to the 0.6 fixed-point attractor. The system tries to loop around the non-existent attractor with a value slightly higher than 0.6; then, it goes through a series of transients before settling on 0.6.

The subject should continue the exercise at load 0.6 for a considerably longer duration. However, the load increases to 0.4 once more. In comparison to the previous transformations, the method now simply converges almost to the 0.4 fixed-point attractor, and the transient processes are much easier to understand (Fig. 7).

The subject may, once again, continue the exercise for longer than he/she is permitted. Convergence to the 0.2 fixed-point attractor is substantially more difficult; in actuality, the sequence of p_k never stabilizes around 0.2. The subject does not appear to be able to hold the load at 0.2 for much longer than he/she has. There is no transition to the 0 fixed-point attractor. The 0 fixed-point attractor has no transition. Instead, “complexity collapses”, and the subject quits the bicycle ergometry test.

It is as well fascinating to see how the body recovers after performing the ergometry test. The “collapse of complexity” has the opposite effect, as seen in Figure 8. The trajectory not only moves away from the point of collapse, but gets more complicated over he time as well.

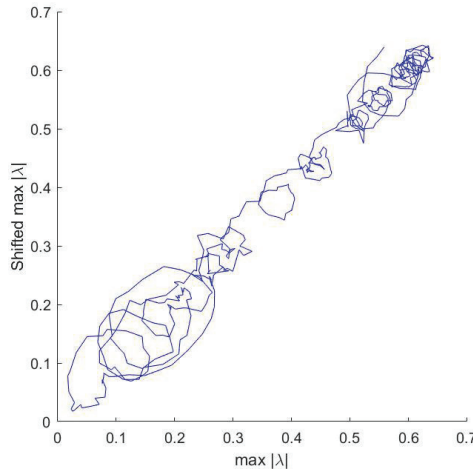


Fig. 8. Phase plane of the optimal RR-JT algebraic relationship after the load; the time delay is $\tau=4$

The trajectory moves quickly at first before stabilizing at 0.35 (Fig. 8). However, as the recovery processes end, this attractor loses its stability. Finally, the system’s trajectory plots a chaotic attractor around 0.6. Since it is known that the heart is a chaotic system, the chaotic behavior of the heart could be considered as a validation of the presented model.

Perhaps, a simple phase plane representation of RR and JT will reveal similar relationships: whether such complex computations are required is a logical question.

Figure 9 depicts the variance of RR/JT intervals during the bicycle ergometry test. Unfortunately, Fig. 9 only shows one relationship: the RR (and JT) intervals shorten as the load increases.

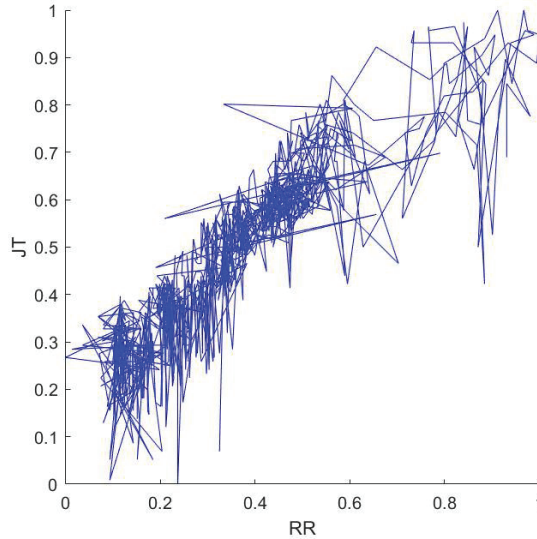


Fig. 9. RR and JT interval series phase plane

The straightforward visualization of RR and JT intervals cannot reveal the complexity of the cardiovascular system dynamics.

The current computational technique reconstructs the optimal set of parameters (s , m , and Δ) for each individual based on his/her RR, JT time series, and load data. The resulting optimum time series p (s , m , Δ) are used to illustrate the self-organization of the cardiac system by minimizing the individual load target function.

The “collapse of complexity” at the end of the bicycle ergometry test, the temporary stability of transitory attractors during the load, and the extensive dynamical behavior of the cardiac system during the recovery phase are all things that a physician might evaluate.

Even though the provided methodologies can only be employed for an individual person's RR and JT data, they opened opportunities for new insights into the dynamics of the cardiovascular system.

In solving specific application problems, the selection of a function representing a two-dimensional square matrix into a scalar is a specific task, as mentioned above. It can be seen how this attractor temporarily stabilizes as the load changes by plotting a simple phase diagram between the RR and JT intervals and noting what the change in the algebraic relationship looks like.

2.5. Synchronization determination algorithms

Synchronization phenomena occur in nature. Human and animal collaborative behaviors, heart rate and breathing regulation, synchronous activity of the neurons are the examples of oscillating elements that synchronize with each other. All of these

mechanisms, as well as many more, have one thing in common: they produce periodic rhythms that can adapt to one another (Pikovsky et al., 2001).

The development of a chaotic system is sensitive to its initial conditions; thus, even if the beginning conditions are slightly different, two similar chaotic systems might separate exponentially over the time. The possibility of cooperation between two chaotic systems due to such delicate reliance has been debated for a long time (Zhang, 2013). The phenomena of synchronization of chaos can emerge when two or more dissipative chaotic systems are connected (Boccaletti et al., 2002). Synchronization is defined as the "correction of oscillating objects' rhythms due to their weak connection" (Pikovsky et al., 2001). This arises when the rhythms of two or more autonomous objects with differing rhythms alter in relation from one to the other (Eroglu et al., 2017).

The following principles for the inclusion and exclusion are suggested by this definition:

1. For synchronization to occur, the objects must be oscillators and autonomous systems. It does not mean that two variables that have identical frequencies are synchronous.

2. The objects must be open systems that receive signals from their environment and interact with other objects; thus, if these external signals are eliminated, the objects will no longer be able to oscillate in typical rhythms.

The synchronization can take several forms depending on the design of the interacting systems, the type of coupling, and the proximity of the systems.

2.5.1. Identical synchronization

A complete synchronization is another term for this type of synchronization. This can be seen in similar chaotic systems. Complete synchronization can be achieved via a variety of coupling techniques. There are two types of complete synchronization: configuration and drive-response coupling. The evolution of one of the connected systems is unaffected by the evolution of the other under the drive response setup, on the opposite, both systems jointly influence each other. Two diffusely coupled dynamics are represented in the simplest case as follows:

$$x' = F(x) + \alpha(y - x), \quad (37)$$

$$y' = F(y) + \alpha(x - y); \quad (38)$$

where F is the vector field modeling the isolated chaotic dynamics and α the coupling parameter. The system $x(t) = y(t)$ denotes the invariant subspace of the coupled system. If this subspace $x(t) = y(t)$ is locally attractive, the coupled system will exhibit identical synchronization.

The oscillators become disconnected if the link is lost, and the chaotic behavior forces neighboring routes to diverge. The diffusive coupling suppresses the chaos-induced divergence of trajectories of interacting systems when the coupling parameter is strong enough, and the perfect synchronization occurs as a result of the contact. The behavior of the difference to determine the essential coupling strength $v = x - y$ was investigated. It is possible to expand the vector field in a series and derive a linear

differential equation describing the behavior of the difference by eliminating the Taylor remainder and assuming that v is small as:

$$v' = DF(x(t))v - 2\alpha v; \quad (39)$$

where the Jacobian of the vector field along the solution is denoted by $DF(x(t))$. If $\alpha = 0$, then:

$$\|v(t)\| \leq \|u(0)\|e^{(-2\alpha+\lambda)t}. \quad (40)$$

It yields a critical coupling strength $\alpha_c = \lambda/2$ for all $\alpha > \alpha_c$, and the system exhibits complete synchronization. The presence of a critical intensity of the coupling is related to the isolated chaotic nature of the dynamics. Regarding synchronization, this logic leads to the right critical coupling value. In certain situations, synchronization loss could be observed for coupling strengths greater than the critical value. This happens because the nonlinear terms that are ignored in the critical coupling value derivation play a significant role and break the exponential limit for the different behavior (Ashwin, 2006).

However, a comprehensive solution to this problem can be given, and a critical value is obtained such that the nonlinearities would not affect the stability (Pereira, 2011).

2.5.2. Generalized synchronization

Generalized synchronization suggests that a functional relationship is fulfilled by the states of two coupled systems or asymptotically satisfies a functional relationship as time goes to infinity (Ouannas et al., 2015). Mostly, this type of synchronization appears when the chaotic oscillators that are coupled are different. When the state of the oscillators is determined by the dynamical variables (x_1, x_2, \dots, x_n) and (y_1, y_2, \dots, y_m) , the generalized synchronization emerges when there is a functional, Φ , such as $[y_1(t), y_2(t), \dots, y_m(t)] = \Phi[x_1(t), x_2(t), \dots, x_n(t)]$. This implies that the dynamic state of one of the oscillators is dictated absolutely by the state of the other. If the oscillators are mutually connected, this function must be invertible. However, if there is a drive-response arrangement, the drive determines the response evolution, and Φ does not need to be invertible.

2.5.3. Phase synchronization

In recent years, the phase synchronization has been an object of great interest, particularly regarding its application to biological rhythm synchronization. In most cases, this form of synchronization implies locking the frequencies of the coupled oscillators with certain oscillating variables, while the signal amplitudes remain uncorrelated. Even if the oscillators are not similar, this phenomenon happens. Phase synchronization observation includes a previous concept of a chaotic oscillator phase (Zhong et al., 2018). The projection of oscillator trajectories around a well-defined core can be observed in a phase-space plane in numerous practical contexts. The phase is defined, if this is the case, by the angle, $\varphi(t)$, represented by the segment joining the center of rotation and the trajectory point projection onto the plane. In other cases, the

signal processing theory concepts, such as the Hilbert transformation, can still be used to characterize a step. When the phases of the two coupled oscillators are denoted by $\varphi_1(t)$ and $\varphi_2(t)$, the synchronization of the phase is given by the relation $n\varphi_1(t)=m\varphi_2(t)$, where m and n are whole numbers.

2.5.4. Anticipated and lag synchronization

The synchronized state is defined in these circumstances by a time interval, such that the dynamical variables of the oscillators (x_1, x_2, \dots, x_n) and $(x'_1, x'_2, \dots, x'_n)$ are related by $x'_i(t) = x_i(t + \tau)$. This implies that the dynamics of one oscillator follows or anticipates the other. Anticipated Synchronization (AS) is a unique type of synchronization that occurs when two systems are unidirectionally coupled, and the information is transmitted from the sender to the receiver, but the receiver leads the sender in time (Dalla, 2019). Anticipated synchronization may emerge between the chaotic oscillators linked in a drive-response system, which dynamics are described by differential equations of delay. In this case, the reaction predicts the dynamics of the drive. Lag synchronization can occur when the connection between the phase-synchronized oscillators is strengthened. Lag synchronization can be achieved by increasing the intensity of the coupling between the phase-synchronized oscillators. The driving signal is composed of several nonlinear delayed state variable modifications (Pyragas, 1998).

2.5.5. Amplitude envelope synchronization

Amplitude envelope synchronization is a type of synchronization of weakly coupled chaotic oscillators. In this situation, there is no relationship between the phases or amplitudes. The oscillations of the two systems are developed by a periodic envelope with the same frequency in both. The order of magnitude is the same as the difference between the two chaotic oscillators' average oscillation frequencies. In a sense, that phase synchronization occurs when the frequency of the coupling between two synchronized oscillators of the amplitude envelope is enhanced; the amplitude envelope synchronization precedes the stage synchronization. The property of asymptotic stability is shared by all these modes of synchronization. This means that the effect of a minor perturbation that breaks synchronization is easily dampened until the synchronized state has been reached and the synchronization is restored again. A positive system exponent of Lyapunov, consisting of two oscillators, which becomes negative when chaotic synchronization is achieved, mathematically defines the asymptotic stability (Qiu et al., 2020).

Individual properties alone are not enough to understand the complex systems. The analysis of interconnections between those properties is required. The statistical approaches require a significant amount of data and are inconvenient when instantaneous estimation is needed; therefore, the matrix analysis approaches create new options.

In this work, it is shown that the synchronization of Human Heart Rhythms with the Earth's Time-Varying Magnetic Field plays an essential role in self-organization of human cardiovascular system. In order to compute the local magnetic field power

in the frequency range $\omega \in [0; 1]$ Hz, the time interval $t_0 = 2015/02/26$ 01:00:02 through $t_1 = 2015/02/26$ 01:00:03, the corresponding spectrogram is calculated as described above. The spectrogram is then cropped to $S = \min\{S; 0.25\}$. The signal power $P = 7.7405$ ((pT)²/Hz) is computed from the filtered spectrogram.

Let a signal $X = (X_1, \dots, X_n)$ be a scalar time series of size n . It is possible to embed the time series into a 2D delay coordinate space:

$$X_i, i = \overline{1, n} \rightarrow (X_i, X_{i+\tau}), i = \overline{1, n-\tau}, \tau \in \mathbb{N}. \quad (41)$$

For $\tau = 1$, the following trajectory matrix is obtained:

$$\begin{bmatrix} X_1 & X_2 \\ X_2 & X_3 \\ \vdots & \vdots \\ X_{n-1} & X_n \end{bmatrix}; \quad (42)$$

where each row of the matrix corresponds to the coordinates of a delay coordinate space embedded point. The time lag τ can be different ($\tau \in \mathbb{N}$). Thus, at $\tau = k$, the trajectory matrix reads as:

$$\begin{bmatrix} X_1 & X_k \\ X_2 & X_{k+1} \\ \vdots & \vdots \\ X_{n-k+1} & X_n \end{bmatrix}. \quad (43)$$

The arranged set of integrated points is referred to as the attractor, and the 2D plane is referred to as the state space (Sauer et al., 2009). It is worth mentioning that the area occupied by the embedded attractor is one of the attributes that characterize the time series dynamics. However, the area of the attractor is determined by the time lag τ used in the reconstruction of the state space. The maximum area of the embedded attractor is a characteristic that can be used to describe the underlying model that governs the time series evolution (Ragulskis, Lukoseviciute, 2009).

A simple algorithm was used to compute the area of the embedded attractor based on the direct assessment of the geometric area occupied by the set of points of the trajectory matrix in the state space. The steps of the algorithm are as follows:

- (1) Determine the center of mass of the points that make up the attractor, shift the origin of the state space to the mass's center.
- (2) Divide the attractor's state space into slices that have equal central angles of a circle centered on the origin; the number of slices is proportional to the number of points in the time series observation window.
- (3) Establish the radius of each slice to the greatest distance possible between a slice point and the origin.
- (4) As the sum of the areas of all slices, compute the area of the attractor S_τ .

The algorithms for the synchronization between different time series play a particularly important role in finding links between HRV and other factors influencing the human environment (e.g., local Earth magnetic field).

III. ALGORITHMS AND APPLICATIONS IN THE CARDIAC SIGNAL ANALYSIS

Among all non-invasive methods for identifying the functioning of the cardiovascular system, electrocardiography (ECG) is the most basic and well-studied one. Clinical practice cannot be conducted without incorporating ECG parameters. With the help of ECG parameters, monitoring heart rate and conductance abnormalities, as well as cardiac hypertrophies and ischemic processes, can be detected. A sensitive indicator of cardiac dysfunction can still be identified by analyzing cardiac intervals, even if no cardiac dysfunction can be detected with traditional echocardiography (Biering-Sorensen et al., 2016). Some argue that the diagnostic properties of ECG parameters are well understood, and alternative analysis techniques are not needed. This is most likely due to the reasons mentioned below:

- Poor identification of the precision of links between ECG parameters,
- A fixed model of ECG parameter relationships does not always work even for the same person,
- Time-averaged ECG parameter relationships are unable to portray the complexity of correlations across the time scale lengths.

Despite this, the relationships between ECG parameters remain an active area of research. Many physiological and pathological factors can alter the relationships between ECG parameters. It is believed that chaotic processes play a vital role in the interaction between different systems and according to holistic models, in generating reactions between them (Malik et al., 2002). As a result, looking for a single deterministic model that can explain the relationships between ECG parameters is possibly illogical. It is natural to pay attention to the dynamic processes and relationships that can show complex chaotic behavior (Bonomini et al., 2012).

3.1. The algorithm for the detection of anaerobic threshold

The anaerobic threshold is a limit at which the body is no longer able to compensate for the need for oxygen to produce energy during intense physical exercise. Complicated assessments, such as a cardiopulmonary exercise test, are used to determine the anaerobic threshold. The anaerobic threshold can as well be measured by taking blood samples during the stress test. Therefore, there exists a strong need for a rapid, convenient, and non-invasive method to determine the anaerobic threshold.

The term "anaerobic threshold" (AnT) is commonly used in sports medicine. The AnT is a dependable and powerful predictor of load performance. The lactate threshold (LT) and the AnT are sometimes used interchangeably. The LT refers to the point at which blood lactate concentration is no longer linearly connected to the exercise intensity, but instead rises with both intensity and duration of the exercise (Maud et al., 1995). The "maximum steady-state lactate concentration" is the blood lactate concentration at the AnT (Gladden et al., 1985). The AnT is a point during

exercise when higher lactic acid levels cause increased carbon dioxide generation and minute ventilation. Even though the LT and the AnT are sometimes used alternately, they are not the same thing (Wilmore et al., 2005).

The AnT is calculated by using several approved methods. Blood lactate accumulation is still a good indicator of fatigue onset; therefore, blood lactate accumulation and maximal lactate steady state can be utilized to accurately determine the LT. A graded exercise test in a laboratory setting is the most accurate approach to determine the LT (McArdle et al., 2000). At regular intervals, the resistance of the cycle ergometer is raised, and the blood samples are obtained at each increment. Plotting blood lactate against each exertion period produces the lactate performance curve. The lactate curve can be used to calculate the AnT. The AnT is stated to be indicated by a quick or sharp rise in the curve above the base level (McArdle et al., 2000). However, detecting this abrupt increase in blood lactate might be difficult (McArdle et al., 2000).

According to Conconi et al. (1982), the AnT relates to a deflection point in the heart rate during the exercise. The Conconi test is based on the idea that heart rate and exercise intensity are proportional. Conconi showed that at near-maximal exercise intensities, all of their subjects' heart rates reached a plateau (Ballarin et al., 1989). The Conconi test is appealing because of its simplicity. However, other researchers significantly doubt the Conconi test's accuracy (Tokmakidis, 1992). According to the studies, the heart rate deflection point or plateau occurs in a limited number of persons, and when it does, it greatly overestimates the LT when measured directly (Conconi et al., 1996). Many subsequent studies have both confirmed and disputed the Conconi test's utility (Bourgois, 1998).

During a workout, VO_2 max, maximum heart rate, and other physiological dynamics are typically measured at the same time (Maud, Foster, 1995). However, during the physical load, the heart rate has never been completely reliable and varied greatly across and within people (Maud, Foster, 1995; Wilmore, 2005; McArdle et al., 2000). The Conconi test is regarded to be less reliable than a combination of heart rate and lactate values (Conconi et al., 1982).

An easy way to calculate the AnT is to suppose that it happens when the heart rate hits 85–90 percent of its maximum during the activity (for 20 age healthy subjects). However, as previously stated, the heart rates vary widely between individuals, and even for the same individual, this test is not valid.

Some researchers have questioned the validity of detecting the LT and AnT even in the laboratory conditions (Gladden, 1985; Yeh, 1983). More researchers (Yeh, 1983; Hughson, 1987) questioned if there is such a thing as a precise point or threshold. Conversely, they claim that blood lactate accumulation is continuous, and a single threshold point cannot be defined.

Any physiological test that is commonly recognized is only as reliable as the tester's ability to follow a predetermined protocol. Even when an appropriate assessment has been chosen, numerous variables must be maintained to ensure that the test is accurate and dependable.

All necessary standards for the experimentation ethics were met in this study. On December 23, 2015, Kaunas Regional Ethics Committee for Biomedical Investigations, No. BE-2-51, approved permission to conduct biomedical research. The cardiac RR and QRS intervals were measured by using ECG cycle ergometry workout. Before the trial, the participants signed a written informed permission form.

The cardiac intervals were measured by using the ECG analysis system "Kaunas-Load" (Vainoras et al., 1998) that was developed at the Institute of Cardiology, Lithuanian University of Health Sciences. The QRS (duration of QRS) interval was estimated by using the II lead of the ECG depolarization time of the heart ventricles. The system allows for the simultaneous recording of 12 different ECG standard parameters. The measurement is initiated at zero load and continues for one minute. The load is then increased by 25W per minute after that. Throughout the entire cycle ergometry exercise, the participant must maintain a consistent 60 revolutions per minute spinning rate. According to the American Heart Association, the exercise should be continued until the first clinical signs of the load limitation appear. During the recovery period, the measurement is repeated for additional 10 minutes. Throughout the experiment, systolic and diastolic pressures are taken and recorded in the middle of every minute. During the cycle ergometry exercise and recovery process, the ratio of oxygen to carbon dioxide in exhaled air is measured as well.

Throughout the experiment, two ECG parameters (RR and QRS) are measured and denoted as vectors: $x = (x_1, x_2, \dots, x_n)$ and $y = (y_1, y_2, \dots, y_n)$. The given computational technique is used to examine the relationship between the time series x and y (Ziaukas et al., 2017). The algorithm is split into three stages:

1. Elements of the time series x and y are embedded in a series of perfect Lagrange differences matrices $L_{\delta,k} = \begin{bmatrix} x_k & x_{k+\delta} - y_{k+\delta} \\ x_{k-\delta} - y_{k-\delta} & y_k \end{bmatrix}$; $k = (1 + \delta), (2 + \delta), \dots, (n - \delta)$; $\delta \in N$. From the topological standpoint, a three-dimensional trajectory matrix contains two scalar trajectories.

2. The sequence of matrices $L_{\delta,k}$ is transformed into a scalar sequence of maximum modulus values of eigenvalues of matrices $L_{\delta,k}$; this scalar sequence is denoted as $s_{\delta,k} = \max|\lambda(L_{\delta,k})|$.

3. Lastly, the internal and external smoothing for $s_{\delta,k}$ is applied. The internal smoothing radius is R_i , and the external smoothing radius is R_e ($R_i, R_e \in N$). The smoothed sequence then reads as follows (Ziaukas et al., 2017):

$$p_k(R_i, R_e) = \frac{1}{(2R_e+1)R_i} \sum_{j=k-R_e}^{k+R_e} \sum_{\delta=1}^{R_i} s_{\delta,j}. \quad (44)$$

It should be noted that the computation of $p_k(R_i, R_e)$ requires multiple embeddings of x and y into different trajectory matrices. In order to analyze the relationship between scalar time series x and y , the parameter sequence $p_k(R_i, R_e)$ is applied.

Ziaukas et al. (2017) propose an optimization problem in terms of the parameters R_i, R_e (assessing the whole cohort of persons). Optimization procedures are not repeated and maintain $R_i = 3$ and $R_e = 4$ constant throughout the rest of the

computations. The algorithm for investigating RR-DQRS relationships will be the same as in Ziaukas et al. (2017), except now, y represents the DQRS sequence.

Apart from the ECG, systolic and diastolic blood pressures as well as the oxygen-to-carbon dioxide ratio in exhaled air are all monitored during the cycle ergometry exercise and recovery.

Throughout the study, the systolic and diastolic pressures were measured once every minute. The oxygen-to-carbon dioxide ratio in exhaled air is continually measured (the patient wears a mask with a gas analyzer), but the data are averaged for each minute of the experiment.

Experiment 1

Figure 10 depicts the evolution of the relationships between RR and DQRS cardiac intervals for the first individual. The x -axis in parts A, B, and C shows the number of cardiac cycles since the commencement of the cycle ergometry exercise. The power of the load is depicted in Figure 10B. The subject sits for 1 minute at rest at the start of the experiment. For each minute after that, the load is increased by 25 W. The cycle ergometry exercise continues for another 13 minutes, stopping at 325 W in the middle of the 14th minute (Fig. 10B). The interval lengths in Fig. 10B are not equal due to the increased heart rate (different number of cardiac cycles fit into each minute). The recovery processes are monitored further for 10 minutes after the cycle ergometry exercise.

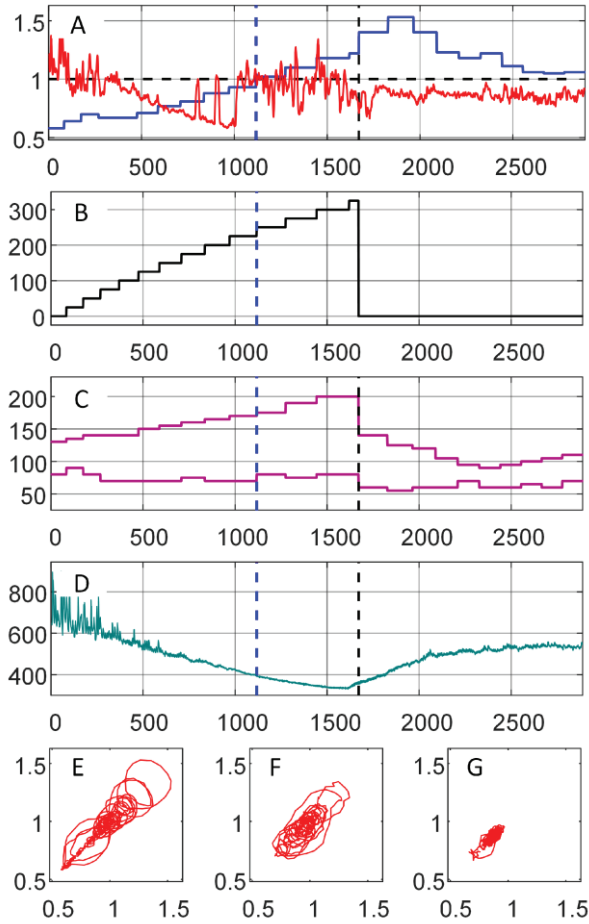


Fig. 10. Visualization of the transit through the AnT for person 1

Part (A): the red solid line illustrates the relationship between RR and DQRS cardiac intervals; the blue solid line, the ratio between CO₂ and O₂ in the exhaled air (the horizontal dashed black line marks when this ratio is equal to 1). Part (B): the black solid line shows the load during the cycle ergometry exercise. Part (C): the pink solid lines show the variation of the systolic and diastolic blood pressures during the exercise. Part (D): the cyan solid line shows the variation of the RR interval during the exercise. Vertical dashed blue lines mark the AnT threshold; vertical dashed black lines, the termination of the exercise in parts (A), (B), (C) and (D). The horizontal axes in parts (A)–(D) stand for the consecutive number of the heartbeat. The reconstructed attractor in the time interval from the beginning of the measurement until the AnT is shown in part (E); from the AnT until the termination of the exercise, in part (F); from the termination of the exercise until the end of measurement, in part (G).

The vertical dashed black line shows the exercise termination moment, and the systolic and diastolic blood pressures are shown in Fig. 10 C.

Figure 10A depicts the oxygen-to-carbon dioxide ratio in the exhaled air during the cycle ergometry exercise and recovery process (the blue solid line). A vertical dashed blue line denotes the anaerobic threshold (when the ratio of oxygen to carbon dioxide in exhaled air equals to one).

The thin solid red line in Fig. 10A represents the algebraic link between the RR and DQRS intervals. It is important to highlight that the collapse of complexity depicted by this connection occurs at the anaerobic threshold, not at the end of the cycle ergometry test (Ziaukas et al., 2017). The cardiac system begins to seek a new stable state before the anaerobic threshold (notice multiple intermittent peaks in Fig. 10A), but the transition is too early, and the system returns to the progressive collapse of the complexity regime. However, just before the anaerobic threshold, the relationship between RR and DQRS changes completely (Fig. 10A). The necessity to generate a new pattern of cardiac system self-organization that opens up new functional possibilities under increasing physical strain explains this change. The cardiac system continues to operate in this new state during the rest and recovery periods of the workout.

The cardiac system's approach to the collapse of the complexity before the anaerobic threshold is depicted in the phase-plot diagram in Fig. 10E. A two-dimensional embedding strategy with a near-optimal time delay is used to reconstruct the attractor (Ziaukas et al., 2017). The attractor in Fig. 10E was displayed by using the time signal's observation window (the relationship between RR and DQRS), which encompasses the period from the start of the experiment to the anaerobic threshold.

In the time interval between the anaerobic threshold and the termination moment of the cycle ergometry workout, the attractor in Fig. 10F is recreated. Finally, in Fig. 10G, the attractor depicts the time period between the end of the ergometry exercise and the end of the measurement.

The geometric shape of the attractor in Fig. 10E indicates a steady decrease in the cardiac system complexity followed by a wandering process to a new state. The attractor in Fig. 10F depicts the shifting dynamics of the cardiac system in the new post-anaerobic state. The recovery process is represented by the attractor in Fig. 10G.

The participant was able to complete the cycle ergometry exercise without difficulty, as evidenced by the fluctuation in systolic and diastolic pressures throughout and after the activity (Fig. 10C). The diastolic blood pressure dropped at the onset of the physical strain and did not climb above it until the ergometry exercise was finished. The systolic blood pressure raised steadily during the ergometry workout, but it did not reach 200 mmHg at the end. After the exercise, both systolic and diastolic pressures decreased and then were restored to the normal throughout the recovery time.

The growth of the direct relationships between RR and DQRS intervals at this stage of cycle ergometry exercise is signaled by the movement of the algebraic relationship between RR and DQRS intervals towards the collapse of complexity right before the anaerobic threshold. The cardiac system's efforts to reorganize as a new mode of action are illustrated by the fluctuation of these connections before the anaerobic threshold. This form of self-reorganization reveals that the cardiac system's

regulatory activities are physically executed not just through the ability to change the heart rate, but the ability to restructure the heart's internal processes (by changing the DQRS interval) as well.

Experiment 2

Figure 11 shows the results of the second person. This person's systolic blood pressure was already elevated at the start of the experiment (150 mmHg). The drift towards the complexity collapse is very rapid; it was already over by the end of the second minute (Fig. 11A). The system then fluctuates about the temporarily stabilized attractor until it reaches the AnT (Fig. 11E). After the threshold is reached, the system begins to look for a way to reorganize into a different mode of operation (Fig. 11A); however, increasing systolic and diastolic pressures does not allow the cardiac system to converge towards the new attractor. Only when the load has been removed, and the systolic and diastolic pressures have decreased, the cardiac system shift to the new attractor appears. Nevertheless, because the recovery processes are already underway, the new attractor becomes unstable, and the system reverts to its original condition (Fig. 11G).

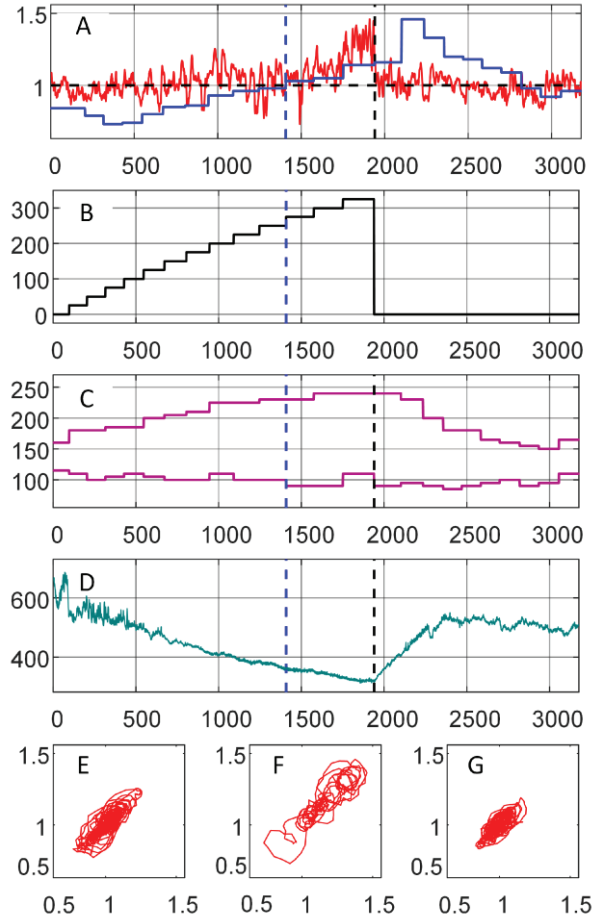


Fig. 11. Visualization of the transit through the AnT for person 2; all lines in all parts have the same notions as in Fig. 10

Experiment 3

The third person had a hypertonic state at the start of the experiment (systolic blood pressure is 160 mmHg) as well as a hypertensive reaction to the load (Fig. 12).

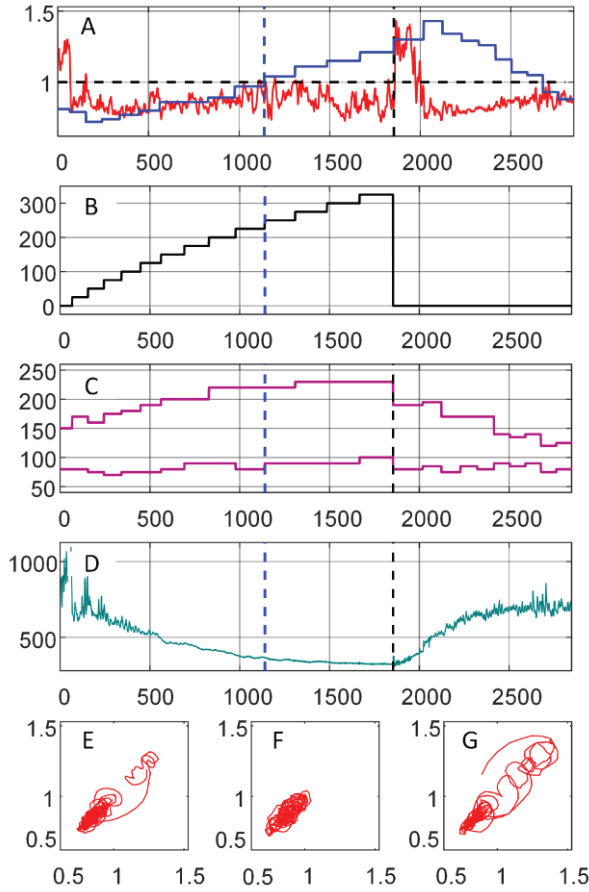


Fig. 12. Visualization of the transit through the AnT for person 3; all lines in all parts have the same notions as in Fig. 10

During the cycle ergometry exercise, the algebraic relationship between RR and DQRS cardiac intervals can be used to show the transition through the AnT. Furthermore, it appears that the transition via the AnT is far from straightforward, and it varies depending on a person's physiological characteristics.

It has been found that the algebraic relationship between RR and DQRS cardiac intervals can be used to characterize the heart system's self-organization before, during, and after the load. This relationship depicts the cardiac system's ability to transition to the different state after crossing the AnT threshold. The proposed visualization technique stands in stark contrast to the existing available methods for identifying the AnT, which is based on the O_2/CO_2 ratio in the exhaled air, blood lactate concentration, or RR fluctuation during the load. In addition, the diversity in RR intervals (parts (D) in Fig. 10, 11, 12) makes it impossible to establish the AnT (or even to classify people's performance).

When comparing the RR-DQRS relationship to the RR-JT intervals relationship, the RR-DQRS relationship reveals completely different properties

(Ziaukas et al., 2017). The RR-JT connection measures the degree of self-organization of the cardiac system during the load (the collapse of complexity occurs at the end of the cycle ergometry exercise). However, the RR-DQRS relationship demonstrates the reorganization of the cardiac system into a distinct mode of operation during the AnT transit.

The final point to consider is that the presented relationship can be utilized to classify performance under stress. Furthermore, the RR-DQRS connection might be employed as a stand-alone indication for both determining the AnT threshold and characterizing the patient's performance.

The primary goal of this study was not to develop a novel biomarker. Instead, a new visualization technique was presented that might help to characterize and classify transit through the AnT threshold. The future research should focus on building pattern categorization algorithms based on the RR-DQRS relationship for the automatic analysis of transitory processes.

For the first time, a methodology has been proposed for the detection of an anaerobic threshold by using only the ECG signal that does not require any additional measurements, such as measuring the level of lactate in the blood or measuring the ratio of carbon dioxide to oxygen in the exhaled air.

The algebraic relationship between RR and DQRS cardiac intervals can be used to describe the self-organization of the cardiac system before, during, and after the transit through the anaerobic threshold.

3.2. The algorithm for the detection of ischemic heart episodes

At the early stage, the ischemic heart disease does not cause any symptoms and is usually detected only in the presence of significant disease progression.

The examination of the disease takes a long time because the examination methods, such as computed tomography or angiography, are complex and costly. Therefore, the main objective of this section is to propose a quick, convenient, and non-invasive technique capable to detect this insidious disease in its initial phase of development. This technique is based on the JT/ST algebraic relationship. This relationship is used to describe the individual response of the human body during the physical load and the recovery processes as well as to determine the early symptoms of the ischemic heart disease.

In this research, the JT/ST relationship was investigated, which has been used to characterize the individual performance during the load and recovery cycles and identify the ischemic changes in the heart.

The presented research was complied with all ethical guidelines for the experimentation. Kaunas Regional Ethics Committee for Biomedical Investigations, No. BE-2-51, approved the permit to conduct biomedical investigations on December 23, 2015. The heart intervals and their properties were recorded by using the ECG stress test on a cycle ergometer. The system “Kaunas-Load” (Vainoras et al., 1996) that was developed at the Institute of Cardiology (Lithuanian University of Health Sciences) was used to perform synchronous registration of 12 leads and different

standard parameters of the ECG (including the duration of JT and the amplitude of ST intervals for each cardiac cycle).

The registration of the ECG has started at the beginning of the bicycle ergometry exercise with the load set to 50W. The load was kept constant for two minutes and then increased by 50W. The person is asked to maintain a constant cycle ergometer spinning rate at 60 revolutions per minute during the whole bicycle ergometry exercise. The stress test is terminated when the person fails to maintain the spinning rate, or the first clinical indications for load limitation are observed, according to the American Heart Association.

The group consisted of ten physically active males who were not professional athletes. The average age is 41.86 years with a standard deviation of 1.80 m, a weight of 80.29 kg, and a BMI of 24.54 kg/m². Because three patients showed clinical signs of load restrictions, the load was held fixed for one minute before being increased by 50W.

Step 1

Throughout the experiment, the length of the JT interval and the ST amplitude is continuously and synchronously registered and denoted as vectors $x = (x_1, x_2, \dots, x_n)$ and $y = (y_1, y_2, \dots, y_n)$, respectively; where n is the total number of heartbeats recorded throughout the entire experiment. The algorithm introduced experiments are used to recreate the algebraic relationship between the time series x and y .

The sequence of matrices $L_{\delta,k}^{(\beta)}$ is transformed into a scalar sequence by using a mapping $\mathcal{F}: \mathbb{R}^{2 \times 2} \rightarrow \mathbb{R}^1$, where $\beta \in \{1, 2, \dots, 18\}$. The mapping \mathcal{F} is defined as the maximal modulus of the two eigenvalues of $L_{\delta,k}^{(\beta)}$ in Ziaukas et al. (2017) and Saunoriene et al. (2019). The mapping is generalized by setting $\mathcal{F} = \|L_{\delta,k}^{(\beta)}\|$ in this research. The norm of the matrix $\|A\| = \sup_{z \in \mathbb{R}^2} \left(\frac{\|Az\|_2}{\|z\|_2} \right) = \sup_{z, \|z\|_2=1} (\|Az\|_2) \geq \max(|\lambda_1|, |\lambda_2|)$ where λ_1 and λ_2 are two eigenvalues of A and 2-norm is the Euclidian norm (Saunoriene et al., 2019). It should be noted that the inequality becomes equality when the matrix A is symmetric. Therefore, the sensitivity of the method was increased by replacing the maximal modulus of the eigenvalues by the norm in the definition of the mapping.

Lastly, the scalar sequence is smoothed internally and externally $\|L_{\delta,k}^{(\beta)}\|$. If the internal smoothing radius is R_i and the external smoothing radius is R_e , then the smoothed sequence depicting the algebraic relationship between time series x and y reads as follows:

$$s_k(R_i, R_e, \beta) = \frac{1}{R_i(2R_e+1)} \sum_{j=k-R_e}^{k+R_e} \sum_{\delta=1}^{R_i} \|L_{\delta,j}^{(\beta)}\|; \quad (45)$$

where $k = (1 + R_i + R_e), (2 + R_i + R_e), \dots, (n - R_i - R_e)$. The optimization problem in respect of the smoothing parameters is formulated in the experiment above for the whole cohort of persons resulting into $R_i = 3, R_e = 4$ and $\beta = 1$. These values

of the parameters are kept fixed as well. All further numerical computations are based on $s_k(3,4,1)$.

The hypothesis was raised that two consecutive declines in algebraic relationships between the duration of the JT interval and the ST amplitude during the bicycle ergometry exercise can be used for the early detection of episodes of ischemic heart disease.

The following algorithm is proposed in order to quantitatively describe two consecutive declines.

The determination of the average value of the algebraic relationship between the duration of the JT interval and the ST amplitude in the observation window centered around the termination of the ergometry exercise moment. The averaging is required to minimize the local effects induced by the inevitable additive noise. The recommendation is to use observation windows with the averaging radius of 3-time steps around the termination moment:

$$\bar{S} = \frac{1}{7} [s_T(3,4,1) + \sum_{j=1}^3 (s_{T-j}(3,4,1) + s_{T+1}(3,4,1))] . \quad (46)$$

Step 2

The upper boundary at \bar{S} should be fixed, and the areas below \bar{S} and the JT/ST algebraic relationship should be marked separately for the load and recovery processes in different colors.

The dynamics of the JT/ST relationship throughout the load and recovery phases are illustrated and discussed for seven healthy persons and three persons with suspected ischemic heart disease. A few examples of the results will be shown.

Person 1

The total area of the algebraic relationship function under \bar{S} during the load is marked in red in Figure 13A. The total area of the algebraic relationship function under \bar{S} during the recovery process is marked in blue in Figure 13A. It should be noted that the thick black vertical line represents the end of the load (and the start of the recovery process), and the thin black dashed horizontal line represents the numerical value of \bar{S} in Figure 13A.

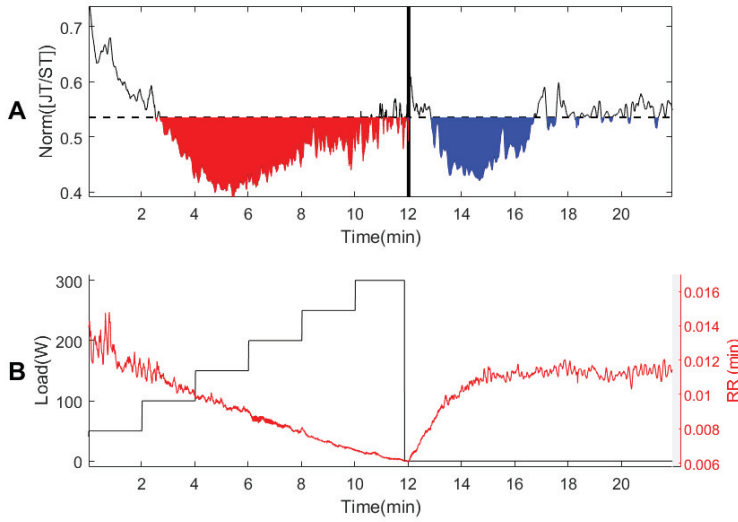


Fig. 13. The dynamics of the JT/ST relationship during the load and the recovery processes for person 1; the x-axis in parts (A, B) represents the time (measured in minutes) from the beginning of the cycle ergometry exercise; the left y-axis in part (B) represents the power of the load in Watts; the right y-axis in part (B) represents the variation of the RR interval in min; the algebraic JT/ST relationship is represented by the thin dashed black line in part A; the thick black solid vertical line in part A marks the end of the load

The algebraic JT/ST relationship reveals interesting dynamic behavior during the load and recovery processes (Figure 13). It has been shown in Ziaukas et al. (2017) that the collapse of complexity occurs in the algebraic relationship between RR/JT intervals at the end of the load process. However, the situation is completely different now. The JT/ST relationship drops down and reaches the first minimum much earlier than the end of the load process (Figure 13A). After reaching the first minimum, the JT/ST relationship starts rising until the end of the load process. The JT/ST relationships start decreasing again, reach the second minimum, and continue to grow during the recovery process (Figure 13A).

It can be observed that the variability of the JT/ST relationship grows before the termination of the load. Similar growth of low-frequency fluctuations before the end of the exercise is observed in RR/QRS relationship (Saunoriene et al., 2019) and a quasi-isometric arm-curl exercise (Vázquez et al., 2016). However, the behavior of the JT/ST relationship is completely different if compared to the RR/JT or RR/QRS relationships. The JT/ST relationship becomes more fluctuated and grows to a local maximum at the end of the exercise and thus forms the first pit during the load process (marked in red in Figure 13A).

The second pit is formed during the recovery process (marked in blue in Figure 13A). Such a different behavior of the JT/ST relationship, compared to the other

relationships, can be explained by the fact that the JT and ST intervals represent completely different aspects of the self-organization of the cardiovascular system.

Healthy persons

In order to examine and analyze the transient behavior of the cardiovascular system and its self-organization during the load and recovery processes of the bicycle ergometry exercise, a series of tests with other people were performed.

The dynamics of the JT/ST relationship during the load and recovery processes for person 2 are depicted in Figure 14. It can be observed that the global minimum in the first pit is reached a little later for person 2, compared to person 1. However, the fluctuations before the termination of the load are as well higher for person 2. The recovery process can be characterized as well by much more violent fluctuations (Figure 14A). It is assumed that the self-organization of the cardiovascular system of person 2 is much more complex if compared to person 1. This complexity can be characterized by higher fluctuations and a less stable recovery process. Yet, the red and the blue pits are visible in Figure 14A. Indeed, all persons are individual, and one should not expect to reproduce identical transient trajectories of the JT/ST dynamics for different persons. The physical endurance of person 1 is better than person 2. Both persons did terminate the exercise at 300 W load, but person 1 managed to last almost 14 min (person 2 lasted less than 13 min).

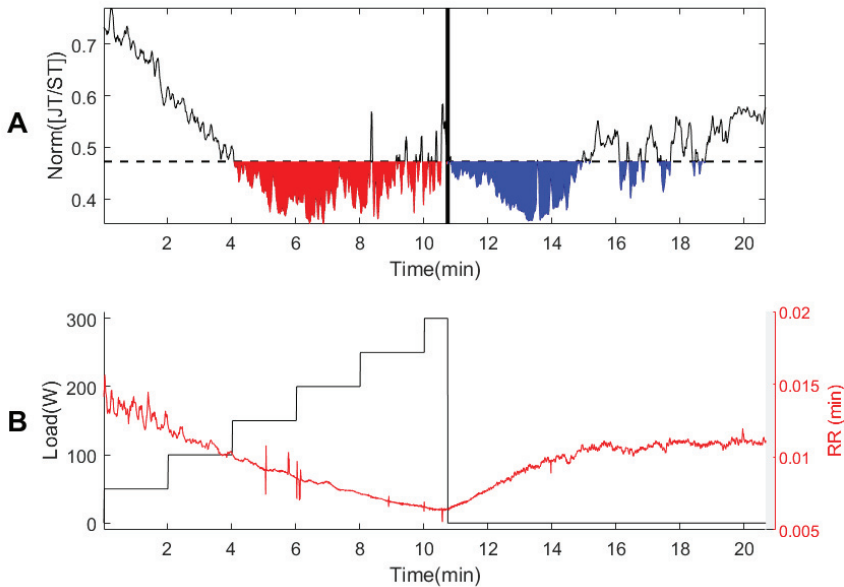


Fig. 14. The dynamics of the JT/ST relationship during the load and the recovery processes for person 2; all lines in all parts have the same notions as in Fig. 13

The dynamics of the JT/ST relationship during the load and the recovery processes for person 3 are depicted in Figure 15. Firstly, it can be observed that person 3 did manage to reach only 250 W maximum load, and the bicycle ergometry exercise

did last for only almost 11 min. Additionally, though both pits (the red and the blue one) are visible in Fig. 15A, the fluctuations before the load termination moment and the complexity of the transient process after the global minimum of the second pit are much higher if compared to person 2 (and person 1, of course). This is a clear indication that the ability of the cardiovascular system of the person 3 to adapt to the load and recover after the load is less pronounced, compared to the other subjects.

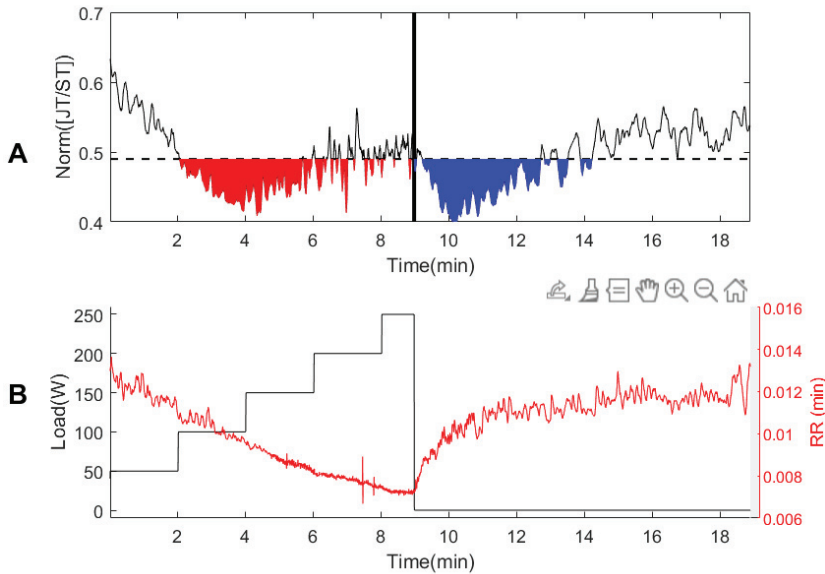


Fig. 15. The dynamics of the JT/ST relationship during the load and the recovery processes for person 3; all lines in all parts have the same notions as in Fig. 13

Persons with suspected ischemic heart disease

The results of bicycle ergometry experiments with healthy persons demonstrate that the double consecutive decline of the JT/ST relationship (the red and the blue pits) can be used for subtle characterization of the self-organization of the cardiovascular system during the load and the recovery processes. It is interesting to observe if similar patterns could be observed in the JT/ST relationship for persons having different suspected ischemic heart disease conditions.

Person 4 had ischemic effects on the myocardium and could continue the exercise for less than 4 min (Figure 16). The first pit during the load did not have enough time to develop (Figure 16A). The blue pit during the recovery process is missing completely. The trajectory of the JT/ST relationship during the recovery process reminds a wandering chaotic process. The ability of the cardiovascular system to self-organize during the recovery process is impaired.

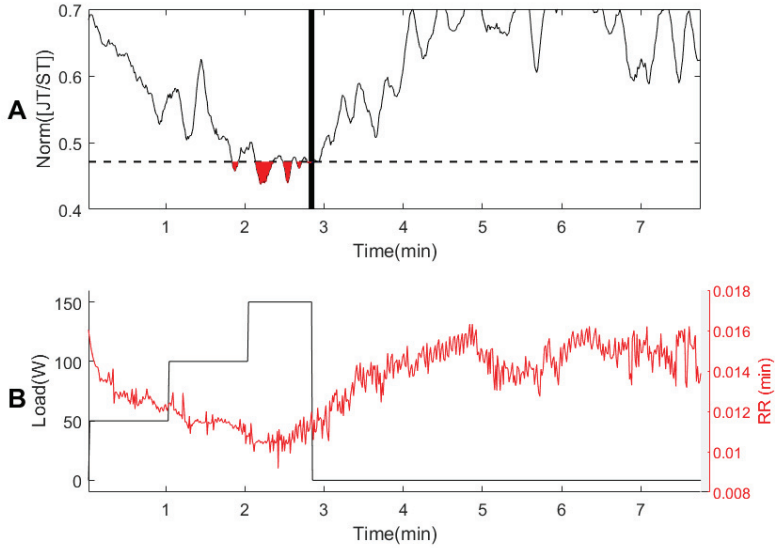


Fig. 16. The dynamics of the JT/ST relationship during the load and the recovery processes for person 4; all lines in all parts have the same notions as in Fig. 13

Similar results are observed in Figure 17. Person 5 managed to reach only 100 W load. The red and the blue pits are completely missing. However, the recovery process for person 5 looks better, compared to person 4. The JT/ST relationship quickly returns and then starts wandering around the initial state (Figure 17A). Person 5 had ischemic changes in the heart. The supply of oxygen to the heart becomes deficient soon after the beginning of the physical exercise.

The dynamics of the JT/ST relationship for person 6 are depicted in Figure 18. The maximal load is 250 W; however, this load is only reached in around 5 min (Figure 18B). Clearly expressed pits are not formed during the load or recovery processes.

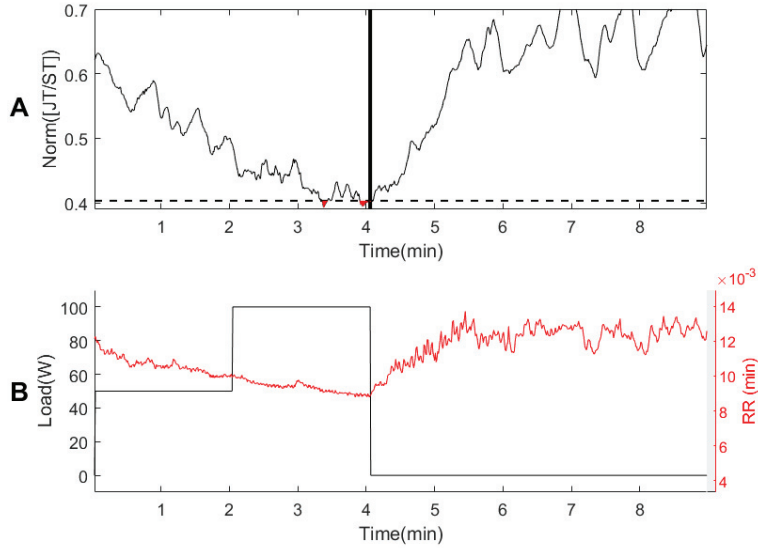


Fig. 17. The dynamics of the JT/ST relationship during the load and the recovery processes for person 5; the x -axis in parts (A, B) represents the time (measured in minutes) from the beginning of the cycle ergometry exercise; the left y -axis in part (B) represents the power of the load in Watts; the right y -axis in part (B) represents the variation of the RR interval in min; the algebraic JT/ST relationship is represented by the thin dashed black line in part A; the thick black solid vertical line in part A marks the end of the load

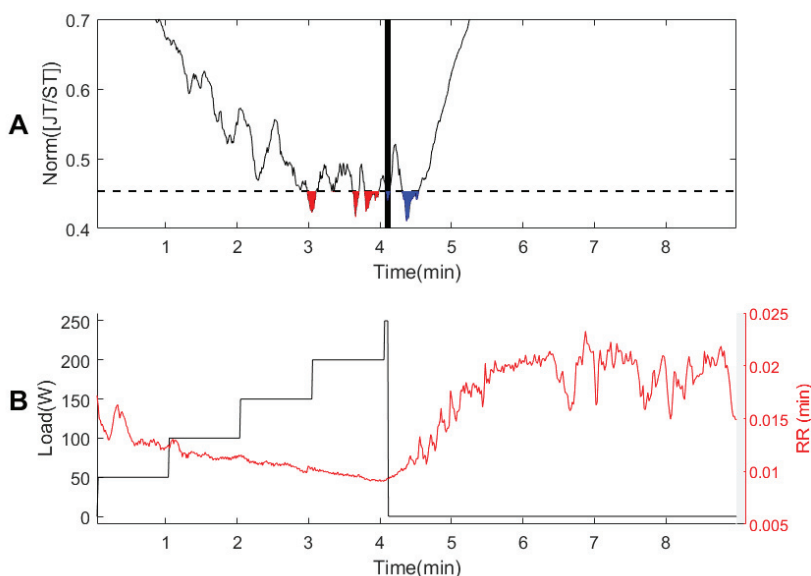


Fig. 18. The dynamics of the JT/ST relationship during the load and the recovery processes for person 6; all lines in all parts have the same notions as in Fig. 13

The depression of the amplitude of the ST segment during the stress exercise is a traditional biomarker for the diagnosis of coronary heart disease (CHD). However, the prognostic efficacy of this metric has yet to be properly examined and compared to more traditional exercise ECG features such as basic end-exercise ST-segment depression, heart rate-adjusted ST/HR index (Detrano, 1986; Kligfield et al., 1987), and ST/HR slope (Elamin et al., 1980; Kligfield et al., 1989). Because ST-segment depression/heart rate (ST/HR) hysteresis and cardiopulmonary exercise test-derived parameters have limited diagnostic definition at exercise electrocardiography (ECG), they have been offered as alternatives for the diagnosis of myocardial ischemia caused by the exercise (Lehtinen et al., 1999).

Other activities, such as ECG variables based on the combined ST/HR data, taken during the exercise and recovery phases (the so-called stress recovery index) (Bigi, 1994), have recently been shown to include predictive information (Bigi et al., 2005; Bigi et al., 2007). The ST/HR hysteresis provides for a recovery phase as well, but it is less sensitive to the maximum heart rate during the workout. In order to obtain more precise information on an individual patient's exercise ability, metabolic equivalents and oxygen consumption should be thoroughly examined (Svart et al., 2010).

The possible transit through the anaerobic threshold could be a factor affecting the JT/ST relationship. As a result, Figures 13B–18B show the fluctuation of the RR interval (inter-beat interval) during the load and recovery phases for all patients. The anaerobic threshold correlates to a deflection point in the heart rate during the exercise, according to Conconi et al. (1982) and Ballarin et al. (1989). However, the

RR interval reaches a sharp minimum at the load termination moment. Therefore, it can be concluded that the anaerobic threshold does not play a role of a causal factor that influences the formation of two consecutive declines in the JT/ST algebraic relationship.

Every assessed parameter reflects only specific physiological information of the human body. It can be assumed that all circuits of the organ control systems that have been activated during the load do return to the baseline levels during the recovery process (for healthy people). The minimum level of the JT/ST relationship was in the range between 0.3 and 0.5 for all observed persons. It is assumed that when the human organism reaches this limit, it can no longer fall below this range, and then the reorganization of the cardiovascular system takes place. There are two possible options during the repolarization process: the compensatory mechanisms are turned on for the healthy persons or are completely imbalanced for the persons with ischemic heart disease.

A new algorithm capable to detect the early onset of ischemic episodes is introduced in this section. A very important feature of this algorithm is that it is exclusively based only on the ECG signal analysis. The new approach provides valuable clinical information on the efficiency of the individual metabolism in respect to the JT/ST algebraic relationship during the load and the recovery processes.

3.3. Synchronization of human heart rhythms with the Earth's time-varying magnetic field

It is well known that Schuman resonances of the local Earth's magnetic field do coincide with the characteristic frequencies of the human brain activity waves (McCraty et al., 2018). The main objective of this section is to demonstrate that a direct relationship between the local Earth's magnetic field and the human cardiovascular system does exist. Moreover, these relationships do have a long-term impact on the human health. Moreover, it is well known that the human brain has a tight connection with the heart's activity. This section raises a hypothesis that the local Earth's magnetic field is synchronized and affects the rhythm of the human heart.

Field-line resonances have been linked to the improvements in cardiovascular function in many studies (Doronin et al., 1998; Khabarova et al., 2009; McCraty et al., 2017; Zenchenko et al., 2014). According to the studies, the changes in the amplitude of resonant frequencies generated by geomagnetic field-line and Schumann resonances can synchronize human autonomic nervous system activity expressed in the heart rate variability (HRV) over longer time periods.

The groups have been gathered from five nations separated by a large geographical distance to see if HRV synchronization to field-line resonances happens globally and if various field-line resonant frequencies exist in different regions for this study. A newly designed and tested strategy using near-optimal chaotic attractor embedding techniques was employed to improve the assessment of physiological synchronization and classify individual response patterns (Timofejeva et al., 2017). As a result, the author of the dissertation was able to identify specific patterns of synchronization between HRV and local magnetic field behavior as well as assess the

impact of HRV coherence on synchronization with each other and the earth's magnetic field in a range of groups of people from across the world. The data signal may be applied to reconstruct the underlying chaotic dynamical system that corresponds to the observed phenomena, which is the essential notion behind this technique (for example, heart rate variability or local magnetic field spectral power, etc.). For the reconstruction to be meaningful and maintain the attributes of the underlying dynamical system, the ideal reconstruction parameters must be specified. By comparing specific ideal parameters related to two data signals, the synchronization between two data signals can be measured.

In total, 104 people from California, Lithuania, Saudi Arabia, New Zealand, and England took part in the study for 15 days between February 26 and March 13, 2015. The magnetometers of the Global Coherence Monitoring Network (McCraty et al., 2015) are in those countries; thus, their selection was based on their geographic locations. The majority of participants were healthy and went to work or university during the day. The Lithuanian group consisted of twenty medical students from Lithuania's Lithuanian University of Health Sciences. The group from California consisted of 20 employees, 16 of whom worked for the HeartMath Institute (HMI) in Boulder Creek, California, and were split between two offices, about 5 miles apart. Two of these workers, one in a neighboring town and the other in the southern California, worked and lived remotely. The remaining four people were local acquaintances. The New Zealand party, which was based in Aotearoa, consisted of 22 people from various cultural backgrounds and roots. The Embassy of Peace was established by eleven members of the Freedom Farms workers. The remaining eleven participants were linked to the organization, and all of the group members were said to have long-standing and meaningful relationships with one another. The Saudi Arabian contingent consisted of 20 medical students from King Faisal University's college of medicine. Seven business leaders from England worked in a shared office space. The remaining seven were people known to the study coordinator who had an interest in HeartMath and personal, social, and global coherence and lived in various parts of the UK. The subjects were enrolled, the logistics were planned, and the participants were trained in study methods and the use of the HRV recorders by a local site coordinator in each location. Even though the research coordinators in each of the five nations recruited a total of 104 volunteers, one individual did not return their HRV recorder after the study.

Data collection on HRV

HRV is a non-invasive test that exposes the dynamic activity of a person's autonomic nervous system (Shaffer et al., 2014). The participants had 24-hour ambulatory HRV recordings taken every day for two weeks, from February 26 to March 12, 2015. At the start of the trial, the site coordinator informed each participant on how to attach, start, and stop the HRV recorders (Bodyguard2, Firstbeat Technologies Ltd., Jyväskylä, Finland), who retrieved the data from the HRV recorders and submitted it to the FTP data collecting site.

The participants were as well given instructions for recording everyday activities such as sleep and waking periods, among other things. After being told how to halt the HRV recorder after waking, they were given up to an hour to bathe before restarting it. In a modified V5 position, Ambu Blue Sensor L microporous disposable electrodes were used. The participants were encouraged to place the electrodes in three separate spots near the V5 position to reduce skating. At a sample rate of 1000 Hz, the HRV recorder calculated the inter-beat-interval (IBI) from the electrocardiogram. The RR intervals were kept in the HRV recorder's memory, which was then uploaded to the study's FTP site at the study's conclusion.

DADiSP 6.7 was used to evaluate the HRV data after it was downloaded to a workstation. The analysis excluded IBIs that were less than or equal to 30% of the mean of the previous four periods. Following the automated editing process, an experienced technician personally examined and corrected all recordings as needed. According to HRV Task Force (Novak et al., 1997) recommendations, all HRV recordings were separated into 5-minute segments. The analysis was excluded from any 5-minute segment that had more than 10% of the IBIs eliminated or absent. The local time stamps in the HRV recordings were transferred to Coordinated Universal Time to guarantee the synchronization between the participants in different locations and with the magnetic field data (UTC).

Due to the participants' different time zones, HRV data was collected over 15 days to obtain 14 full days of data. To sum up, 95 percent (30,621 h.) of the predicted 32,256 h of recording (96 participants, 14 days, 24 h) were accessible after accounting for the missing recordings, data clearing, and editing.

Data of magnetic field

Magnetometers (Zonge Engineering ANT-4) were used to collect data on the local magnetic field intensity at five locations: Lithuania, Boulder Creek, CA, USA, Saudi Arabia's eastern province, and New Zealand's north island. The Global Coherence Monitoring Network (McCraty et al., 2015) includes all of that equipment. Each location has two magnetometers positioned in the north-south and east-west axis to detect time-varying magnetic field strengths (sensitivity 1 pT) throughout a large frequency range (0.01–300 Hz) with flat frequency response. Each magnetometer has a sampling rate of 130 Hz. The magnetic field intensity data is captured by data acquisition equipment, which is then stamped with the global positioning system time and transferred to a common server. The participant groups are not far separated (up to several hundreds of kilometers) from the magnetometer installation sites, as previously indicated.

Heart lock-in procedure

On March 5, each group met in person at their respective sites for a 15-minute Heart Lock-In (HLI) session (McCraty et al., 2018). A group Skype call was put up to help the groups feel more connected to each other. The HLI approach's steps were read aloud over the computer speakers that everyone in the room could hear them.

The HLI approach aims to increase one's ability to sustain heartfelt happy emotions (McCraty et al., 2006). According to McCraty et al., these are the steps of HLI:

“Step 1: Concentrate on the heart area. Imagine your breath going in and out of your chest or heart, a little slower and deeper than normal.

Step 2: Initiate and maintain a regenerative emotion like gratitude, care, or compassion.

Step 3: Share that revitalizing sensation with others” (McCraty et al., 2006).

This technique is generally associated with the feelings of calm, harmony, and inner warmth and has been proved to be a dependable approach to boosting heart rhythm coherence (McCraty et al., 2006). It is as well an excellent way to diffuse the collected stress and unpleasant feelings.

Computation of the power of the local magnetic field

The key parts of the method were to compute the magnetic field intensity spectrogram for successive one-second time intervals, determine a spectrum amplitude and the total spectral power values in the frequency band between 0.2 and 3.5 Hz, which were previously described as the ultra-low frequency (ULF) power (Timofejeva et al., 2017; McCraty et al., 2017; Alabdulgader et al., 2018).

After that, a Hampel filter was employed to remove the transit noise caused by lightning, human-made sources, and other factors from the magnetic field spectral power time series at each site (Hampel et al., 1971). This function substitutes a value in a data window with the median if it deviates from it by more than three standard deviations. The optimal size of the data window for the Hampel filter was determined by using the formula below: Local magnetic field spectral power time series were filtered by using data windows varying in size from 2 to 24 hours.

Participants HRV and Earth's magnetic field synchronization

The degree of synchronization between group HRV and local magnetic field spectral power was determined by using techniques that were published and validated by Timofejeva et al. (2017). The presence of such a mapping that permits data signals to be reduced to a single integer that defines the dynamical characteristics of the investigated series from a geometrical perspective is the central idea of the methodology. The integer is the time lag that optimizes the reconstructed attractor's area from the processed signal. The technique labeled as Algorithm C in Timofejeva et al. (2017) was adjusted to provide a single scalar value matching to the synchronization between the assessed data signals. The short outline of the modified method is presented below.

Two synchronously sampled data series could be taken as an example: $RR = (RR_1, \dots, RR_n)$ and $M = (M_1, \dots, M_n)$, proportional to the spectral power of the participant's HRV (RR) and local magnetic field (M).

- The RR and M data signals are separated into T 5-min observation windows (per HRV analysis guidelines) (Novak, 1997), and suitable time lag values for the HRV time series are constructed for each observation window

$(\tau_*^{(RR)} = (\tau_{*1}^{(RR)}, \dots, (\tau_{*T}^{(RR)}))$ and magnetic field spectral power data signal $(\tau_*^{(M)} = (\tau_{*1}^{(M)}, \dots, (\tau_{*T}^{(M)}))$. This approach describes the dynamical and geometrical features of RR and M data series by mapping them to the integer vectors. $(\bar{\tau}_*^{(RR)})$.

- In order to find the averaged changes in time delays for $HRV(\bar{\tau}_*^{(RR)})$ and magnetic field data $(\bar{\tau}_*^{(M)})$, the obtained ideal time lag vectors are smoothed by using a moving average algorithm. The moving average is calculated by using a 20-data-point observation window.
- Pearson correlation coefficient $C^{RR,M} = \rho(\bar{\tau}_*^{(RR)}, \bar{\tau}_*^{(M)})$ is calculated by using the optimal time lag vectors that have been averaged. The resultant value $C^{RR,M}$ denotes the degree of synchronization between the analyzed HRV and magnetic field spectral power signals. Naturally, a higher $C^{RR,M}$ value indicates a greater degree of synchronization and vice versa ($C^{RR,M} \in [-1,1]$). It is worth noting that the assumption of normality of the data series employed in subsequent analyses was confirmed.

Let $RR^{(k)} = RR_1^{(k)}, \dots, RR_n^{(k)}$, $k = 1, \dots, K$ is set of HRV data signals, where $RR^{(k)}$ corresponds to k -th participant from one of the considered countries. The mean correlation coefficient $C^{(RR^{(1,\dots,K)},M)} = \frac{1}{K} \sum_{k=1}^K C^{(RR^{(k)},M)}$ is used to calculate the mean synchronization between each group's HRV and respective magnetic field spectral power signal.

Statistical analysis

In order to assess the statistical significance of the acquired results, the following statistical tests are performed in the subsequent study:

- The Pearson correlation significance test is used to examine the statistical significance of the synchronization between the participant's HRV and the Earth's magnetic field obtained by using the approach mentioned in the preceding subsection (Null Hypothesis $H_0: C^{(RR^{(1,\dots,K)},M)} = 0$).
- Using the Repeated Measures design, multiple measurements of the same variable are obtained on the same participants in different contexts or at two or more times. The assumption of sphericity was tested by using Mauchly's Test of Sphericity, and any breaches were noted in the result tables along with their remedial technique. The Bonferroni test was employed to adjust the observed significance level for the fact that multiple comparisons were done when the post hoc multiple comparison tests were utilized. The researchers utilized a Repeated Measures ANOVA to look at changes in the mean LMF-HRV correlations over time in this investigation. It was used as well to see if there were any differences in the HRV coherence and heart rhythm synchronization before, during, and after the Heart Lock-In technique was practiced.

Synchronization of HRV and local magnetic field power between participants

Because the local magnetic field power varied by nation, the methodologies for assessing synchronization between participants HRV and LMF power time series were developed separately for each site. Since the HLI took place for a 15-minute period at 5:00 p.m. (UTC) on 5th of March in 2015, the participants LMF-HRV synchronization was calculated throughout 11 days between 28 February and 11 March. In this study, a "day" is defined as a 24-hour period that starts at 5:00 p.m., the time of the Global Heart Lock-In. This allowed researchers to evaluate the synchronization of individuals HRV and magnetic field activity on the HLI day to the days before and after the HLI.

A repeated measure analysis of variance was used to examine the statistical significance of the differences in the LMF-HRV correlations. ANOVA looks at the mean difference between the subjects throughout the experiment's ten days (February 28–March 11).

The LMF-HRV correlation coefficients were evaluated for all participants throughout the 11-day research to determine if they vary by location, knowing that the LMF varied by region. Using Repeated Measures ANOVA, significant differences between participants in the five separate location groups were identified across the 11-day study period (Day * Location, $p < 0.001$). Partial η^2 (Partial Eta Squared) is one of the characteristics that is the most commonly calculated using ANOVA. It helps to answer the question how the value of a measured variable depends on the conditions under which it was measured (i.e., what effect does the factor has on the dependent variables compared to the random error). As a result of this discovery, the initial goal to assess all participants as a single group became unsuitable and was dropped.

Then, for each of the groups at each location, the repeated measures ANOVA were ran independently. Table 2 shows that there were significant differences in the mean LMF-HRV-correlations between days for each group.

In order to investigate the differences in LMF-HRV correlation, the ANOVA test was performed separately for each group at each site. In Table 3, one can see that the mean LMF-HRV-correlation for each group varies dramatically between days.

Table 2. The results of repeated measures

	<i>N</i>	Mean Sq.	df	F	$p <$	Partial η^2
California	17	0.50	10	8.46	0.001	0.35
Lithuania	19	0.44	10	9.26	0.001	0.34
New Zealand	21	0.40	10	6.22	0.001	0.24
Saudi Arabia	19	0.18	10	2.62	0.01	0.13
The United Kingdom	11	0.18	10	2.88	0.01	0.22

The statistical significance of the mean synchronization between participants HRV and LMF activity was determined by using the Pearson correlation significance

test. Table 3 displays the outcomes of the test. On day 6 (HLI day), the mean LMF-HRV synchronization for all five groups was substantially different from zero.

Table 3. The results of the correlation coefficient statistical significance test (* $p < 0.05$, ** $p < 0.01$, *** $p < 0.001$); the mean LMF-HRV synchronization on day 6 (HLI day) for all five groups was significantly different from zero

	California Correlation <i>p-value</i>	Lithuania Correlation <i>p-value</i>	New Zealand Correlation <i>p-value</i>	Saudi Arabia Correlation <i>p-value</i>	The United Kingdom Correlation <i>p-value</i>
February 28	-0.297 0.000***	0.001 0.983	0.094 0.114	-0.114 0.054	0.042 0.481
March 1	0.056 0.342	-0.214 0.000***	-0.056 0.345	-0.033 0.574	-0.096 0.106
March 2	-0.068 0.251	-0.051 0.391	-0.092 0.120	0.017 0.769	-0.125 0.034*
March 3	0.058 0.329	-0.004 0.952	-0.056 0.348	-0.044 0.455	0.128 0.031*
March 4	-0.139 0.019*	-0.096 0.104	0.128 0.031*	0.005 0.928	0.005 0.928
March 5	0.335 0.000***	0.320 0.000***	0.366 0.000***	0.183 0.002**	0.254 0.000***
March 6	0.115 0.053	-0.074 0.212	0.075 0.205	-0.137 0.020*	0.090 0.130
March 7	-0.070 0.236	-0.201 0.001***	-0.041 0.495	-0.083 0.161	-0.184 0.002**
March 8	-0.127 0.031*	-0.146 0.013*	-0.073 0.220	0.045 0.446	-0.138 0.019*
March 9	0.017 0.771	-0.101 0.088	-0.071 0.232	0.114 0.053	0.054 0.364
March 10	0.088 0.139	0.047 0.430	-0.056 0.344	-0.043 0.469	0.086 0.148

The pattern of differences is best depicted in Figure 19. Surprisingly, the only day during the study period when all of the groups HRV was positively related to the LMF was day 6, the day of the HLI, when all of the groups HRV and LMF correlations were significantly higher.

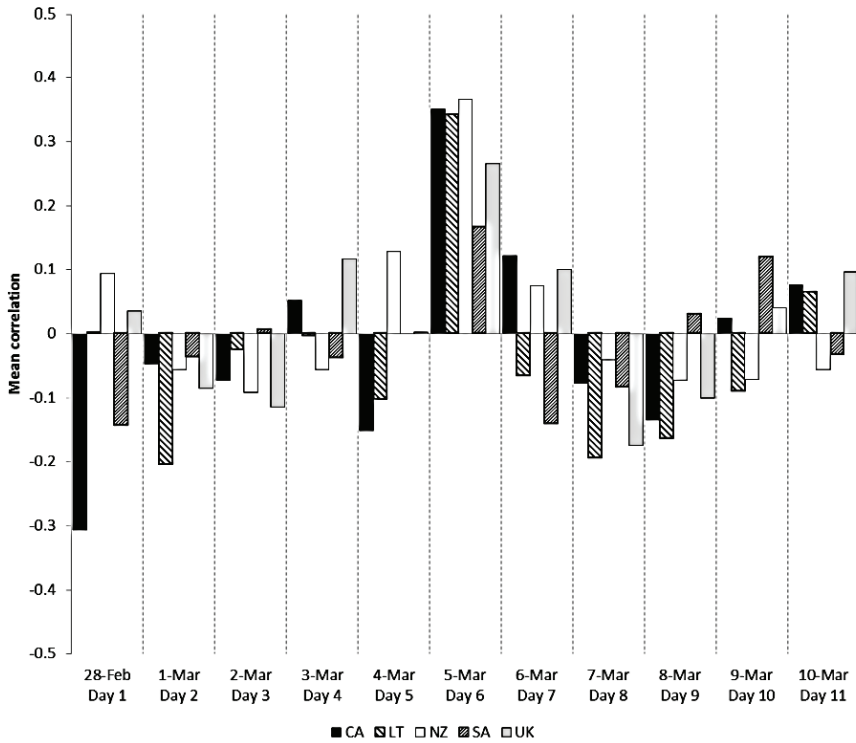


Fig. 19. LMF-HRV correlations by day and group on average (Abbreviations CA, LT, NZ, SA, and the UK correspond to California, Lithuania, New Zealand, Saudi Arabia, and the United Kingdom, respectively)

Figure 20 shows how Day 6 (HLI day) in the Lithuania group differed significantly from all other days during the study period. The eleventh day was distinct from the prior three (including day 6). In terms of significant differences across days, the California and New Zealand groups finished in second and third, respectively, the HLI day (day 6) being significantly different from six of the other days.

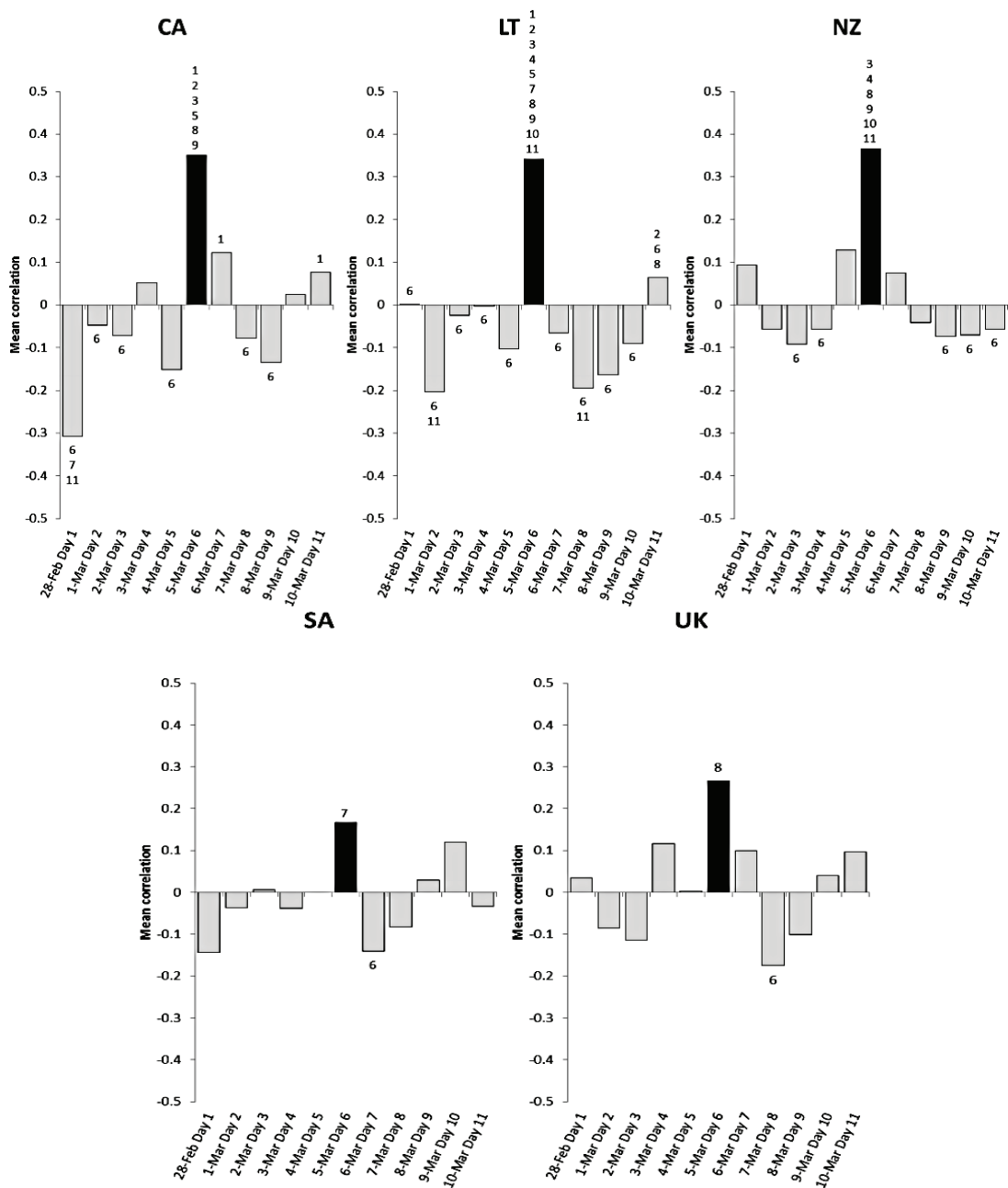


Fig. 20. Averaged LMF-HRV correlation by day and group; day 6 when all of the groups engaged in the 15-minute Heart Lock-In at the same time is represented by the dark color; pairwise importance is indicated by the day markers above each bar

The group locations were chosen to be close to the magnetic field monitoring stations that the HRV of the groups could be compared to the local magnetic fields, which varied depending on where they were. As a result, the research of synchronization between participants HRV and LMF power was done separately for each group's location. Because the worldwide HLI took place for 15 minutes at 5:00 p.m. (UTC); a "day" was defined as 24 hours commencing at 5:00 p.m. (UTC) (UTC). The daily LMF-HRV synchronization of participants was calculated during the 11-day period, which included 5 days before the HLI day, 5 days on the HLI day, and 5 days following the HLI day.

The day of the HLI was the only day where all of the groups' HRV was positively correlated with the LMF, and the synchronization between the HRV and LMF for all of the groups was significantly higher than on most of other days. Individuals with significantly different levels of sensitivity to the changes in the Earth's magnetic field have been seen, and they can react to the changes in the same environmental variable in opposing ways (Alabdulgader et al., 2015). Other environmental factors, without a doubt, influence HRV. Altitude, for example, is one of the elements that influence HRV. However, it is worth noting that all of the subjects stayed in the same geographic region for the whole 11-day experiment, ensuring that their altitude remained constant. On a longer timeline, the average daily temperature is linked to the time of the year. LMF is once again inextricably linked to the season (Alabdulgader et al., 2018). The average intensity of the solar wind received at each geographic position varies due to the slope of the Earth's rotation axis. The solar wind has an impact on the Earth's magnetic field. However, the time of year can be ignored once more as a slowly changing variable throughout the 11 days. As a result of changing local climatic conditions, the average daily temperature, humidity, air pressure, oxygen level, and lightning storms can vary. Those fluctuations are not linked across different geographic regions. On the same day, however, the greatest degree of synchronization was discovered in all geographic areas around the planet. Based on the findings of the statistical study, it can be stated that the HLI technique improves HRV and LMF coherence statistically.

Participants slower HRV rhythms on the day of the Heart Lock-In technique application can and do synchronize to the global changes in the local magnetic field, according to the findings. The participants HRV synchronization with the local magnetic field activity was measured every day for 11 days, encompassing 5 days before, the day of, and the 5 days after the 15-minute heart-focused meditation. The analysis of group members' heart rhythm synchronization revealed that all groups heart rhythms were significantly more synchronized during the meditation period, and the evaluation of participants HRV coherence before, during, and after the Heart Lock-In confirmed that most groups showed significantly increased coherence during the meditation period. The day of the meditation was the only day where all of the groups' HRV was positively linked with the local magnetic field activity, and the synchronization between the participants HRV and local magnetic field activity was significantly higher than on the other days.

Specific synchronization phenomena between HRV and the local magnetic field variation are identified and visualized in this section. The day of application of the HLI session was the only one in which the HRV of the whole group was positively correlated with the LMF, and the synchronization of the HRV and LMF in all groups was significantly higher than on the other days. Based on the findings of the statistical study, it can be argued that the HLI technique improves the coherence between the LMF and HRV.

3.4. Visualization of complex processes in the cardiovascular system during the electrical auricular vagus nerve stimulation

Researchers have long been interested in the vagus nerve activation because of its major effect on numerous bodily systems and importance in maintaining homeostasis (Yuan et al., 2016). The vagus nerve is stimulated by activating the parasympathetic nervous system to relieve the pain of various origins and localizations, increase peripheral blood flow, promote tissue regeneration benefits, etc. (Kaniusas et al., 2019). The stimulating effect is only noticeable over time when combined with other treatments. Until now, no approaches for determining the precise mechanism of action of this electrical stimulation have been established. A hypothesis that it is possible to assess this influence of the vagus nerve stimulation by analyzing only ECG parameters is raised in this section.

The vagus nerve (VN) is the longest cranial nerve in the human body, regulating several systems (Yuan et al., 2016). The vagus nerve has long been known as both an efferent nerve and an antagonist of the sympathetic nervous system. Most organs get parasympathetic and sympathetic afferents from the vagus nerve, whereas the splanchnic nerves receive sympathetic afferents. The parasympathetic nervous system, in concert with the sympathetic nervous system, controls vegetative activities by opposing each other (Olshansky et al., 2008; Browning et al., 2014). Researchers have long been interested in activating the VN to control the function of related organs due to its extensive effect on multiple systems and crucial role in maintaining homeostasis (Yuan et al., 2016).

The external ear is the only location on the body where VN transmits its lone peripheral branch. In actuality, the auricular branch of VN appears in the pinna of the ear as the afferent auricular VN (aVN), generating a cutaneous receptive field. This area responds to the environmental inputs in terms of peripheral nerve activity. In particular, aVNS, which links directly and favorably the applied stimuli to the brainstem, as shown in Figure 21B, allows for simple external access through electrical stimulation. The brainstem even delivers aVNS input to the higher brain areas via broad projections to the second and third order neurons inside the brain (Mercante et al., 2018). The auricle, particularly its aVN endings, could provide a potent direct doorway for modulating numerous brain functions, providing the most cost-effective non-invasive central nervous system manipulation. The center area of the pinna, the central concha, is primarily innervated by aVN, as illustrated in Figure 21A, whereas aVN was discovered in 100% of cases in cymba concha (Peuker, 2002).

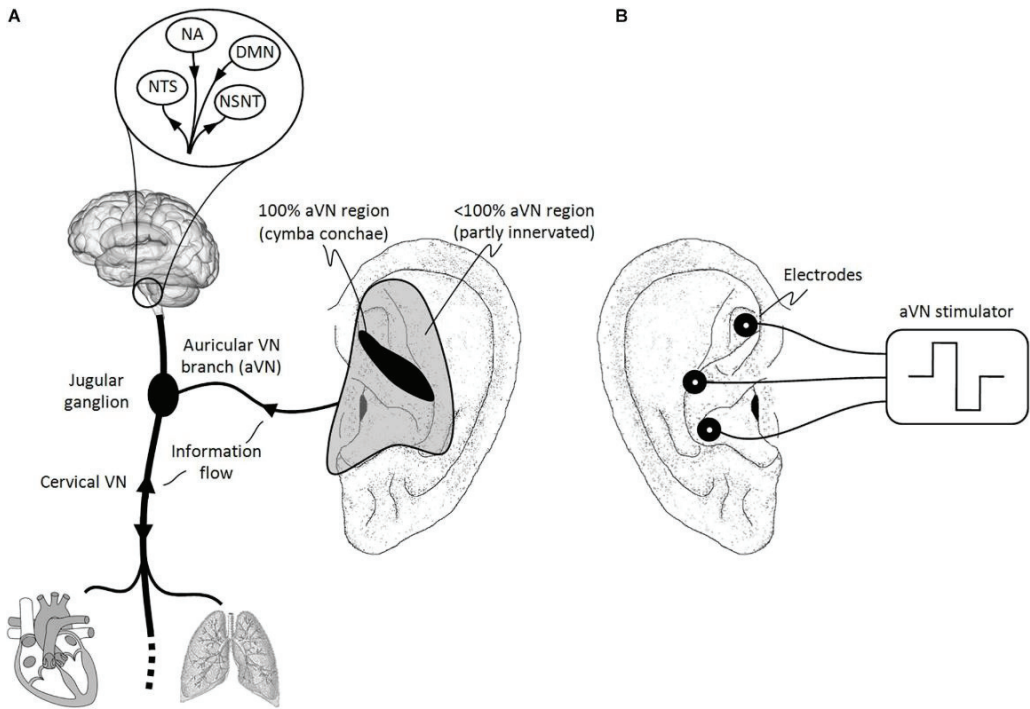


Fig. 21. The auricle's natural sensory innervation contrasts its artificial stimulation;

A) the vagus nerve (VN) connects the brain to the majority of the thoracic and abdominal organs; auricular afferent branches (aVN) emerge from the cervical VN at the level of the jugular ganglion immediately outside the cranium and innervate the pinna of the outer ear's central regions (Peuker, Filler, 2002); (B) with needle electrodes placed within these core areas, electric stimulation of aVN endings was performed; the nucleus of the solitary tract (NTS), the nucleus spinalis of the trigeminal nerve (NSNT), the nucleus ambiguus (NA), and the dorsal motor nucleus (DMN) are all acronyms for nucleus of the solitary tract; this figure and figure caption were originally published in Kaniusas et al. (2019), which was published in *Frontiers of Neuroscience* under the creative commons' attribution license CC BY 4.0

Human functional state changes as a result of vagus nerve stimulation. In terms of neuromodulation, it recruits sensory aVN fibers and simulates/projects the sensory information to the brainstem, forming the auriculo-vagal afferent pathway (He et al., 2013). Both the autonomic nervous system (ANS) and the central nervous system (CNS) are controlled by auricular vagus nerve stimulation (aVNS) because it projects directly to the nucleus of the solitary tract (NTS). As a result, since the autonomic nervous system (ANS), which is formed of sympathetic and parasympathetic branches, regulates systemic factors of cardiovascular, respiratory, and immunological functions to maintain them within homeostatic limits, and because aVNS modulates the parasympathetic auricular branch, the effects of aVNS on the body can be expected to be systemic. The vagus nerve, which is part of the

parasympathetic nervous system, counteracts the sympathetic stress response (Breit, 2018). The parasympathetic system is activated in several ways, one of which is the arterial baroreflex activation. The principle of negative feedback governs the regulation of vascular tone, as it does in many other systems. Arterial baroreceptors in the aortic arch transmit blood pressure to the brainstem via the afferent VN and provide feedback for controlling arterial blood pressure in the near term (baroreflex). The arterial blood pressure (ABP) and vascular tonus often fluctuate in a wave-like pattern due to these causes. The afferent vagus nerve sends signals to the brainstem when hypertension triggers baroreceptors in the aortic arch (Kaniusas et al., 2020). In reaction to hypertension, the brain, particularly the nucleus of the solitary tract (NTS), restricts sympathetic outflow to the heart and periphery instinctively, whilst stroke volume and total peripheral resistance decrease, respectively. The parasympathetic outflow is automatically enhanced by efferent VN fibers, decreasing the heartbeat through the efferent VN link to the sinoatrial node. As a result, blood pressure falls and returns to normal. Because of these brain-mediated effects, auricular VNS can be used as systemic therapy, affecting the entire human body and its complex subsystems (Berthoud et al., 2001). For this reason, systemic monitoring methods are required for the registration, validation, and optimization of systemic effects induced by the auricular VNS. The methods of interest reflect the non-linear complex systems of the human body, coupled mutually with the feedback loops (Siauciunaite et al., 2018). Thus, ECG is of particular importance. The relationships between ECG parameters do vary according to various physiological and pathological reasons (Malik et al., 2002).

However, the individual tuning of stimulation settings remains an unresolved issue in the actual deployment of aVNS. Several investigations have demonstrated that the therapeutic benefits of aVNS are found in long-term therapy (Szeles et al., 2021; Kampush et al., 2015). In order to tailor the personalized approach to the patient's situation, the stimulation protocol and settings must be optimized (Ziaukas et al., 2017). Only by observing systemic changes in the human body in real-time throughout the stimulation process could achieve optimal treatment results for individual patients as well as minimizing of consequences caused by over-stimulation and under-stimulation. Numerical algorithms for the identification of algebraic relationships between cardiac intervals have already been designed and implemented in several previous studies (Saunoriene et al., 2019). These algorithms are utilized in this paper for the construction of phase plots, representing complex dynamical processes during the self-organization of the cardiovascular system. The main objective of this work was to present a computational framework able to visualize complex reactions of the cardiovascular system during aVNS.

A single ECG characteristic, such as the RR interval, which is a systemic parameter, reveals the overall functional status of the organism's regulatory system and is employed as a measure of neurocardiac function that reflects heart-brain interactions and ANS dynamics (Shaffer et al., 2014; McCraty et al., 2009). For example, when the heart fails, not only do the various regulating systems fail (decrease in multiplicity), but their tight connection, such as arterial or cardiopulmonary

baroreceptor activity, deteriorates, making the regulating system and the RR interval less complicated (Rostagno et al., 1999; Kaye et al., 1998).

The duration of ventricular repolarization is described by the JT interval. The JT range, which is split into the JT_a interval (from the point J to the peak of the T wave) and the T_e interval, which controls certain electrophysiological events (from the T wave peak to the end of T). JT intervals are related to the changes in the heart metabolism (Vainoras et al., 1996). The JT interval corresponds to the cardiac electric systole and is connected to the degree of myocardial metabolism. The regulatory nerve system influences DJT (length of JT interval) changes. The changes in repolarization are closely related to the metabolic changes in the organism. ECG leads with a shorter JT interval suggest that repolarization occurs earlier, and metabolic changes occur faster in certain myocardial locations. Longer DJT results in delayed repolarization and metabolic responses (Gargasas et al., 1998). The QRS complex is a component of the heart's regulatory system that reflects depolarization spreading in the ventricle and synchronization of depolarization spreading between the ventricles. The larger QRS complex indicates slower conduction in the ventricle of the heart (Muntianaitė-Dulkinienė, 2010). The changes in the patterns of interconnection (connectivity) and patterns of variation over time (variability) offer essential information about the state of the overall system, since the spatial and temporal organization of a complex system defines its character (Seely, 2000). Measuring the absolute value of a clinical parameter like the heart rate provides highly important and therapeutically useful data. However, analyzing the interconnections of ECG characteristics provides additional clinical information that is often more informative than the heart rate alone, especially when the heart rate is within normal limits (Que et al., 2001). For example, RR-JT interconnection shows how to tide the regulatory system that is connected to the metabolism in the heart; its intervals reveal the evolution of complex dynamical processes in the self-organization of the heart system during the load and the recovery processes (Ziaukas et al., 2017). Moreover, this relationship is used for the detection of prolonged repolarization in ventricular conduction defects (Batzel, 2007), but the JT interval is constructed as a linear function of the RR interval in the mentioned study. Similarly, it is shown by Misigoj-Durakovic et al. (2016) that the heart rates-corrected JT interval is a good estimate of specific repolarization time in a cohort of physically fit university students. There is a well-known parabolic relationship between the HR and JT interval when HR rises, JT interval shortens, and vice versa. This JT interval shortening shows the accelerating metabolism of the heart.

RR-QRS interconnection reflects the interconnection between organism regulatory system and heart regulatory system by the reaction of the duration of the QRS complex to RR interval shortening. Specific feedback reactions (depending on the type of stress-induced) could include changes in vascular tone, with or without affecting HR, and certain aspects of the individual cardiopulmonary, and the arterial reflexes may involve counteracting or inhibiting influences on other elements (Batzel, 2007). Small changes may indicate ischemic tissue islets, sympathetic tone, coronary flow, or myocardial contraction pattern (Sornmo et al., 1998). For the evaluation of the human functional state during the vagus nerve stimulation, the model of integral

health evaluation was used. This model is shown together with the short-term neural baroreflex feedback loop response model in Fig. 22, adapted from (Batzel, 2007).

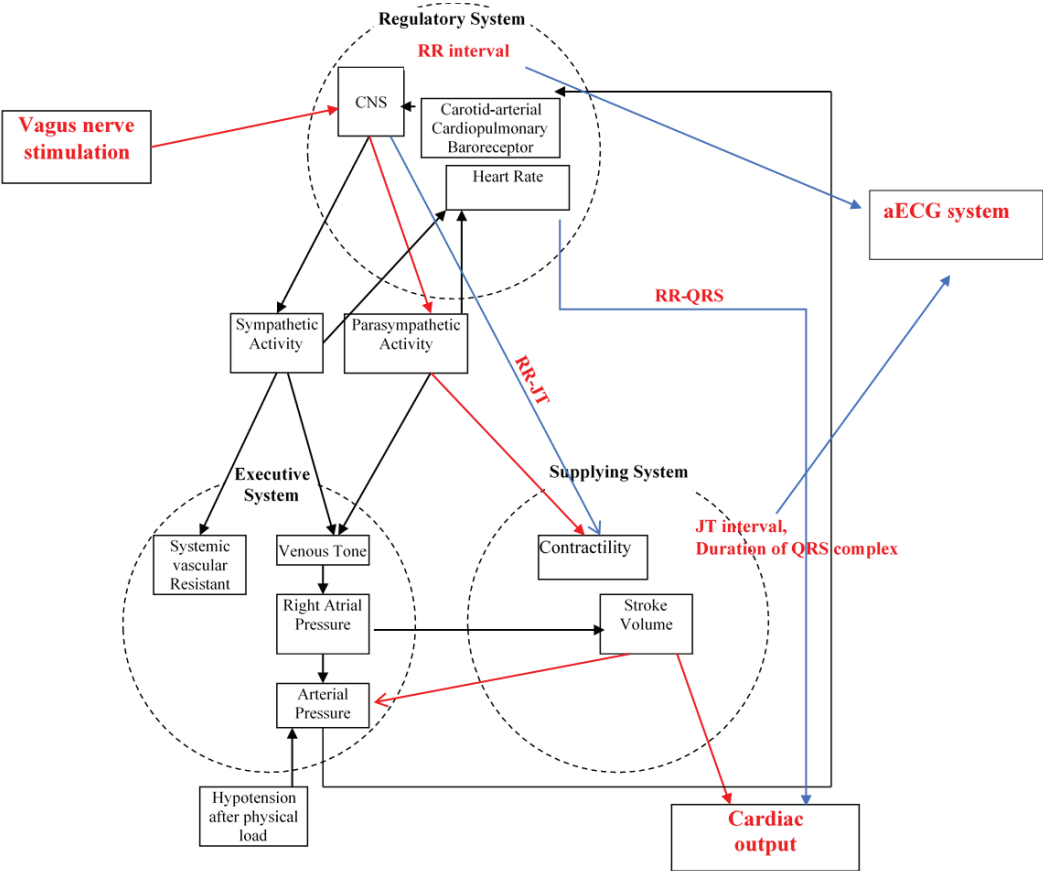


Fig. 22. Baroreceptor control loops in the context of the model of integral evaluation

This study consisted of 4 single cases for the preparation of the ethics proposal. Each of the volunteers signed a consent form to take part in this research. They were assessed four times: two verum and two placebo experiments (Table 4). In this study, four healthy persons (two males and two females), at the age of 27.8 (± 2.22), were investigated.

Table 4. The description of subjects participating in the experiment

Gender	Age, y	Height, m	Weight, kg	BMI, kg/m ²
M	31	1.81	83	25.34
F	27	1.72	65	21.97
M	26	1.77	65	20.75
F	27	1.69	55	19.26

Twelve lead ECG were assessed and analyzed using the Kaunas–Load system (Vainoras, 1998). Twenty-five different parameters and their interconnections were measured per cardiac cycle using advanced ECG analysis. The experiment started with a baseline, represented with a black line in Fig. 23, recording phase of 10 min without pVNS, continued with a verum phase of 20 min with pVNS (red line), a resting phase of 20 min without pVNS (black line), another verum phase of 20 min (red line), and a follow-up period of recovery phase for 20 min (black line). In total, more than 5000 cardio cycles were recorded and estimated.



Fig. 23. The time protocol of the experiment

Four-needle electrodes were placed in vagally innervated parts of the auricle, in/around the cyma conchae, to perform percutaneous auricular VNS (pVNS) (Fig. 24). The stimulation sequence consisted of alternating polarity monophasic pulses that were repeated every 1 second (amplitude 4 V, pulse duration 1 ms).



Fig. 24. The location of four needle electrodes

Step 1. It is considered that the vectors $x = (x_1, x_2, \dots, x_n)$ and $y = (y_1, y_2, \dots, y_n)$ represent synchronous measurement data, representing two different cardiac intervals; where n is the total number of heartbeats recorded during the experiment. The algebraic relationship between the time series x and y is reconstructed by using the algorithm presented in Ziaukas et al. (2017). This algorithm comprises three basic parts.

Step 1. Six elements: $x_{k-\delta}$, x_k , $x_{k+\delta}$, $y_{k-\delta}$, y_k , $y_{k+\delta}$, are mapped into a two-dimensional perfect matrix of Lagrange differences (the concept of perfect matrices

of Lagrange differences is introduced in Saunoriene et al. (2019), where δ is the time lag, $k = (1 + \delta), (2 + \delta), \dots, (n - \delta)$). The structure of the perfect matrix of Lagrange differences is in Ziaukas et al. (2017).

Step 2. Every matrix $L_{\delta,k}$ is transformed into a scalar value $s_{\delta,k} = \max(|\lambda_1|, |\lambda_2|)$ where λ_1 and λ_2 are the two eigenvalues of $L_{\delta,k}$ (Ziaukas et al., 2017; Saunoriene et al., 2019).

Step 3. Lastly, the generated scalar sequence of maximal eigenvalues is smoothed internally and externally. If the internal smoothing radius is R_i , and the external smoothing radius is R_e , the smoothed sequence representing the algebraic relationship between the time series x and y follows (43), where $k = (1 + R_i + R_e), (2 + R_i + R_e), \dots, (n - R_i - R_e)$. A well-posed optimization problem in respect of the smoothing parameters is formulated in Ziaukas et al. (2017) for the whole cohort of persons resulting into $R_i = 3$ and $R_e = 4$. These values of the smoothing parameters are kept fixed in this paper as well. All further analysis is based on $\bar{s}_k(3,4)$.

The use of phase maps of bioelectrical signals for the analysis of dynamical processes is widely recognized (Erem et al., 2016). In order to describe the attractors (and measure their stability), the dynamical processes of vagus nerve stimulation are visualized in a phase plane. The graphs below depict the entire vagus nerve stimulation experiment dynamics.

The case reports suggest that the right vagus can be used in circumstances where approaching the left vagus is inadvisable. Since the right vagus innervates the sinoatrial node, stimulating on the right is best conducted with the ECG monitoring (Johnson et al., 2018). It is well known that the phase maps of bioelectrical signals may be useful for the investigation of dynamical processes (Erem et al., 2016). In order to represent the attractors better (and to assess their stability), the dynamical processes of vagus nerve stimulation in a phase plane are visualized as well. The graphs below show the full dynamics of the vagus nerve stimulation experiment.

In the first case, it can be observed that when the body relaxes, the curve goes to the upper right corner (Figure 25). Both JT–QRS and RR–JT relations values are increasing (Figure 25). After the first stimulation, the black curve (rest after the first stimulation) makes a loop (Figure 25), circuiting in one place, then the red curve, the second stimulation phase, go up again. This means that the independence of the two systems and the complexity of the parameters increase, then, during the recovery again, it makes a loop to go back to the initial body phase state. A different behavior is seen when the stimulation session with the placebo session is compared. There are no clear changes in the process dynamics, but there are small fluctuations in the initial body state.

The second subject shows more complicated changes: during the second stimulation, the tension in both fractal levels (RR/JT and JT/QRS) is reduced as well (Figure 26). The system in the phase plane goes to the right-top part of Figure 26. During the sham stimulation (Placebo), the black curves make a loop, but the general trend for both systems is to go into a state of relaxation. If it was just a lying effect,

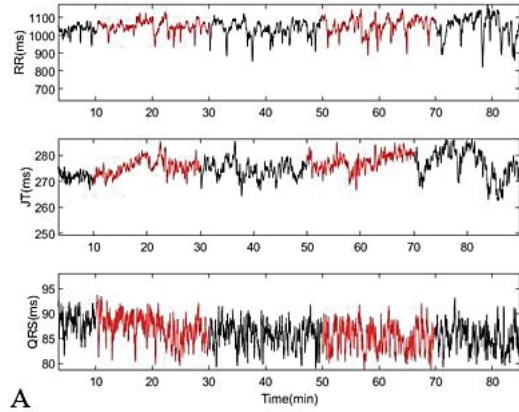
the black line at the end of the experiment would not go back, but it always rises (effect of long-lasting rest).

The third case (Figure 27) has a classical pattern of the vagus nerve stimulation dynamics that appeared in most of the cases. The complexity between relations grew; the systems became more independent from each other. In the sham stimulation (placebo), there is a similar effect as in the real stimulation. This could be due to the insertion of the needles providing excitation to the parasympathetic nervous system; the body already has a memory of the effect of the needle penetration.

The fourth subject showed the classical behavior in the same way as in the first stimulation; however, for some reason, the second stimulation did not show much effect (second red curve) (Figure 28). This could be due to many factors, for example, psychological state or stressful thoughts during the experiment.

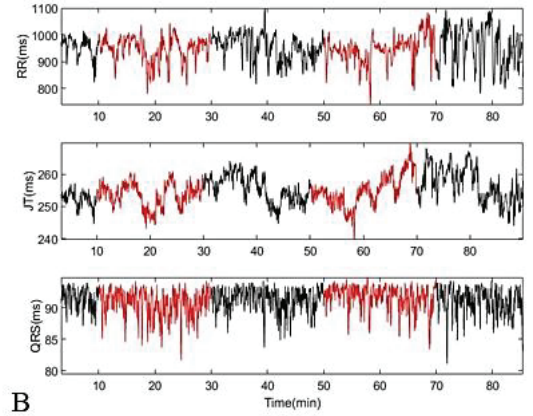
Subject 1

STIMULATION

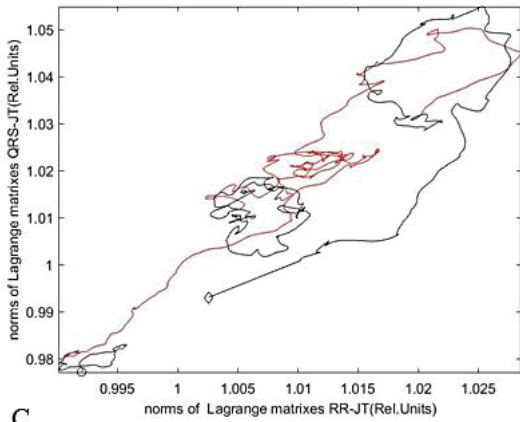


A

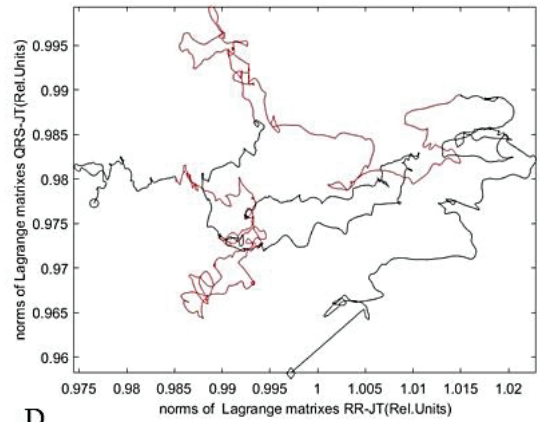
PLACEBO



B



C



D

Fig. 25. The transit through the stimulation and placebo for Subject 1; (A) dynamic of parameters RR interval, JT interval, and QRS duration during the investigation (Stimulation); (B) dynamic of parameters RR interval, JT interval, and QRS duration during the investigation (Placebo); (C) phase plane for JT/QRS and RR/JT norms during the stimulation; (D) phase plane for JT/QRS and RR/JT norms during placebo; the beginning of the experiment is marked as a black circle, the end of the experiment is marked as a black diamond marker; in total, more than 5000 cardio cycles were recorded and estimated

Subject 2

STIMULATION

PLACEBO

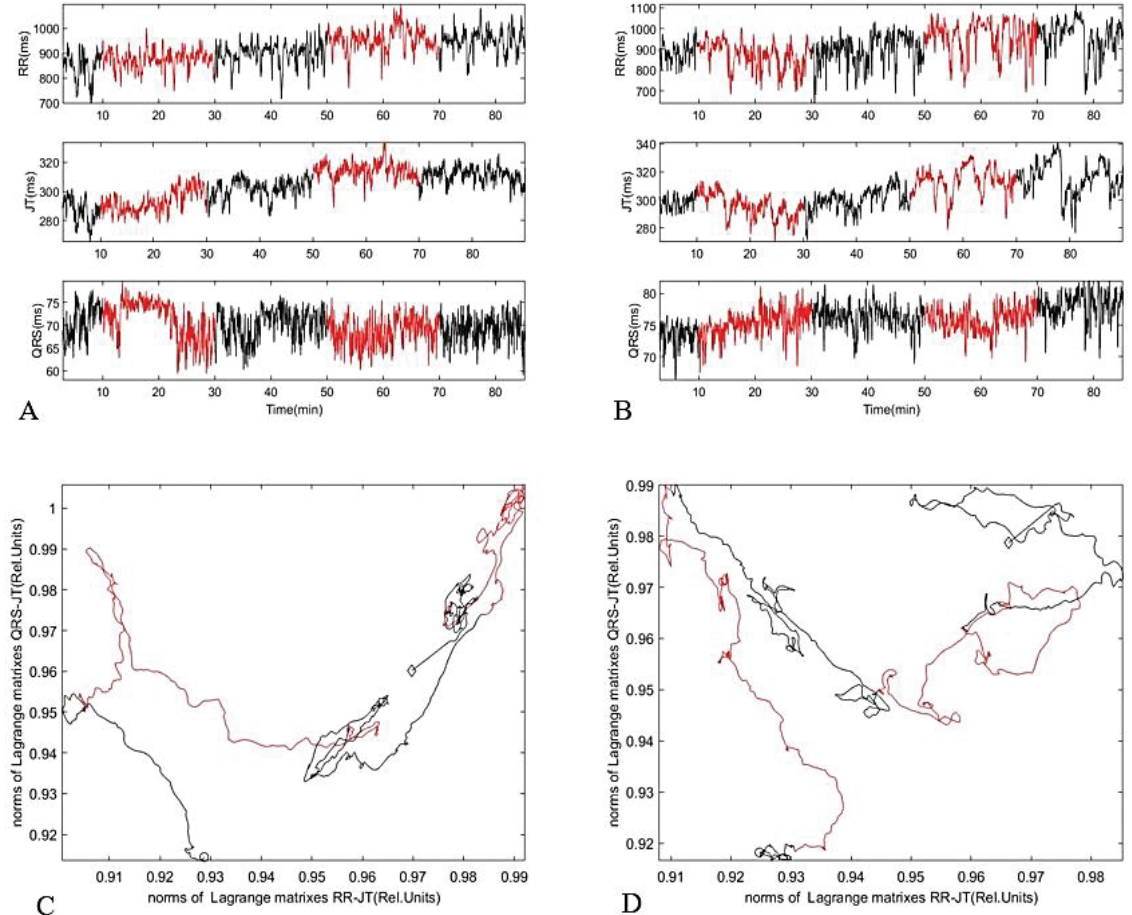


Fig. 26. The transit through the stimulation and placebo for Subject 2; (A) dynamic of parameters RR interval, JT interval, and QRS duration during the investigation (Stimulation); (B) dynamic of parameters RR interval, JT interval, and QRS duration during the investigation (Placebo); (C) phase plane for JT/QRS and RR/JT norms during the stimulation; (D) phase plane for JT/QRS and RR/JT norms during placebo

Subject 3

STIMULATION

PLACEBO

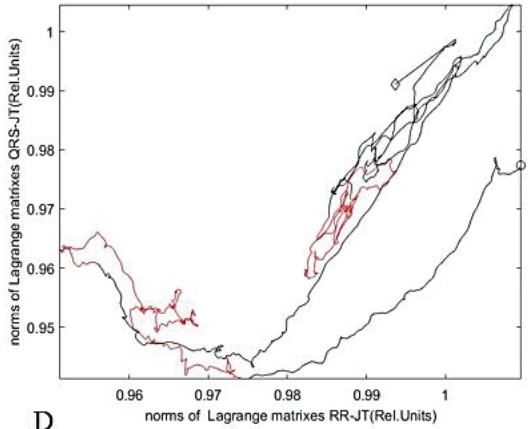
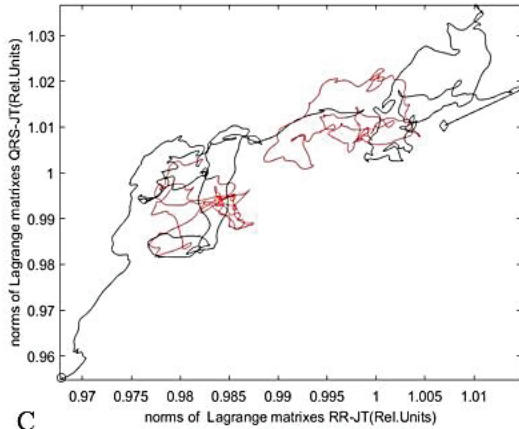
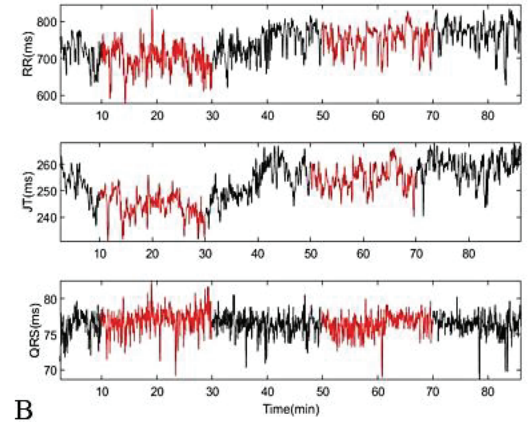
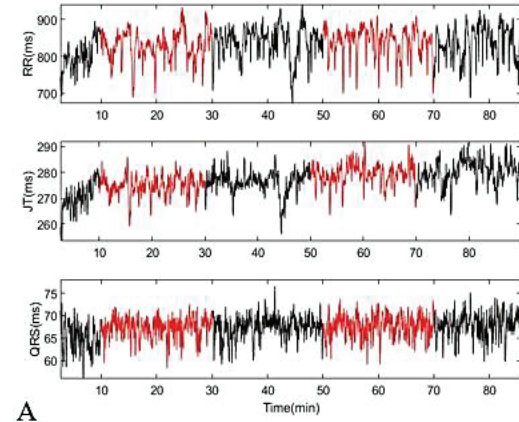


Fig. 27. The transit through the stimulation and placebo for Subject 3; (A) dynamic of parameters RR interval, JT interval, and QRS duration during the investigation (Stimulation); (B) dynamic of parameters RR interval, JT interval, and QRS duration during the investigation (Placebo); (C) phase plane for JT/QRS and RR/JT norms during the stimulation; (D) phase plane for JT/QRS and RR/JT norms during placebo

Subject 4

STIMULATION

PLACEBO

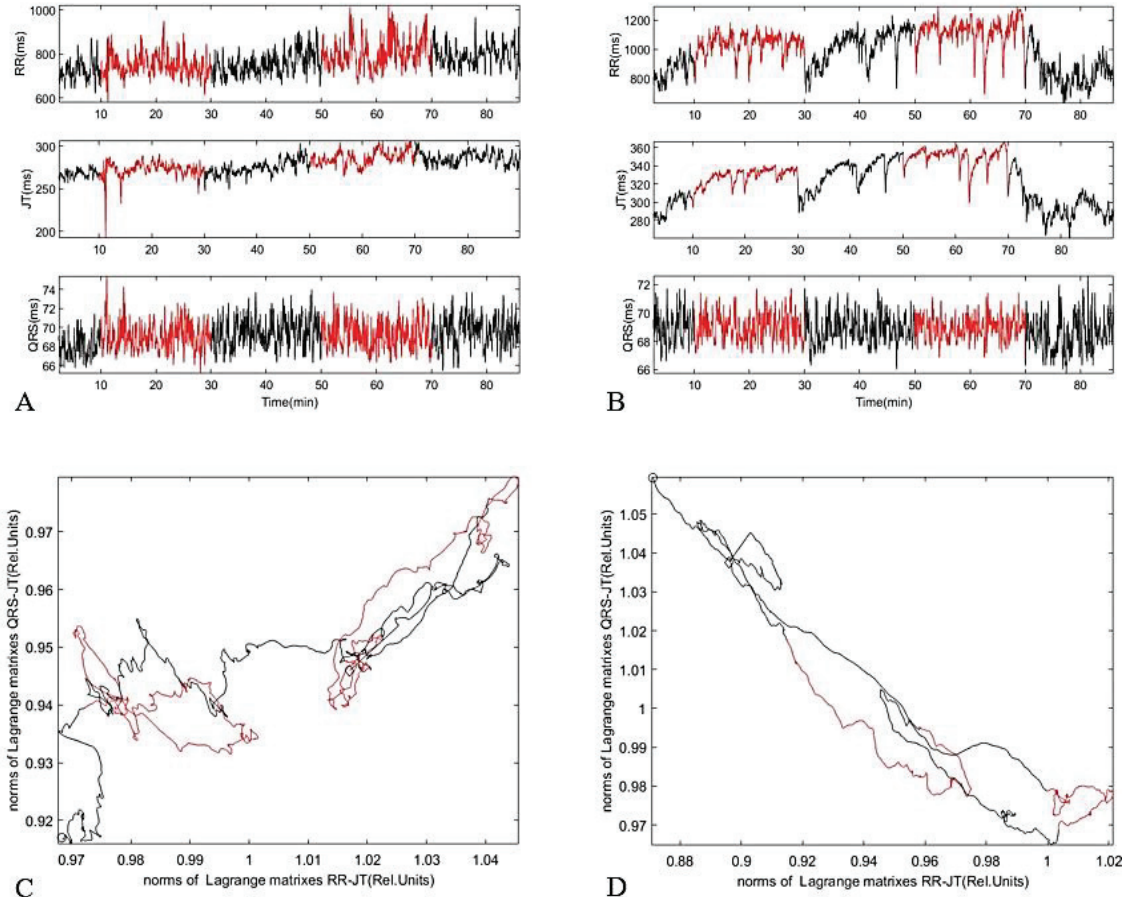


Fig. 28. The transit through the stimulation and placebo for Subject 4; (A) dynamic of parameters RR interval, JT interval, and QRS duration during the investigation (Stimulation); (B) dynamic of parameters RR interval, JT interval, and QRS duration during the investigation (Placebo); (C) phase plane for JT/QRS and RR/JT norms during the stimulation; (D) phase plane for JT/QRS and RR/JT norms during placebo

When the body's responses can be objectively measured, the parameters such as the period of stimulation may be improved. Even though the human body's reaction

to every stimulus might be quite distinct and unique, it was possible to effectively trace the whole process of electrical auricular vagus nerve stimulation at two different fractal levels of the human organism by using the visualization approach. The suggested approach for tracking small modifications in algebraic connections between cardiac intervals during aVNS can follow individual patient reactions in the real time. The presented techniques provide a unique insight into the complex dynamical processes, taking place in a patient's cardiovascular system during the stimulation. The ability to track these dynamical processes can build the ground for the optimization strategy, which could lead to personalized aVNS treatment. The development of such a personalized approach to aVNS treatment is a definite objective of the future research.

IV. CONCLUSIONS

1. It has been demonstrated that the anaerobic threshold can be determined by using mathematical models and algorithms, using only the algebraic relationship between RR and DQRS cardiac intervals (other standard techniques based on the lactate or exhale gas concentration measurement are not required for that purpose).
2. Early onset of ischemic episodes in the heart can be detected based on the algebraic relationship between JT and ST cardiac parameters.
3. The visualization of inter-relationships between RR/DQRS and RR/JT cardiac intervals in the phase plane enables a unique insight into the complex processes of the self-organization of the cardiovascular system during the electrical auricular vagus nerve stimulation.
4. The novel synchronization detection algorithm enabled to detect inter-connections between the human heart rate variability (HRV) and the Earth's local magnetic field (LMF). That did help to validate the positive effect of the Heart-Lock-In technique for the coherence between the LMF and HRV.

REFERENCES

1. Aboy M, Hornero R, Abasolo D, Alvare D. Interpretation of the Lempel-Ziv complexity measure in the context of biomedical signal analysis. *IEEE Transactions on Biomedical Engineering* 2006;11(53): 2282-2288
2. Ahmad S, Tejuja A, Newman KD, Zarychanski R & Seely AJ Clinical review: A review and analysis of heart rate variability and the diagnosis and prognosis of infection. *Crit. Care* 13, 232 (2009). [PubMed: 20017889]
3. AKTARUZZAMAN, M. and R. SASSI. Parametric estimation of sample entropy in heart rate variability analysis. *Biomedical Signal Processing and Control*. 2014, 14(0), 141– 147. ISSN: 1746-8094.
4. Alabdulgade, A.; Macraty, R.; Atkinson, M.; Vainoras, A.; Berškiene, K.; Mauriciene, V.; Daunoraviciene, A.; Navickas, Z.; Šmidtaitė, R.; Landauskas, M. Human heart rhythm sensitivity to earth local magnetic field fluctuations. *J. Vibroeng.* 2015,17, 3271–3278.
5. Alabdulgader, A.; McCraty, R.; Atkinson, M.; Dobyns, Y.; Vainoras, A.; Ragulskis, M.; Stolc, V. Long-term study of heart rate variability responses to changes in the solar and geomagnetic environment. *Sci. Rep.* 2018, 8, 1–14. [CrossRef] [PubMed]
6. Alexander, F. (2012). A multifaceted mathematical approach for complex systems.
7. Ballarin, E.; Borsetto, C.; Cellini, M.; Patracchini, M.; Vitiello, P.; Ziglio, P.G.; Conconi, F. Adaptation of the “Conconi test” to children and adolescents. *Int. J. Sports Med.* 1989, 10, 334–338.
8. Baranger M. Chaos, complexity and entropy. New England Complex Systems Institute, Cambridge 2001. Available at: <http://necsi.org/projects.html>
9. Barella, L. F., Miranda, R. A., Franco, C. C. S., Alves, S., Malta, A., Ribeiro, T. A. S., et al. (2014). Vagus nerve contributes to metabolic syndrome in high-fat diet-fed young and adult rats. *Exp. Physiol.* 100, 57–68. doi: 10.1113/expphysiol.2014.082982
10. Bartocci, E., & Lió, P. (2016). Computational modeling, formal analysis, and tools for systems biology. *PLoS computational biology*, 12(1), e1004591.
11. Bar-Yam, Yaneer (2002). "General Features of Complex Systems" (PDF). *Encyclopedia of Life Support Systems*. Retrieved 16 September 2014.
12. Batzel J.J., Kappel F., Schneditz D., Tran H.T. Cardiovascular and Respiratory Systems Modeling, Analysis, and Control. Society for Industrial and Applied Mathematics, Philadelphia. 2007. P. 105-119.
13. Bazett, H.C. An analysis of the time relations of electrocardiograms. *Heart* 1920, 7, 353–370.
14. Beckers F, Rameakers D, Aubert AE. Approximate entropy of heart rate variability: validation of methods and application in heart failure. *Cardiovasc Eng* 2001;1:177-182.
15. Beckers F, Verheyden B, Aubert AE. Aging and nonlinear heart rate control in healthy population. *Am J physiol heart Cric Physiol* 2006; 290:2560-2570.

16. Behzad Mozaffary and Mohammad A. Tinati, "ECG Baseline Wander Elimination using Wavelet Packets", *World Academy of Science, Engineering and Technology*, vol. 3, no. January, pp. 14– 16, 2005.
17. Berthoud, H. R., and Neuhuber, W. L. (2001). Functional and chemical anatomy of the afferent vagal system. *Auton. Neurosci.* 85, 1–17. doi: 10.1016/S1566-0702(00)00215-0
18. BIALEK, William. *Biophysics: searching for principles*. Princeton University Press, 2012.
19. Biering-Sorensen T, Mogelvang R, de Knecht MC, Others. Cardiac Time Intervals by Tissue Doppler Imaging M-Mode: Normal Values and Association with Established Echocardiographic and Invasive Measures of Systolic and Diastolic Function. *PLOS ONE*. 2016; 11(4):1–14. <https://doi.org/10.1371/journal.pone.0153636> PMID: 27093636
20. Biggiero L. Sources of complexity in human systems. *J. Nonlinear Dynamics. Psychology and Life Sciences*, 2001, January;5 (1): 379
21. Bigi, R.; Cortigiani, L.; Gregori, D.; Bax, J.; Fiorentini, C. Prognostic Value of Combined Exercise and Recovery Electrocardiographic Analysis. *Arch. Intern. Med.* 2005, 165, 1253.
22. Bigi, R.; Cortigiani, L.; Gregori, D.; Fiorentini, C. Comparison of the Prognostic Value of the Stress-Recovery Index Versus Standard Electrocardiographic Criteria in Patients with a Negative Exercise Electrocardiogram. *Am. J. Cardiol.* 2007, 100, 605–609.
23. Bigi, R.; Maffi, M.; Occhi, G.; Bolognese, L.; Pozzoni, L.; Curti, G. Improvement in identification of multivessel disease after acute myocardial infarction following stress-recovery analysis of ST depression in the heart rate domain during exercise. *Eur. Heart J.* 1994, 15, 1240–1246.
24. Blecker, W. K., Mackaay, A. J., Masson-Pévet, M., Bouman, L. N., & Becker, A. E. (1980). Functional and morphological organization of the rabbit sinus node. *Circulation research*, 46(1), 11-22.
25. Boccaletti S, Kurths J, Osipov G, Valladares DL& Zhou CS.. 2002 The synchronization of chaotic systems. *Phys. Rep.* 366, 1–101. doi:10.1016/S0370-1573(02)00137-0 (doi:10.1016/S0370-1573(02)00137-0).
26. Bonomini MP, Arini PD, Gonzalez GE, Buchholz B, Valentinuzzi ME. The allometric model in chronic myocardial infarction. *Theoretical Biology and Medical Modelling*. 2012; 9(1):1. <https://doi.org/10.1186/1742-4682-9-15>
27. Botting K, Trzeciakowski JP, benoit MF, Salama SA, Diaz-Arrastia CR. Sample entropy analysis of cervical neoplasia gene-expression signatures. *BMC Bioinformatics* 2009; 66(10).
28. Bourgois, J., & Vrijens, J. (1998). The Conconi test: a controversial concept for the determination of the anaerobic threshold in young rowers. *International journal of sports medicine*, 19(08), 553-559.
29. Breit, Sigrid, et al. "Vagus nerve as modulator of the brain–gut axis in psychiatric and inflammatory disorders." *Frontiers in psychiatry* 9 (2018): 44.
30. Bretscher, O. *Linear Algebra with Applications*; Pearson/Prentice Hall: Upper Saddle River, NJ, USA, 2005.

31. Browning KN, Travagli RA. Central nervous system control of gastrointestinal motility and secretion and modulation of gastrointestinal functions. *Compr Physiol* (2014) 4:1339–68.10.1002/cphy.c130055
32. CHAZOTTES, J. R. and B. FERNANDEZ. The CML2004 Project. Lecture Notes in Physics, 2005.
33. Chen JL, Tseng YJ, Chiu HW, Hsiao TC, Chu WC. Nonlinear analysis of heart rate dynamics in hyperthyroidism. *Physiological Measurements* 2007; 28(4):427-437.
34. Chen KY (2011) Combining linear and nonlinear model in forecasting tourism demand. *Exp Syst Appl* 38(8):10368–10376
35. Cilliers, P. (1998). *Complexity and Postmodernism: Understanding Complex Systems*, Routledge, London.
36. Conconi, F., Grazi, G., Casoni, I., Guglielmini, C., Borsetto, C., Ballarin, E., ... & Manfredini, F. (1996). The Conconi test: methodology after 12 years of application. *International journal of sports medicine*, 17(07), 509-519.
37. Conconi, F.; Ferrari, M.; Ziglio, P.G.; Droghetti, P.; Codeca, L. Determination of the anaerobic threshold by a noninvasive field test in runners. *J. Appl. Physiol.* 1982, 52, 862–873.
38. Costa M, Goldberger AL, Peng CK. Multiscale entropy analysis of biological signals. *Phys. Rev E Stat Nonlin Soft mater Phys* 2005; 71:021906.
39. Cripps TR, Malik M, Farrell TG & Camm AJ Prognostic value of reduced heart rate variability after myocardial infarction: clinical evaluation of a new analysis method. *Br Heart J* 65, 14–9 (1991). [PubMed: 1704246]
40. Dalla Porta, L., Matias, F. S., Dos Santos, A. J., Alonso, A., Carelli, P. V., Copelli, M., & Mirasso, C. R. (2019). Exploring the phase-locking mechanisms yielding delayed and anticipated synchronization in neuronal circuits. *Frontiers in systems neuroscience*, 13, 41.
41. Dekker, J.; Schouten, E.; Klootwijk, P.; Pool, J.; Kromhout, D. Association between QT interval and coronary heart disease in middle-aged and elderly men. The Zutphen Study. *Circulation* 1994, 90, 779–785.
42. Detrano, R.; Salcedo, E.; Passalacqua, M.; Friis, R. Exercise electrocardiographic variables: A critical appraisal. *J. Am. Coll. Cardiol.* 1986, 8, 836–847.
43. DiFrancesco, D. (2005). Cardiac pacemaker/f current and its inhibition by heart rate-reducing agents. *Current medical research and opinion*, 21(7), 1115-1122.
44. Dong-xiao N, Hui-feng S, Desheng DW (2012) Short-term load forecasting using bayesian neural networks learned by hybrid monte carlo algorithm. *Appl Soft Comput* 12(6):1822–1827
45. Doronin, V.; Parfentev, V.; Tleulin, S.; Namvar, R.; Somsikov, V.; Drobzhev, V.; Chemeris, A. Effect of variations of the geomagnetic field and solar activity on human physiological indicators. *Biofizika* 1998, 43, 647–653. [PubMed]
46. Easton JF, Stephens CR, Angelova M (2014) Risk factors and prediction of very short term versus short/intermediate term post-stroke mortality: a data mining approach. *Comput Biol Med* 54:199–210

47. Elamin, M.; Mary, D.; Smith, D.; Linden, R. Prediction of severity of coronary artery disease using slope of submaximal ST segment/heart rate relationship. *Cardiovasc. Res.* 1980, 14, 681–691.
48. Elgendi M On the Analysis of Fingertip Photoplethysmogram Signals. *Curr. Cardiol. Rev* 8, 14–25 (2012). [PubMed: 22845812]
49. Erem, B.; Orellana, R.M.; Hyde, D.E.; Peters, J.M.; Duffy, F.H.; Stovicek, P.; Warfield, S.K.; MacLeod, R.S.; Tadmor, G.; Brooks, D.H. Extensions to a manifold learning framework for time-series analysis on dynamic manifolds in bioelectric signals. *Phys. Rev. E* 2016, 93, 42218.
50. Eroglu, Deniz; Lamb, Jeroen S. W.; Pereira, Tiago (2017). "Synchronization of chaos and its applications". *Contemporary Physics*. 58 (3): 207–243]
51. Firmino PRA, de Mattos Neto PS, Ferreira TA (2014) Correcting and combining time series forecasters. *Neural Netw* 50:1–11
52. Freitas U, Roulin E, Muir JF, Letellier Ch. Identifying chaos from heart rate: The right task? *Chaos* 2009;19.
53. Gao, J., Cao, Y., Tung, W. W., & Hu, J. (2007). *Multiscale analysis of complex time series: integration of chaos and random fractal theory, and beyond*. John Wiley & Sons.
54. Gargasas, L., Vainoras, A., Schwela, H., Jaruševičius, G., Ruseckas, R., & Miškinis, V. (1998). JT interval changes during bicycle ergometry. *Kardiologia Polska: II międzynarodowy kongres Polskiego towarzystwa kardiologicznego: 4-6 września/September 1998, Katowice, Poland. Katowice., 1998, t. 49, supl. 1, abstract no. P153.*
55. Gargasas, L.; Vainoras, A.; Ruseckas, R.; Jurkonienė, R.; Jurkonis, V.; Miskinis, V. A new software for ECG monitoring system. In *NCeHT2006, Proceedings of the 6th Nordic Conference on eHealth and Telemedicine, Helsinki, Finland, 31 August–1 September 2006*; Doupi, P., Ed.; Valopaino Oy: Helsinki, Finland, 2006; pp. 255–256.
56. Gidea, M., Gidea, C., & Byrd, W. (2011). Deterministic models for simulating electrocardiographic signals. *Communications in Nonlinear Science and Numerical Simulation*, 16(10), 3871–3880.
57. Gierałtowski J, Żebrowski JJ & Baranowski R Multiscale multifractal analysis of heart rate variability recordings with a large number of occurrences of arrhythmia. *Phys. Rev. E* 85, 021915 (2012).
58. Gladden, L. B., Yates, J. W., Stremel, R. W., & Stamford, B. A. (1985). Gas exchange and lactate anaerobic thresholds: inter-and intraevaluator agreement. *Journal of Applied Physiology*, 58(6), 2082–2089.
59. Goldberger AL. Fractal variability versus pathologic periodicity: complexity loss and stereotypy in disease. *Perspect Biol Med* 1997; 40:543–561.
60. Goldenberg I, Moss AJ, Zareba W, Others. QT interval: how to measure it and what is “normal”. *Journal of cardiovascular electrophysiology*. 2006; 17(3):333–336. <https://doi.org/10.1111/j.1540-8167.2006.00408.x> PMID: 16643414
61. Goncalves H, Pinto P, Silva M, Ayres-de-Campos D & Bernardes J Electrocardiography versus photoplethysmography in assessment of maternal heart rate variability during labor. *Springerplus* 5, 1079 (2016). [PubMed: 27462527]

62. GOSHVARPOUR, A. Classification of Heart Rate Signals during Meditation using Lyapunov Exponents and Entropy. *International Journal of Intelligent Systems and Applications*. 2012, 4(2), 6.
63. GRAFF, B. et al. Entropy Measures in the Assessment of Heart Rate Variability in Patients with Cardiodepressive Vasovagal Syncope. *Entropy*. 2015, 17(3), 1007–1022. ISSN: 1099- 4300.
64. Hampel, F.R. A general qualitative definition of robustness. *Ann. Math. Stat.* 1971, 42, 1887–1896. [CrossRef]
65. Hazewinkel, M. (Ed.). (2012). *Encyclopaedia of Mathematics: Reaction-Diffusion Equation-Stirling Interpolation Formula* (Vol. 8). Springer Science & Business Media.
66. He, W., Zhu, B., Zhu, X.-L., Li, L., Bai, W.-Z., and Ben, H. (2013). The auriculo-vagal afferent pathway and its role in seizure suppression in rats. *BMC Neurosci.* 14:85. doi: 10.1186/1471-2202-14-85
67. HODGKIN, A. L. and A.F. HUXLEY. A quantitative description of membrane current and its application to conduction and excitation in nerve. *The Journal of physiology.* 1952,117(4), 500.
68. Householder, Alston S. (1975), *The theory of matrices in numerical analysis*, New York, NY: Dover Publications, MR 0378371
69. Huke, J.P.; Broomhead, D.S. Embedding theorems for non-uniformly sampled dynamical systems. *Nonlinearity* 2007, 20, 2205–2244. [CrossRef]
70. Iaizzo, P. A. (Ed.). (2010). *Handbook of cardiac anatomy, physiology, and devices*. Springer Science & Business Media.
71. IBARZ, B. et al. Map-based models in neuronal dynamics. *Physics Reports*. 2011, 501(1–2), 1–74. ISSN: 0370-1573.
72. Iida T, Miyakawa T, edamatsu Ch, Onodera Sh. Effect of working speed on the complexity of the cycle of head fluctuation during walking using approximate entropy. *The Japanese Society of Physical Fitness and Sport Medicine* 2007;56;481-488
73. Jia C, Wei L, Wang H, Yang J (2014) Study of track irregularity time series calibration and variation pattern at unit section. *Comput Intell Neurosci* 2014;14. <http://dx.doi.org/10.1155/2014/727948>
74. Johnson, R.L.; Wilson, C.G. A review of vagus nerve stimulation as a therapeutic intervention. *J. Inflamm. Res.* 2018, 11, 203–213, doi:10.2147/JIR.S163248.
75. Johnson, Rhaya L, and Christopher G Wilson. “A review of vagus nerve stimulation as a therapeutic intervention.” *Journal of inflammation research* vol. 11 203-213. 16 May. 2018, doi:10.2147/JIR.S163248
76. Kampusch S., Kaniusas E., Szeles J.C.: New approaches in multipunctual percutaneous stimulation of the auricular vagus nerve. *Proceedings of the 6th International IEEE EMBS Conference on Neural Engineering*. 263-266 (2013).
77. Kampusch, S.; Thürk, F.; Kaniusas, E.; Széles, J.C. Autonomous nervous system modulation by percutaneous auricular vagus nerve stimulation: Multiparametric assessment and implications for clinical use in diabetic foot ulcerations. In *Proceedings of the 2015 IEEE Sensors Applications Symposium (SAS)*, Zadar, Croatia, 13–15 April 2015; pp. 1–6.
78. Kaniusas, E., Kampusch, S., Tittgemeyer, M., Panetsos, F., Gines, R. F., Papa, M., ... & Šarolić, A. (2019). Current directions in the auricular vagus

- nerve stimulation II—an engineering perspective. *Frontiers in neuroscience*, 13, 772.
79. KARAGUEUZIAN, H. S. et al. Bifurcation theory and cardiac arrhythmias. *American journal of cardiovascular disease*. 2013, 3(1), 1.
 80. Kaye, D. M., Jennings, G. L., Dart, A. M., & Esler, M. D. (1998). Differential effect of acute baroreceptor unloading on cardiac and systemic sympathetic tone in congestive heart failure. *Journal of the American College of Cardiology*, 31(3), 583-587.
 81. Khabarova, O.; Dimitrova, S. On the nature of people's reaction to space weather and meteorological weather changes. *Sun Geosph*. 2009, 4, 60–71.
 82. Kim H. S., Eykholt R., Salas J. D., Nonlinear dynamics, delay times, and embedding windows. *Physica D*, 1999, 127, p. 48-60.
 83. Kligfield, P.; Ameisen, O.; Okin, P. Heart rate adjustment of ST segment depression for improved detection of coronary artery disease. *Circulation* 1989, 79, 245–255.
 84. Kurakin, V. L. (2001). Linear complexity of polylinear sequences.
 85. Kurakin, VL, Kuzmin AVMAS, Nechayev AA (1995) Linear complexity of polinear sequences. *J Math Sci* 76:2793–2915
 86. Landauskas, M., Navickas, Z., Vainoras, A., & Ragulskis, M. (2017). Weighted moving averaging revisited: an algebraic approach. *Computational and Applied Mathematics*, 36(4), 1545-1558.
 87. Lang, Serge (2002), *Algebra*, Graduate Texts in Mathematics, 211 (Revised third ed.), New York: Springer-Verlag, ISBN 978-0-387-95385-4, MR 1878556
 88. Lehtinen, R. ST/HR hysteresis: Exercise and recovery phase ST depression/heart rate analysis of the exercise ECG. *J. Electrocardiol*. 1999, 32, 198–204.
 89. Li, Y.; Li, G.; Yang, Y.; Liang, X.; Xu, M. A fault diagnosis scheme for planetary gearboxes using adaptive multi-scale morphology filter and modified hierarchical permutation entropy. *Mech. Syst. Signal Process* 2018, 105, 319–337. [CrossRef]
 90. Lin DC & Sharif A Common multifractality in the heart rate variability and brain activity of healthy humans. *Chaos Interdiscip. J. Nonlinear Sci* 20, 023121 (2010).
 91. Lombardi F Chaos Theory, Heart Rate Variability, and Arrhythmic Mortality. *Circulation* 101, 8–10 (2000). [PubMed: 10618296]
 92. Ma R, Hu SJ, Xu HH (2013) Very short-term wind speed prediction of a wind farm based on artificial neural network. *Adv Mater Res Trans Tech Publ* 608:677–682
 93. Malik M, Camm AJ. Heart rate variability. (Futura Pub. Co., 1995).
 94. Malik M, Färbon P, Batchvarov V, Hnatkova K, Camm AJ. Relation between QT and RR intervals is highly individual among healthy subjects: implications for heart rate correction of the QT interval. *Heart*. 2002;87(3):220–228. pmid:11847158
 95. Malik, M., Andršová, I. A., Hnatkova, K., Šišáková, M., Toman, O., Smetana, P., ... & Schmidt, G. (2021). Influence of heart rate correction formulas on QTc interval stability.

96. Manabe, Y.; Chakraborty, B. A novel approach for estimation of optimal embedding parameters of nonlinear time series by structural learning of neural network. *Neurocomputing* 2007, 70, 1360–1371. [CrossRef]
97. Mandel Y et al. Human embryonic and induced pluripotent stem cell-derived cardiomyocytes exhibit beat rate variability and power-law behavior. *Circulation* 125, 883–93 (2012). [PubMed:22261196]
98. Manikandan MS, Soman K (2012) A novel method for detecting R-peaks in electrocardiogram (ECG) signal. *Biomed Signal Process Control* 7(2):118–128
99. Manpreet Kaur, Birmohan Singh and Seema, “Comparisons of Different Approaches for Removal of Baseline Wander from ECG Signal”, *International Journal of Computer Applications*, pp. 1290- 1294, 2011.
100. Marmarelis P, Marmarelis V. *Anglysis of physiological systems: The white-noise approach*. New York: Plenum press;1978.
101. Maud, P. J., & Foster, C. (2006). *Physiological assessment of human fitness*. Human Kinetics.
102. Mayra O., Ahola T., Leiviska K., Time delay estimation and variable grouping using genetic algorithm, *Control Engineering Laboratory* ,2006, Report A no. 32.
103. McArdle WD, Katch FI, Katch VL. *Essentials of exercise physiology*. 2nd ed. Philadelphia, PA: Lippincott Williams & Wilkins, 2000.
104. McCraty R, Atkinson M, Tomasino D, Bradley RT. *The coherent heart: heart-brain interactions, psychophysiological coherence, and the emergence of system-wide order*. Boulder Creek, CA: Institute of Heartmath; 2009.
105. McCraty, R., Atkinson, M., Timofejeva, I., Joffè-Luinienè, R., Vainoras, A., Landauskas, M., ... & Ragulskis, M. K. (2018). The influence of heart coherence on synchronization between human heart rate variability and geomagnetic activity. *Journal of complexity in health sciences*, 1(2), 42-48.
106. McCraty, R.; Atkinson, M.; Stolz, V.; Alabdulgader, A.A.; Vainoras, A.; Ragulskis, M. Synchronization of human autonomic nervous system rhythms with geomagnetic activity in human subjects. *Int. J. Environ. Res. Public Health* 2017, 14, 770. [CrossRef] [PubMed]
107. McCraty, R.; Deyhle, A. The global coherence initiative: Investigating the dynamic relationship between people and earth’s energetic systems. *Bioelectromagn. Subtle Energy Med.* 2015, 2, 411–425.
108. McCraty, R.; Moor, S.; Goelitz, J.; Lance, S.W. *Transforming Stress for Teens: The Heartmath Solution for Staying Cool under Pressure*; Instant Help Books, an Imprint of New Harbinger Publications, Inc.: Oakland, CA, USA, 2016.
109. McCraty, R.; Tomasino, D. Emotional Stress, Positive Emotions, and Psychophysiological Coherence. In *Stress in Health and Disease*; Wiley-VCH: Hoboken, NJ, USA, 2006.
110. Mercante, B., Ginatempo, F., Manca, A., Melis, F., Enrico, P., and Deriu, F. (2018b). *Anatomo-physiologic basis for auricular stimulation*. *Med. Acupunct.* 30, 141–150. doi: 10.1089/acu.2017.1254
111. MICHAELS, Donald C.; MATYAS, Edward P.; JALIFE, Jose. Dynamic interactions and mutual synchronization of sinoatrial node pacemaker cells. A mathematical model. *Circulation research*, 1986, 58.5: 706-720.

112. MISHRA, A. K. and S. RAGHAV. Local fractal dimension based ECG arrhythmia classification. *Biomedical Signal Processing and Control*. 2010, 5(2), 114–123. ISSN: 1746- 8094.
113. Misigoj-Durakovic M, Durakovic Z, Prskalo I. Heart rate-corrected QT and JT intervals in electrocardiograms in physically fit students and student athletes. *Annals of Noninvasive Electrocardiology*. 2016;21(6):595–603. pmid:27194642
114. Nan X, Li Q, Qiu D, Zhao Y, Guo X (2013) Short-term wind speed syntheses correcting forecasting model and its application. *Int J Electric Power Energy Syst* 49:264–268
115. Ning, et al. Application of parallel RBF network on iterative prediction of chaotic time series. In: 2010 International Workshop on Chaos-Fractal Theories and Applications. IEEE, 2010. p. 341-345.
116. Novak, V.; Saul, J.P.; Eckberg, D.L. Task Force report on heart rate variability. *Circulation* 1997, 96, 1056.
117. OFULLA, A. *The Secrets of Hidden Knowledge: How Understanding Things in the Physical Realm Nurtures Life*. 2013.
118. Olshansky, B., Sabbah, H. N., Hauptman, P. J., and Colucci, W. S. (2008). Parasympathetic nervous system and heart failure: pathophysiology and potential implications for therapy. *Circulation* 118, 863–871. doi: 10.1161/circulationaha.107.760405
119. Ouannas, A., & Odibat, Z. (2015). Generalized synchronization of different dimensional chaotic dynamical systems in discrete time. *Nonlinear Dynamics*, 81(1), 765-771.
120. Packard, N.H.; Crutchfield, J.P.; Farmer, J.D.; Shaw, R.S. Geometry from a time series. *Phys. Rev. Lett.* 1980,45, 712–716. [CrossRef]
121. Palivonaite R, Ragulskis M (2014) Short-term time series algebraic forecasting with internal smoothing. *Neurocomputing* 127:161–171
122. Pandey, V., & Giri, V. K. (2016, March). High frequency noise removal from ECG using moving average filters. In 2016 International Conference on Emerging Trends in Electrical Electronics & Sustainable Energy Systems (ICETEESES) (pp. 191-195). IEEE.
123. Park H, Elden L (2003) Matrix rank reduction for data analysis and feature extraction. Tech. rep., technical report
124. Pearson, R.K.; Neuvo, Y.; Astola, J.; Gabbouj, M. The class of generalized hampel filters. In *Proceedings of the IEEE 2015 23rd European Signal Processing Conference (EUSIPCO)*, Nice, France, 31 August–4 September 2015; pp. 2501–2505
125. Peitgen H-O, Jürgens H & Saupe D *Chaos and Fractals: New Frontiers of Science*. (Springer Science & Business Media, 2006).
126. PEREIRA, Tiago. Stability of Synchronized motion in complex networks. arXiv preprint arXiv:1112.2297, 2011.
127. Perkiomaki SJ. Nonlinear dynamics of heart rate and repolarization. *International Journal of Bioelectromagnetism* 2003; 1(5):300.
128. Peuker, E. T., and Filler, T. J. (2002). The nerve supply of the human auricle. *Clin. Anat.* 15, 35–37. doi: 10.1002/ca.1089
129. Pikkujamsa SM, Makikallio TM, Airaksinen KEJ, Huikuri HV. Determinant and interindividual variation of R-R interval dynamics in healthy middle-age subjects. *Am J physiol heart Circ Physiol* 2001; 3:1400-1406.

130. Pikovsky A, Rosenblum M, Kurths J (2001) Synchronization: a universal concept in nonlinear sciences. Cambridge Nonlinear Science Series 12. Cambridge University Press, Cambridge, New York, Melbourne, Madrid, Cape Town, Singapore, São Paulo
131. Poderys, J., Bikulčienė, L., Trinkūnas, E., Poderienė, K., Buliuolis, A., & Vainoras, A. (2015). Matrix analysis of ECG parameters may be a way to improve quality of functional state monitoring during exercising. *Baltic Journal of Sport and Health Sciences*, 4(99).
132. PORTA, A. et al. Cardiovascular control and time domain Granger causality: insights from selective autonomic blockade. 2013
133. Pyragas K., "Synchronization of coupled timedelay systems: analytical estimations," *Physical Review E*, vol. 58, pp. 3067–3071, 1998.
134. Qiu, Q., Zhou, B., Wang, P., He, L., Xiao, Y., Yang, Z., & Zhan, M. (2020). Origin of amplitude synchronization in coupled nonidentical oscillators. *Physical Review E*, 101(2), 022210.
135. Quarteroni A, Fornaggia L, Veneziani A.. *Complex Systems in Biomedicine*. Springer, 2006.
136. Que CL, Kenyon CM, Olivenstein R, Macklem PT, Maksym GN: Homeokinesis and short-term variability of human airway caliber. *J Appl Physiol* 2001, 91:1131-1141.
137. Ragulskis M, Lukoseviciute K, Navickas Z, Palivonaite R (2011) Short-term time series forecasting based on the identification of skeleton algebraic sequences. *Neurocomputing* 74(10):1735–1747
138. Ragulskis M, Lukoseviciute K. Non-uniform attractor embedding for time series forecasting by fuzzy inference systems. *Neurocomputing*. 2009; 72(10):2618–2626. <https://doi.org/10.1016/j.neucom.2008.10.010>
139. Rautaharju, P.M.; Zhang, Z.M.; Prineas, R.; Heiss, G. Assessment of prolonged QT and JT intervals in ventricular conduction defects. *Am. J. Cardiol*. 2004, 93, 1017–1021.
140. Rostagno, C., Felici, M., Caciolli, S., Olivo, G., Comeglio, M., Galanti, G., & Sereni, G. G. N. (1999). Decreased baroreflex sensitivity assessed from phase IV of Valsalva maneuver in mild congestive heart failure. *Angiology*, 50(8), 655-664.
141. Sauer T, Yorke JA, Casdagli M. Embedology. *Journal of statistical Physics*. 1991; 65(3-4):579–616. <https://doi.org/10.1007/BF01053745>
142. Saunoriene, L.; Siauciunaite, V.; Vainoras, A.; Bertasiute, V.; Navickas, Z.; Ragulskis, M. The characterization of the transit through the anaerobic threshold based on relationships between RR and QRS cardiac intervals. *PLoS ONE* 2019, 14, e0216938.
143. Savitzky A, Golay MJE. Smoothing and differentiation of data by simplified least squares procedures. *Analytical chemistry*. 1964; 36(8):1627–1639. <https://doi.org/10.1021/ac60214a047>
144. Schmitt DT, Ivanov PC. Fractal scale-invariant and nonlinear properties of cardiac dynamics remain stable with advanced age: a new mechanistic Picture of cardiac control in healthy elderly. *Am J Physiol Integr Comp Physiol* 2007; 293:1923-1937
145. Schumaster A. Linear and nonlinear approaches to the analysis of RR interval variability. *Biological Research For Nursing* 2004; 3(5): 211-221.

146. Seely AJ, Christou NV: Multiple organ dysfunction syndrome: exploring the paradigm of complex nonlinear systems. *Crit Care Med* 2000, 28:2193-2200.
147. Segerstrom SC, Nes LS. Heart rate variability reflects self-regulatory strength, effort, and fatigue. *Psychol Sci.* 2007;18(3):275–81.
148. Shaffer F, McCraty R, Zerr CL. A healthy heart is not a metronome: an integrative review of the heart's anatomy and heart rate variability. *Front Psychol.* 2014;5: 1040.
149. Sharma V Deterministic chaos and fractal complexity in the dynamics of cardiovascular behavior: perspectives on a new frontier. *Open Cardiovasc Med J* 3, 110–23 (2009). [PubMed: 19812706]
150. Shen M., Chen W.-N., Zhang J., Chung H. S.-H., Kaynak O. Optimal selection of parameters for nonuniform embedding of chaotic time series using ant colony optimization. *Cybernetics*, Vol. 43, Issue 2, 2013, p. 790-802. [Search CrossRef]
151. Siauciunaite, V., Kaniusas, E., Kampusch, S., Szeles, J. C., & Vainoras, A. (2018, September). Auricular vagus nerve stimulation affects fractality of the human body as resolved by advanced ECG. In 2018 EMF-Med 1st World Conference on Biomedical Applications of Electromagnetic Fields (EMF-Med) (pp. 1-2). IEEE.
152. Sidorenko AV, Ovsyankina GI, Solonovich NA. Complex analysis of human electroencephalograms with circulatory disturbance of the brain. *An Interdisciplinary Journal* 2006; 9(1):97-104.
153. Skinner JE, Anchin JM, Weis DN. Nonlinear analysis of the heartbeats in public patient ECGs using an automate PD2i algorithm for risk stratification of arrhythmic death. *The Clin Risk manag* 2008; 4(2): 549-557.
154. Šliupaitė A, Navickas Z, Vainoras A. Evaluation of complexity of ECG parameters using sample entropy and Hankel matrix. *Electronics and Electrical Engineering* 2009; 4(92):107-110.
155. Small M., *Applied Nonlinear Time Series Analysis: Applications in Physics, Physiology and Finance* (World Scientific Series on Nonlinear Science Series a), World Scientific Pub. Co Inc., 2005.
156. Sornmo L, Wohlfart B, Berg J, Pahlm O. Beat-to-Beat QRS Variability in the 12-Lead ECG and the Detection of Coronary Artery Disease. *J Electrocardiol* 1998;31(4):336–44.
157. Spurlin JW & Nelson CM Building branched tissue structures: from single cell guidance to coordinated construction. *Philos. Trans. R. Soc. Lond. B. Biol. Sci* 372, (2017).
158. Sun Y, Chan KL, Krishan SM. Life-threatening ventricular arrhythmia recognition by nonlinear descriptor. *Biomedical Engineering OnLine* 2005; 4:1-11.
159. Svart, K.; Lehtinen, R.; Nieminen, T.; Nikus, K.; Lehtimäki, T.; Kööbi, T.; Niemelä, K.; Niemi, M.; Turjanmaa, V.; Kähönen, M.; et al. Exercise electrocardiography detection of coronary artery disease by ST-segment depression/heart rate hysteresis in women: The Finnish Cardiovascular Study. *Int. J. Cardiol.* 2010, 140, 182–188.
160. Széles, J.C.; Kampusch, S.; Le, V.H.; Enajat, D.P.; Kaniusas, E.; Neumayer, C. Clinical Effectiveness of Percutaneous Auricular Vagus Nerve

- Stimulation in Chronic Back Pain Patients-A Single-Centre Retrospective Analysis. *Ann. Pain Med.* 2021, 3, 1009.
161. Takens F., Detecting strange attractors in turbulence, *Lecture Notes in Mathematic*, 1980, 898, p. 366-381
 162. Takens F., Detecting strange attractors in turbulence: dynamical systems and turbulence, *Warwick 1980 (1981)* 366-381.
 163. Tao D., Hongfei X., Chaotic Time Series Prediction Based on Radial Basis Function Network, *Eighth ACIS International Conference*, 2007.
 164. TAO, Mei, et al. Permutation entropy based on non-uniform embedding. *Entropy*, 2018, 20.8: 612.
 165. Theiler, J. Estimating the fractal dimension of chaotic time series. *Lincoln Lab. J.* 1990, 3, 63–86. [CrossRef]
 166. Timofejeva, I.; McCraty, R.; Atkinson, M.; Joffe, R.; Vainoras, A.; Alabdulgader, A.A.; Ragulskis, M. Identification of a group's physiological synchronization with earth's magnetic field. *Int. J. Environ. Res. Public Health* 2017, 14, 998. [CrossRef]
 167. Tokmakidis, S. P. Critical Velocity and Lactate Threshold in Young Swimmers.
 168. Trefethen LN (1999) Computation of pseudospectra. *Acta Numerica* 8:247–295
 169. Tulppo MP, Hughson RL, Miakikallio TH, et al. Effects of exercise and passive head – up tilt on fractal and complexity properties of heart rate dynamics. *AJP – heart and Circulatory Physiology*, 2002; 280(3):18081–1087
 170. Tyrtyshnikov, E. E. (2012). A brief introduction to numerical analysis. Springer Science & Business Media.
 171. UBEYLI, E. Detecting variabilities of ECG signals by Lyapunov exponents. *Neural Computing and Applications*. 2009, 18(7), 653–662. ISSN: 0941-064
 172. Ursino M. Interaction between carotid baroregulation and the pulsating heart: a mathematical model. *Am J Physiol* 1998; 275:1733- 1747.
 173. Uzal L.C., Grinblat G.L., Verder P. F., Optimal reconstruction of dynamical systems: A noise amplification approach, *Physical Review E* 84, 2011.
 174. Vainoras A, Ašeriškytė D, Poderys J, Navickas Z. Fractal dimensions in evaluation in heart fluctuation parameters during physical investigations. *Education, Physical Training, Sport* 2005; 3(57):61-66.
 175. Vainoras A, Daunoravičienė A, Šiupšinskas L, Zaveckas V, Poderys J, Mauricienė V ir kt. *Kineziologija. Kaunas: Vitae Litera*; 2005.
 176. Vainoras A. Functional model of human organism reaction to load – evaluation of sportsman training effect. *Education, Physical Training, Sport*. 2002; 3: 88–93.
 177. Vainoras A. *Kardiovaskulinė sistema ir sportinė veikla. Kardiovaskulinė sistema ir sportinė veikla. Vilnius*; 1996. p. 3-8.
 178. Vazquez P, Hristovski R, Balague N. The Path to Exhaustion: Time-Variability Properties of Coordinative Variables during Continuous Exercise. *Frontiers in physiology*. 2016; 7. <https://doi.org/10.3389/fphys.2016.00037> PMID: 26913006
 179. Walker, H. K., Hall, W. D., & Hurst, J. W. (1990). Clinical methods: the history, physical, and laboratory examinations.

180. Wang J, Hu M, Ge P, Ren P, Zhao R (2014) A forecasting model for short term tourist arrival based on the empirical mode decomposition and support vector regression. In: Proceedings of 2013 4th international Asia conference on industrial engineering and management innovation (IEMI2013). Springer, Berlin, pp 1009–1021
181. Wilmore JH, Costill DL. Physiology of sport and exercise. 3rd ed. Champaign, IL: Human Kinetics, 2005.
182. Wright TG, Trefethen LN (2002) Pseudospectra of rectangular matrices. IMA J Numer Anal 22(4):501–519
183. Wu, Chai Wah (2007). Synchronization in Complex Networks of Nonlinear Dynamical Systems.
184. Yaneer Bar Yan. Complexity rising: from human beings to human civilization, a complexity profile. NESCI research projects 2003. Available at: <http://nesci.net/projects/yaneer/Civilization.html>
185. Yaragani VK, Rachunandan MS, Yaragani S, Desai N, Mallavaparapu M. Increased chaos of beat-to-beat QT interval variability in patients with congestive cardiac failure: decrease chaos of QT with clinical improvement. Cardiovascular Engineering 2002; 2:161-167.
186. Yeh, M. P., Gardner, R. M., Adams, T. D., Yanowitz, F. G., & Crapo, R. O. (1983). " Anaerobic threshold": problems of determination and validation. Journal of Applied Physiology, 55(4), 1178-1186.
187. Yuan H, Silberstein SD. Vagus nerve and vagus nerve stimulation, a comprehensive review: part I. Headache (2016) 56(1):71–8.10.1111/head.12647
188. Yuan TF, Li A, Sun X, Arias-Carrion O, Machado S. Vagus nerve stimulation in treating depression: a tale of two stories. Curr Mol Med (2016) 16(1):33–9.10.2174/1566524016666151222143609
189. Yuan, H., & Silberstein, S. D. (2016). Vagus nerve and vagus nerve stimulation, a comprehensive review: part II. Headache: The Journal of Head and Face Pain, 56(2), 259-266.
190. Yunfeng Wu, Rangaraj M. Rangayyan, Yachao Zhou and Sin-Chun Ng, "Filtering electrocardiographic signals using an unbiased and normalized adaptive noise reduction system", Medical Engineering & Physics, vol. 31, no. 1, pp. 17–26, 2009.
191. ZANIN, M. et al. Permutation Entropy and Its Main Biomedical and Econophysics Applications: A Review. Entropy. 2012, 14(8), 1553–1577. ISSN: 1099-4300. 205.
192. Zarafshar, S.; Wong, M.; Singh, N.; Aggarwal, S.; Adhikarla, C.; Froelicher, V.F. Resting ST amplitude: Prognosis and normal values in an ambulatory clinical population. Ann. Noninvasive Electrocardiol. 2013, 18, 519–529.
193. ZAYLAA, A. et al. Reducing sojourn points from recurrence plots to improve transition detection: Application to fetal heart rate transitions. Computers in biology and medicine. 2015, 63, 251–260. ISSN: 0010-4825.
194. Zenchenko, T.; Medvedeva, A.; Khorseva, N.; Breus, T. Synchronization of human heart-rate indicators and geomagnetic field variations in the frequency range of 0.5–3.0 mHz. Izv. Atmos. Ocean. Phys. 2014, 50, 736–744. [CrossRef]
195. Zhang W, Wang J, Wang J, Zhao Z, Tian M (2013) Short-term wind speed forecasting based on a hybrid model. Appl Soft Comput 13(7):3225–3233

196. Zhong, Y., & Boumal, N. (2018). Near-optimal bounds for phase synchronization. *SIAM Journal on Optimization*, 28(2), 989-1016.
197. Ziaukas P, Alabdulgader A, Vainoras A, Navickas Z, Ragulskis M. New approach for visualization of relationships between RR and JT intervals. *Plos One*. 2017; 12(4):0174279. <https://doi.org/10.1371/journal.pone.0174279>
198. Zunino, L.; Olivares, F.; Scholkmann, F.; Rosso, O.A. Permutation entropy based time series analysis: Equalities in the input signal can lead to false conclusions. *Phys. Lett. A* 2017, 381, 1883–1892. [CrossRef]

SANTRAUKA

Tyrimų objektas

Pritaikyti procesų dydžių skirtumų matricas, kad būtų galima įvertinti dinamines EKG signalo sąsajas, kiekvieną atvejų integruojant pradinius signalo duomenis į matricų sekas.

Darbo tikslas

Ištirti sukurtus netiesinės dinamikos metodus, pasiūlyti naujus algoritmus ir juos pritaikyti elektrokardiografinio signalo dinamikai stebėti.

Uždaviniai:

1. Elektrokardiografijos parametų sąsajų analizė.
2. Dinaminių procesų ir kompleksinių žmogaus kūno sistemų santykių stebėjimas kintančiomis aplinkos sąlygomis (lokalus geomagnetinis laukas, klajoklio nervo stimuliacija).
3. Naujų algoritmų, biomarkerių kūrimas esant skirtingoms fiziologinėms sąlygoms (pvz., veloergometrijos metu).
4. Lagranžo matricų skirtumų taikymas širdies parametų santykių dinamikai įvertinti.

Ginti pateikiama:

- Dviejų naujų elektrokardiografijos parametų sąsajų analizės algoritmai, nagrinėjantys širdies ir kraujagyslių sistemos dinamiką esant fiziniam krūviui.
- Elektrokardiografijos parametų ir parametų sąsajų analizės algoritmai, skirti stebėti išorinės aplinkos poveikį žmogaus širdies ir kraujagyslių sistemai.

Darbo mokslinis naujumas ir praktinė svarba:

- Naujai sukurti algoritmai, nagrinėjantys elektrokardiografijos parametų sąsajas gali būti taikomi širdies ir kraujagyslių sistemos dinamikai stebėti ir patologinėms būklėms nustatyti.
- Naujos analizės technikos, tiriančios dviejų elektrokardiografinių signalų charakteristikas, leidžia kokybiškai aptikti ir įvertinti naujus signalo pokyčius. Šios metodikos gali būti naudojamos žmonių sveikatos būklei stebėti ir įvertinti.

Metodai ir programinė įranga

Sukurti ir pritaikyti informacijos redukcijos metodai, algoritmai optimaliam atraktorių atstatymui į vėlinimo fazės plokštumas, algebrinės koreliacijos tarp širdies parametų, lokalaus magnetinio lauko ir klajoklio nervo stimuliavimo algoritmai. Visoms programoms ir algoritmams sukurti buvo naudojama MATLAB programavimo ir skaitmeninio skaičiavimo platforma. EKG parametų registracijai buvo naudojama „Kaunas-Krūvis“ sistema, lokaliai magnetiniam laukui registruoti – „HeartMath Institute“ magnetometrų tinklas, Austrijos technikos universitete sukurta technika buvo stimuliuojamas klajoklis nervas.

Darbo rezultatų aprobavimas

Disertacijos tema pateikti 6 moksliniai straipsniai, 4 straipsniai paskelbti mokslinės informacijos instituto duomenų bazės (ISI) leidiniuose, turinčiuose citavimo indeksą, 2 moksliniai straipsniai – kituose tarptautiniuose leidiniuose. Disertacijos rezultatai buvo pristatyti 3 tarptautinėse konferencijose.

Disertacijos apimtis ir struktūra

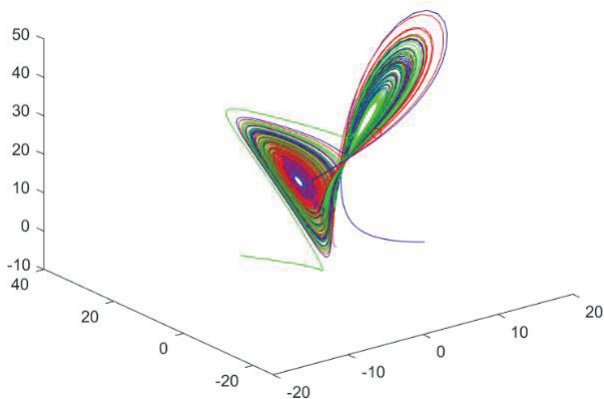
Daktaro disertaciją sudaro įvadas, 3 pagrindiniai skyriai, išvados, literatūros sąrašas ir publikacijų sąrašas. Disertacijos apimtis 126 puslapiai. Disertacijoje yra 28 paveikslai ir 198 šaltinių cituojamos literatūros aprašas.

IVADAS

Žvelgiant sistemiškai, žmogaus organizmas yra kompleksinė sistema arba, tiksliau sakant, tai yra sudėtinga kompleksinių sistemų visuma. Širdies ir kraujagyslių sistema vaidina pagrindinį vaidmenį gyvuose organizmuose. Ją sudaro labai specializuoti posistemiai, kurie sąveikauja tarpusavyje, kad atliktų gyvybiškai svarbias užduotis. Daugybė reguliavimo mechanizmų, tuo pačiu metu veikiančių skirtingomis laiko skalėmis ir galinčių keisti kintamųjų santykius, sukuria kardiovaskulinių kintamųjų dinaminį sudėtingumą (Porta ir kt., 2009). Žmogaus fiziologinių sistemų analizė kompleksinių sistemų teorijos požiūriu išlieka labai ambicinga užduotis. Problemos sudėtingumas dažnai skatina naudoti naujus matematinius metodus, analizuojančius erdvėje ir laike vykstančius procesus. Šioje disertacijoje pasirinkome elektrokardiografijos (EKG) analizę, nes tai pagrindinė ir labiausiai ištirta neinvazinė technika, naudojama šiuolaikiniam širdies ir kraujagyslių sistemos funkcionalumo tyrimui.

I. KOMPLEKSINIŲ IR CHAOTINIŲ SISTEMŲ DINAMIKA

Kompleksinės sistemos turi savybių, kurių negalima visiškai suprasti žinant atskiras sistemos dalis (Quarteroni, 2006). Kiekvienas posistemis turi savo vietinius reguliavimo mechanizmus. Norint užregistruoti, patvirtinti ir optimizuoti sisteminius efektus skirtingomis sąlygomis, reikia sisteminio stebėjimo metodų, atspindinčių netiesines kompleksines žmogaus kūno sistemas. Holistiniai modeliai aiškina žmogų kaip sudėtingą sistemą, o netiesiniai chaotiški procesai vaidina svarbų vaidmenį skirtingų posistemų ir šių posistemų reakcijų santykiuose. Chaoso teorija pradėjo formuotis dar 7-ajame XX a. dešimtmetyje (1961 m. Edvardas Lorenzas orų prognozės skaičiavimuose pastebėjo vadinamąjį „drugelio efektą“ (1 pav.). Norėdamas sumažinti skaičiavimo laiko sąnaudas, Lorenzas sugalvojo panaudoti dalį ankstesnio tyrimo duomenų. Vėliau peržiūrėjus gautus skaičiavimus paaiškėjo, kad tai buvo visiškai nauji rezultatai, nors skaičiavimai buvo analogiški anksčiau atliktiems. Atlikęs tolesnį tyrimą, jis pažymėjo, kad jo pateikti skaičiai buvo šiek tiek suapvalinti.



1 pav. Lorenzo atraktoriaus sprendinio pavyzdys

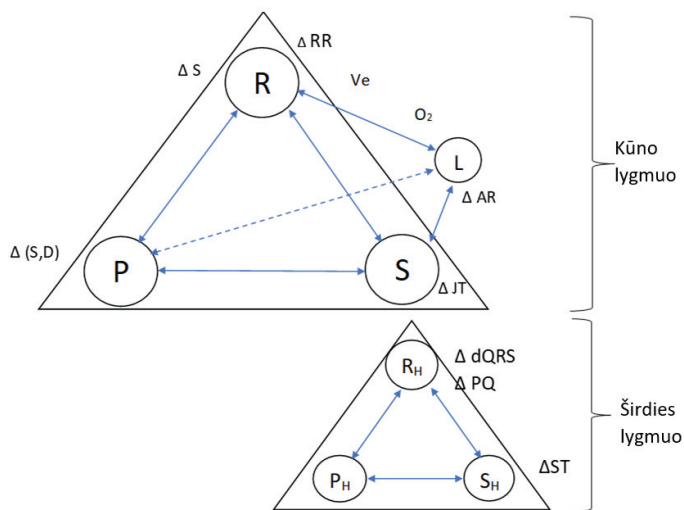
Kitas naujojo mokslo pradininkas buvo Harvis Feigenbaumas. Feigenbaumas atrado dėsni, būdingą visoms chaotiškoms sistemoms – konstantą, apibūdinančią skalių santykį tarp gretimų taško padvigubėjimo taškų. Richardas J. Cohenas su kolegomis gydytojais (Karagueuzian ir kt., 2013) pastebėjo, kad laikotarpio dvigubai padidėję išsišakojimai yra susiję su artėjančiu

širdies priepuoliu. Šis atradimas chaoso teoriją, tapusią neatsiejama širdies ir kraujagyslių (kardiologijos) mokslo dalimi, įsitvirtino ir medicinoje.

1.2. Žmogus kaip kompleksinė sistema

Apsvarstykime galimybę sukurti visų ląstelėje vykstančių cheminių reakcijų modelį. Tūkstančiai kintamųjų neabejotinai bus apibrėžti tūkstančiais diferencialinių lygčių. Pagrįsta manyti, kad tolesnė dinamika bus chaotiška, jei šias diferencialines lygtis užrašysime bendrąja forma, bet parametrus pasirinktume atsitiktinai. Nepaisant to, kad kartais kyla susidomėjimas chaoso galimybėmis biologinėse sistemose, toks bendras masinių dinaminė sistemų elgesys, teoriškai, nėra įgyvendinamas. Kiekvienas parametras yra sureguliuotas pagal tikslią teisingą vertę – parametrai visų pirma priklauso nuo detalių, kurių ląstelė negali kontroliuoti, pavyzdžiui, nuo temperatūros ar maistinių medžiagų koncentracijos aplinkoje. Pusiausvyra tarp tikslumo ir tikslaus prisitaikymo yra iššūkis, kylantis daugelyje biologinių sistemų organizacijos lygių (Bialek, 2012).

XVI amžiuje Vesalijus įvardindamas esmines žmogaus kūno sudedamąsias dalis pastebėjo išskirtines šių sistemų savybes. Šios sistemos apima visą žmogaus organizmą ir vadinamos holistinėmis: kaulų ir raumenų – periferijos sistema (P), širdies ir kraujagyslių – aprūpinančioji (angl. *Supplying*) sistema (S), o nervų – reguliacinė sistema (R). Jos veikia kiekvienos kūno ląstelės funkciją ir reaguoja į kiekvienos ląstelės poreikius, integruojant visų elementų funkcionalumą į vieningą organizmo funkcionalumą. (2 pav.). Be šių trijų sistemų, gali būti paminėta ir kvėpavimo (L) sistema, tačiau ji nėra savarankiška S sistemos atžvilgiu. Žiūrint sisteminiu požiūriu, kiekviena šios sistemos dalių sudaro atskirus posistemius (Kūno lygmens, širdies lygmens ir t. t.). Dėl to kiekvieną posistemę galime vaizduoti nauju trikampiu: R_H – širdies reguliacinė, S_H – širdies aprūpinimas maistinėmis medžiagomis (koronarinė kraujotaka), P_H – širdies periferija (miokardas). Sistemos savybių suma negali apibrėžti ir paaiškinti visų jos savybių. Kita vertus, sistema nustato, kaip veikia jos komponentai.



2 pav. Integralusis žmogaus vertinimo modelis, kaip kompleksinė sistema (adaptuota iš Vainoras, 1996)

Ryšius tarp kelių žmogaus kūno sistemų ir jų atliekamos funkcijos galima apibūdinti keliais būdais. Sudarant 2 paveikslą modelį, turimi parametrai buvo pasirinkti visiškai

neinvaziški: S – sistolinis arterinis kraujospūdis, D – diastolinis arterinis kraujospūdis, RR – laiko tarpas tarp dviejų širdies dūžių, JT – laiko intervalas elektrokardiogramoje nuo taško J iki T bangos pabaiga, ST – segmento amplitudė, dQRS – QRS komplekso trukmė, PQ – laiko intervalas EKG nuo P bangos pradžios iki Q bangos pradžios (3 pav.), Ve – įkvepiamo oro tūris per minutę, O₂ – deguonies tūris, suvartotas per minutę, AR – R dantelio amplitudė, Δ reiškia tam tikro parametro pasikeitimą.

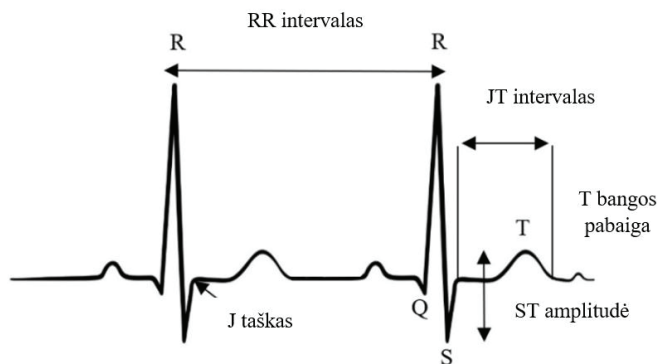
Viso žmogaus kūno funkcinės būklės modeliavimo užduotis šiandieniniam mokslui vis dar yra per sudėtinga. Todėl, remiantis kompleksinių sistemų teorija, bandoma ištirti tik tam tikrų sistemų ypatybes, jų kompleksiskumą, dinamiką ir adaptacinius pokyčius bei remiantis gautais rezultatais siekti suformuoti vieningas, kombinuotas išvadas.

1.3. Širdis kaip kompleksinė sistema

Vienas biologinių kompleksinių sistemų pavyzdžių yra širdis. Chaoso egzistavimas širdies raumenyje (miokarde) aptiriamas atliekant eksperimentinius tyrimus ir atliekant modeliavimo užduotis (Ferreira ir kt., 2011; Qu, 2011; Qu ir kt., 2014). Širdis rodo fraktalinę struktūrą tiek sisteminiu, tiek laiko aspektu. Struktūriniame lygmenyje širdies raumenys yra hierarchiški ir atspindi fraktalo savybę, paremtą skaidulomis. Fraktalų panašumas į save pasireiškia nuo molekulinės skalės mikrofilamento iki ruožuotų ląstelių ir audinių skalių, nuo nm iki μm ir cm. Struktūrizuota hierarchinė organizacija reikalinga darniai širdies audinių funkcijai – sinchronizuotam susitraukimui, kurį valdo širdies elektrinis aktyvumas. Įrodyta, kad įprastas širdies susitraukimų dažnių (ŠSD) variabilumas yra chaotiška deterministinė sistema (Lombardi, 2000), o jai tinkamai analizuoti yra naudojamos fraktalų ir daugiafraktalės analizės (Gierałtowski ir kt., 2012; Lin ir Sharif, 2010). Elektrinis širdies aktyvumas yra kintantis, pradedant nuo sinoatrialinio mazgo, baigiant kardiomiocitais ir visu organu (Sharma, 2009; Mandel ir kt., 2012). Širdies ritmas ir širdies ritmo variabilumas (HRV) priskiria du atskirus, tačiau susijusius parametrus. Abu juos galima gauti iš elektrokardiografijos rodmenų (Goncalves, 2016; Elgendy, 2012).

1.4. Elektrokardiografija

Elektrokardiografijos (EKG) parametrai ir sąajos tarp jų keičiasi atsižvelgiant į įvairias fiziologines ir patologines priežastis (Malik ir kt., 2002). EKG charakteristikos, kad ir tokia kaip RR intervalas, būdamas sisteminiu parametru, atspindi viso organizmo reguliavimo sistemos funkcinę būklę, atspindinčiu širdies ir smegenų sąveiką bei autonominės nervų sistemos (ANS) dinamiką (Shaffer ir kt., 2014; McCraty ir kt., 2009). Optimalus RR intervalų pokyčių lygis organizme atspindi sveiką funkciją, būdingą savireguliacijos pajėgumą ir prisitaikymą skirtingomis sąlygomis (McCraty ir kt., 2009; Segerstrom ir kt., 2007).



3 pav. Pagrindiniai elektrokardiografijos parametrai

Kiekvienas vertinamas parametras atspindi specifinę fiziologinę informaciją, esančią skirtinguose organizmo fraktaliniuose lygiuose. Fiksuotas ryšių tarp EKG parametrų modelis vargiai gali atitikti konkretų asmenį. Todėl tikriausiai nėra tikslinga ieškoti vieningo deterministinio modelio, kuris galėtų apibūdinti ryšius tarp EKG parametrų. Tikslinga stebėti dinaminis tarpusavio ryšių procesus, kurie galėtų parodyti sudėtingą chaotišką jų tarpusavio sąveiką. EKG parametrus galima suskirstyti į sisteminius, rodančius pokyčius aukščiausiame kūno fraktalo lygyje, ir periferinius, nurodant pokyčius organų lygyje arba susijusius su jais (Šiaučiūnaitė ir kt., 2018).

II. VIENOS IR KELIŲ DUOMENŲ SEKŲ ANALIZĖS METODAI, VERTINANTYS KOMPLEKSINIŲ SISTEMŲ DINAMIKĄ

Nors laiko eilučių analizė yra nepaprastai plati matematikos ir statistikos sritis, tačiau šiame darbe gilinsimės į kai kurias laiko eilučių algebrines transformacijas: laiko eilutės atvaizdavimą į vėlinimų erdvę bei Lagranžo matricių transformacijas.

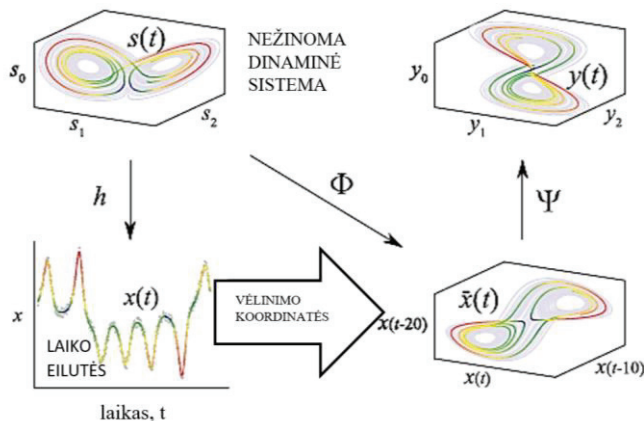
Laiko eilutė yra per tam tikrą laiką surinkta informacija – sekundė, valanda, diena, savaitė, mėnuo, ketvirtis ar metai ir pan. Laiko eilučių analizės tikslas yra rasti modelį, kuris geriausiai atspindi duomenis ir tada naudoti tą modelį, kuris ekstrapoliuotų naujausių laiko eilučių vertes į ateitį. Norint numatyti chaotiškas laiko eiles, pirmiausia reikia rekonstruoti fazinę erdvę (Tao ir Hongfei, 2007). Duomenys paprastai renkami nagrinėjant laiko eilučių dinamiką bei formą (Ning ir kt., 2010).

Skaliarinė laiko eilučių dinamika $\{x(t), t = 1, 2, \dots, N\}$ yra integruota į d -osios dimensijos vėlinimo erdvę, kurioje yra užduoti laiko tarpai. Priklausomai nuo laiko vėlinimo technikos, vėlinimo erdvė išreiškiama (Packard ir kt., 1980):

$$X(t) = (x(t), x(t - \tau), \dots, x(t - (d - 1)\tau)), \quad (1)$$

čia $t = (d - 1)\tau + 1, \dots, N, \tau$ yra laiko vėlinimas, įterpimo matmuo ir laiko linijos ilgis. Erdvės vėlavimo dimensijoje pagal d -osios dimensijos rekonstravimo taškų trajektoriją galima apibrėžti pradines charakteristikas ir dinamikos dėsningumą. Laiko vėlinimo ir rekonstrukcijos matmenys yra svarbūs erdvės rekonstrukcijai (Kim ir kt., 1999).

4 paveiksle parodytas erdvės vėlinimo rekonstrukcijos procesas, pradedant nuo išmatuoto proceso. Bendriausia vėlinimo erdvės formos vektoriaus rekonstrukciją galima apibūdinti d -matmenų vektoriumi $y(t) = \Psi[\bar{x}(t)]$, čia $\bar{x}(t) = \{x(t), x(t - \tau), \dots, x[t - (d - 1)\tau]\}$ yra vėlinimo vektorius laike t ir $\Psi: \mathbb{R}^d \rightarrow \mathbb{R}^n$ yra tolesnė rekonstrukcija, nagrinėjanti bendresnės rekonstrukcijos galimybę (nereguliarus laiko vėlinimas, globalios ar lokalios reikšmės dalijimasis arba triukšmo panaikinimo algoritmai) (Mayra, 2006). Viršutinis grafikas kairėje 4 paveiksle yra tikroji sistema. Jei galime išmatuoti tik vieno sistemos kintamojo reikšmes (apatinis grafikas 4 pav. kairėje), jo rekonstrukcija praktiškai pakartoja pačios sistemos dinamiką (lyginant du grafikus dešinėje).



4 pav. Dinaminės sistemos atraktoriaus rekonstrukcijos ir matavimo proceso schema (Uzal ir kt., 2011)

Laiko eilučių prognozė yra sudėtinga tema įvairiose mokslo srityse. Yra dviejų rūšių laiko eilučių prognozavimo būdai: ilgalaikiai ir trumpalaikiai laiko eilučių prognozavimo metodai. Pratęsus ilgalaikius laiko eilučių prognozavimo metodus, paprastai bandoma sukurti proceso modelį, o vėliau jį panaudoti elgesiui ilgiems laikotarpiams ateityje. Trumpalaikiai laiko eilučių prognozavimo metodai turi tą patį pagrindinį tikslą: sukurti proceso modelį ir jį projektuoti į ateitį. Deja, kadangi pateiktų duomenų kiekis dažnai būna ribotas, metodų taikymas kuriant ilgalaikį laiko eilučių prognozavimo modelį trumpoms laiko eilutėms paprastai yra sudėtingas uždavinys.

Kelių laiko eilučių susietumo analizė turi giliai išsiskynusias tradicijas matematikoje, tačiau šioje disertacijoje nagrinėjame dvimačių kvadratinų matricų transformacijas.

Norint pasirinkti kiekvienai konkrečiai problemai tinkamiausią algoritmą, svarbu nustatyti visų galimų algoritmų efektyvumą ir tikslumą. Kaip ir kitose laiko eilučių analizės situacijose, du pagrindiniai aspektai yra algoritmų kompleksiskumas ir jų skaitinis stabilumas. Nustatyti algoritmo kompleksiskumą reiškia surasti viršutinės ribas arba įvertinti, kiek elementarių operacijų, tokių kaip skaliarų pridėjimas ir dauginimas, reikia tam tikram algoritmui realizuoti, pavyzdžiui, matricų dauginimui.

Matricos skaičiavimus dažnai galima atlikti naudojant skirtingas technikas. Daugelį problemų galima išspręsti tiek tiesioginiais algoritmais, tiek iteraciniais metodais. Pavyzdžiui, kvadratinės matricos tikrinių reikšmių vektorius galima gauti radus vektorių x_n seką, kai n eina į begalybę (Householder ir Alston, 1975).

Jei matrica yra kvadratinė, galima apskaičiuoti kai kurias jos savybes apskaičiuojant jos determinantą. Atsižvelgiant į skaliarinę laiko eilutę, kintamųjų išvestines galima įvertinti skaičiavimais pagal Lagranžo (angl. *Lagrange*) skirtumus laiko eilučių mazgo taške. Gerai žinoma, kad iš skaliarinių laiko eilučių rekonstruoti dariniai linę sustiprinti triukšmą, įtvirtintą toje eilutėje. Tobula Lagranžo skirtumų matrica (Žiaukas ir kt., 2017), antros eilės kvadratinė matrica, o tos matricos elementai atitinka šiuos reikalavimus:

1. Visi matricos elementai yra skirtingi.
2. Nulinės eilės skirtumai yra išdėstyti pagrindinėje įstrižainėje.
3. Pirmos eilės skirtumai yra ant antrinės įstrižainės.
4. x ir y indeksai gali gauti vieną iš trijų galimų reikšmių: $i \in \{n - \delta, n, n + \delta\}$, kur n yra dabartinis laiko momentas ir δ – laiko vėlinimas; $\delta \in \mathbb{N}$.
5. Tobula Lagranžo skirtumų matrica yra leksikografiškai subalansuota – x ir y simbolių skaičius visų matricos elementų išraiškose yra vienodas.

Natūralus klausimas yra apie skirtingų tobulų Lagranžo skirtumų matricų skaičių. Grafinis tobulų Lagranžo skirtumų matricų vaizdavimas padėtų šias matricas klasifikuoti ir interpretuoti jų struktūrą. Nulinės eilės skirtumai ($\pm x$ ir $\pm y$) yra ant pagrindinės įstrižainės, tačiau šių elementų rodikliai gali būti skirtingi.

Kaip minėta anksčiau, turi būti pasirinktas skaliarinis parametras, vaizduojantis vietines sąsajas, aprašytas pagal tobulas Lagranžo skirtumų matricas. Apskritai, tokio parametro parinkimas yra netinkama atvirkštinė parametų identifikavimo problema. Tam, kad būtų galima įvertinti ir palyginti skirtingus parametrus dėl jų reprezentatyvumo, reikia apibrėžti tam tikrą klaidos funkciją.

III. NETIESINĖS DINAMIKOS ALGORITMŲ TAIKYMAS KARDIOSIGNALŲ ANALIZĖJE

3.1. Anaerobinio slenkščio nustatymo algoritmas

Sporto medicinoje dažniausiai vartojamas terminas „anaerobinis slenkstis“ (AeS) yra patikimas ir galingas krūvio efektyvumo prognozuotojas. AeS apskaičiuojamas taikant keletą skirtingų patvirtintų metodų (McArdle ir kt., 2000; Conconi ir kt., 1985; Ballarin ir kt., 1989). Šiame tyrime buvo laikomasi visų būtinų bioetikos standartų. 2015 m. gruodžio 23 d. Kauno regioninis biomedicininis tyrimų etikos komitetas Nr. BE-2-51 patvirtino leidimą atlikti biomedicininis tyrimus. Širdies intervalai buvo matuojami naudojant Lietuvos sveikatos mokslų universiteto Kardiologijos institute sukurta EKG analizės sistemą „Kaunas–Krūvis“ (Vainoras ir kt., 1998). DQRS intervalas buvo įvertintas naudojant EKG II derivacijos širdies skilvelių depoliarizacijos laiką.

„Kaunas–Krūvis“ sistema leidžia vienu metu įrašyti 12 skirtingų EKG standartinių parametrų. Matavimas pradedamas esant nulinei apkrovai ir tęsiamas vieną minutę. Po to apkrova padidinama 25 W per minutę. Viso dviračio ergometrijos pratimo metu dalyvis turi išlaikyti pastovų 60 apsisukimų per minutę sukimosi greitį. Amerikos širdies asociacijos teigimu, pratimas turėtų būti tęsiamas tol, kol pasirodys pirmieji klinikiniai krūvio ribojimo požymiai. Atsigavimo laikotarpiu EKG registruojama dar 10 minučių. Viso eksperimento metu matuojamas sistolinis ir diastolinis kraujo spaudimas, kurie fiksuojami kiekvienos minutės viduryje. Atliekant veloergometrijos pratimą ir atsigavimo proceso metu, taip pat buvo matuojamas deguonies ir anglies dioksido santykis iškvepiamame ore.

Du EKG parametrai (RR ir QRS trukmės intervalai) nuolat matuojami viso eksperimento metu ir atitinkamai žymimi kaip vektoriai $x = (x_1, x_2, \dots, x_n)$ ir $y = (y_1, y_2, \dots, y_n)$. Ryšys tarp laiko eilučių x ir y vertinamas naudojant (Žiaukas ir kt., 2017) pateiktą skaičiavimo techniką. Algoritmą sudaro trys pagrindinės dalys.

1. Visų pirma, laiko eilutės x ir y elementai yra įterpiami į tobulų matricų seką iš Lagranžo skirtumų $L_{\delta,k} = \begin{bmatrix} x_k & x_{k+\delta} - y_{k+\delta} \\ x_{k-\delta} - y_{k-\delta} & y_k \end{bmatrix}$; $k = (1 + \delta), (2 + \delta), \dots, (n - \delta)$; $\delta \in \mathbb{N}$.

Žvelgiant iš topologinės pusės, dvi skaliarinės trajektorijos yra įterptos į vieną trijų dimensijų trajektorijos matricą.

2. Matricų seka $L_{\delta,k}$ transformuojama į matricų $L_{\delta,k}$ savybių didžiausių modulių reikšmių skaliarinę seką, kuri yra žymima kaip $s_{\delta,k} = \max|\lambda(L_{\delta,k})|$. Atkreipkite dėmesį, kad visuose skaičiavimo eksperimentuose naudojamas fiksuotas matricos parametras (didžiausia dviejų $L_{\delta,k}$ savybių reikšmių modulio vertė).

3. Galiausiai taikomas vidinis ir išorinis lyginimas $s_{\delta,k}$. Pažymėkime vidinio lyginimo spindulį R_i ; išorinio išlyginimo spindulys – kaip R_e ($R_i, R_e \in \mathbb{N}$). Tada išlyginta seka skamba:

$$p_k(R_i, R_e) = \frac{1}{(2R_e + 1)R_i} \sum_{j=k-R_e}^{k+R_e} \sum_{\delta=1}^{R_i} S_{\delta j} \quad (2)$$

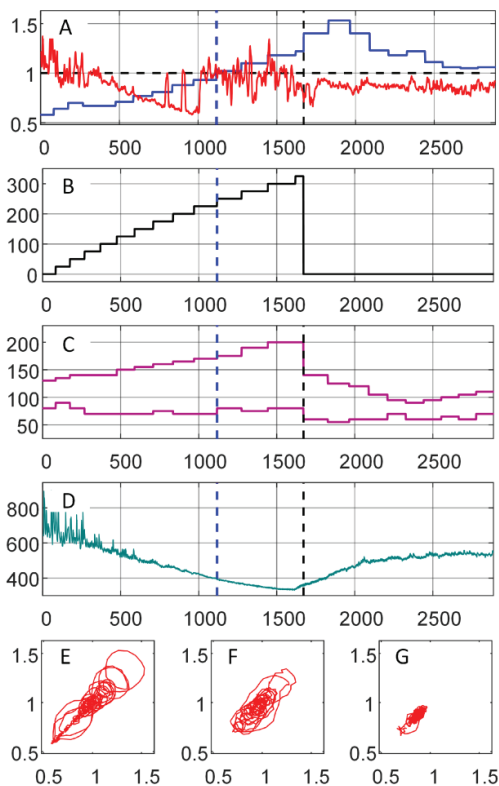
Atkreipkite dėmesį, kad apskaičiuojant $p_k(R_i, R_e)$ reikia kelis kartus įterpti x ir y į skirtingų trajektorijų matricas. Parametrų seka $p_k(R_i, R_e)$ naudojama sąryšiui tarp širdies intervalų RR ir DQRS skaliarinių sekų, žymimų kaip vektoriai x ir y atitinkamai.

Gera išdėstyta optimizavimo problema yra suformuluota (Žiaukas ir kt., 2017) R_i, R_e parametrų atžvilgiu. Mes nekartojame optimizavimo procedūrų ir visuose tolesniuose skaičiavimuose laikome fiksuotus $R_i = 3$ ir $R_e = 4$. Tiriant santykius tarp RR ir QRS trukmės

intervalų, naudojamas algoritmas yra toks pat kaip (Žiaukas ir kt., 2017), išskyrus tai, kad dabar y reiškia QRS trukmės intervalų seką.

Be EKG matavimo, viso krūvio ir atsigavimo proceso metu matuojamas sistolinis ir diastolinis kraujo spaudimas ir santykis tarp anglies dvideginio ir deguonies iškvėpiamame ore.

Pirmojo asmens santykių tarp RR ir DQRS širdies intervalų raida pavaizduota 5 paveiksle. A, B ir C dalyse esanti x ašis rodo širdies ciklą skaičių nuo veloergometrijos pradžios. Krūvio galia parodyta 5B paveiksle. Eksperimento pradžioje asmuo 1 minutę sėdi ramybėje. Tada apkrova padidinama po 25 W kiekvieną minutę iš eilės. Veloergometrija tęsiama 13 minučių ir nutraukiama 14-osios minutės viduryje esant maksimaliai 325 W apkrovai. Atkreipkite dėmesį, kad intervalų ilgis, pavaizduotas 5B paveiksle, nėra vienodas dėl didėjančio širdies ritmo (į kiekvieną minutę telpa skirtingas širdies ciklų skaičius). Atsigavimo procesai dar fiksuojami 10 minučių po veloergometrijos pratimo pabaigos.



5 pav. Perėjimo per AeS vizualizavimas asmeniui Nr. 1. Dalis (A): raudona ištisinė linija iliustruoja ryšį tarp RR ir DQRS širdies intervalų; mėlyna ištisinė linija – santykis tarp CO_2 ir O_2 koncentracijos iškvėpiamame ore (horizontali brūkšniuota juoda linija pažymima, kai šis santykis lygus 1). B dalis: juoda ištisinė linija rodo apkrovą dviračio ergometrijos pratimo metu. C dalis: rausvos vientisos linijos rodo sistolinio ir diastolinio kraujo spaudimo kitimą pratimo metu. D dalis: žydra ištisinė linija rodo RR intervalo kitimą pratimo metu. Vertikalios punktyrinės mėlynos linijos žymi AeS slenkstį; vertikalios punktyrinės juodos linijos – pratimo nutraukimas A, B, C ir D dalyse. Horizontalios ašys dalyse (A)–(D) reiškia iš eilės einantį širdies plakimą. Rekonstruotas atraktorius laiko intervale nuo matavimo pradžios iki AeS rodomas (E) dalyje; nuo AeS iki pratimo (F) dalies pabaigos; nuo pratimo pabaigos iki matavimo pabaigos (G) dalyje.

Anglies dioksido ir deguonies santykis iškvepiamame ore per veloergometrijos pratimą ir atsigavimo procesą parodytas 5A paveiksle (mėlyna vientisa linija). Anaerobinis slenkstis, kai anglies dioksido ir deguonies santykis iškvepiamame ore tampa lygus 1, pažymėtas vertikalia brūkšniuota mėlyna linija. Algebrinis santykis tarp RR ir DQRS intervalų yra pavaizduotas plona vientisa raudona linija 5A pav. Svarbu pažymėti, kad kompleksiskumo mažėjimas, kurį rodo šis ryšys, įvyksta ne veloergometrijos pratimo nutraukimo momentu (Žiaukas ir kt., 2017), bet ties anaerobine riba (5A pav.). Širdies sistema pradeda ieškoti naujos stabilios būsenos prieš anaerobinį slenkstį, tačiau perėjimas į naują būseną yra per anksti ir sistema grįžta į laipsniško kompleksiskumo kritimo režimą. Tačiau santykis tarp RR ir DQRS rodo perėjimą į visiškai kitokią būseną prieš pat anaerobinę ribą (5A pav.). Šį perėjimą galima paaiškinti būtinybe rasti naują širdies sistemos saviorganizacijos režimą, kuris atveria naujas funkcines galimybes atlikti padidėjusį fizinį krūvį. Širdies sistemos reakcija į kompleksiskumo kritimą prieš anaerobinį slenkstį pavaizduota fazinių plokštumų diagramoje 5E pav. Norėdami rekonstruoti atraktorių, mes naudojame dvimatę rekonstravimo procedūrą su beveik optimaliu laiko vėlinimu (Žiaukas ir kt., 2017). 5F pav. atraktorių rekonstruojamas laiko intervale tarp anaerobinės ribos ir veloergometrijos pratimo pabaigos momento. Galiausiai, 5G pav. atraktorių nurodo intervalą nuo veloergometrijos pabaigos iki matavimo pabaigos. Geometrinė atraktoriaus figūra 1E paveiksle iliustruoja laipsnišką širdies sistemos kompleksiskumo kritimą ir naujos būsenos procesą. 5F pav. atraktorių rodo kintančią širdies sistemos dinamiką naujoje poanaerobinėje būsenoje. 5G pav. atraktorių parodo ramų atsigavimo procesą. Mes teigiame, kad toks perėjimas per anaerobinį slenkstį būdingas sveikam žmogui. Tiesą sakant, sistolinio ir diastolinio slėgio kitimas pratimo metu ir po jo (5C pav.) rodo, kad asmuo be problemų galėjo atlikti dviračio veloergometrijos pratimą. Diastolinis kraujospūdis sumažėjo fizinio krūvio pradžioje; jis neviršijo pradinio rodmenų iki veloergometrijos pratimo pabaigos. Sistolinis kraujospūdis nuolat didėjo atliekant pratimą, bet galiniame taške neviršijo 200 mmHg. Ir sistolinis, ir diastolinis slėgis sumažėjo iškart po pratimo pabaigos ir normalizavosi atsigavimo proceso metu. Algebrinio santykio tarp RR ir DQRS intervalų nukrypimas į kompleksiskumo kritimą prieš pat anaerobinį slenkstį signalizuoja apie tiesioginių santykių tarp RR ir DQRS intervalų padidėjimą šio dviračio ergometrijos pratimo metu. Šių santykių svyravimas prieš anaerobinį slenkstį iliustruoja širdies sistemos pastangas persiorganizuoti į naują darbo režimą.

Teigiame, kad šis saviorganizacijos būdas parodo, kad širdies sistemos reguliavimo veiksmas yra fiziškai įgyvendinami ne tik gebant keisti širdies ritmą, bet ir sugebant pertvarkyti vidinius širdies procesus.

3.2. Išeminių epizodų nustatymo algoritmas

Šiame tyrime mes tyrėme JT / ST santykį, kuris bus naudojamas ne tik apibūdinant individualią žmogaus organizmo reakciją krūvio ir atsigavimo procesų metu, bet ir norint nustatyti išeminius pokyčius širdyje. Pateikti tyrimai atitiko visus etikos reikalavimus eksperimentams. Kauno regioninis biomedicininis tyrimų etikos komitetas, patvirtino leidimą Nr. BE-2-51.

EKG registracija pradeda dviračio ergometrijos pratimo pradžioje, kai nustatyta 50 W apkrova. Apkrova dvi minutes laikoma pastovi, o tada padidinama 50 W. Asmens prašoma per visą dviračio ergometrijos pratimą išlaikyti pastovų dviračio ergometro sukimosi greitį, esant 60 apsisukimų per minutę. Testas nutraukiamas, kai asmuo neišlaiko mynimo greičio arba pagal Amerikos širdies asociacijos rekomendacijas pastebimos pirmosios klinikinės krūvio ribojimo indikacijos.

Grupę sudarė dešimt fiziškai aktyvių vyrų, kurie nebuvo profesionalūs sportininkai. Vidutinis amžius yra 41,86 metai, svoris 80,29 kg, o KMI – 24,54 kg / m². Kadangi trims

pacientams pasireiškė klinikiniai krūvio apribojimų požymiai, apkrova buvo fiksuota tik vieną minutę, kol ji padidėjo 50 W.

Viso eksperimento metu JT intervalo ilgis ir ST amplitudė yra nuolat ir sinchroniškai registruojami ir žymimi kaip vektoriai $x = (x_1, x_2, \dots, x_n)$ ir $y = (y_1, y_2, \dots, y_n)$ atitinkamai; kur n yra viso širdies susitraukimų skaičius, užfiksuotas per visą eksperimentą. Algoritmas, įvedęs minėtus dydžius eksperimentus, naudojamas algebriniam ryšiui tarp laiko eilučių x ir y atkurti.

Matricų seka $L_{\delta,k}^{(\beta)}$ transformuojama į skaliarinę seką, naudojant atvaizdavimą $\mathcal{F}: \mathbb{R}^{2 \times 2} \rightarrow \mathbb{R}^1$, kur $\beta \in \{1, 2, \dots, 18\}$. Kartografavimas \mathcal{F} apibrėžiamas kaip didžiausias dviejų $L_{\delta,k}^{(\beta)}$ reikšmių modulis (Ziaukas, 2017) ir (Saunoriene, 2019). Apibendrinami kartografavimą (angl. *mapping*), šiame darbe nustatydami $\mathcal{F} = \|L_{\delta,k}^{(\beta)}\|$. Matricos norma $\|A\| = \sup_{z \in \mathbb{R}^2} \left(\frac{\|Az\|_2}{\|z\|_2} \right) = \sup_{z, \|z\|_2=1} (\|Az\|_2) \geq \max(|\lambda_1|, |\lambda_2|)$, kur λ_1 ir λ_2 yra dvi A tikrinės reikšmės, o 2-norma yra euklidinė norma (Saunoriene ir kt., 2019) Atkreipkite dėmesį, kad nelygybė tampa lygybe, kai matrica A yra simetriška. Todėl padidiname metodo jautrumą, pakeisdami maksimalų tikrinių reikšmių modulį kartografavimo apibrėžime esančią normą.

Galiausiai skaliarinei sekai yra taikomas vidinis ir išorinis glodinimas $\|L_{\delta,k}^{(\beta)}\|$. Jei vidinio glodinimo spindulys yra R_i , o išorinio glodinimo spindulys yra R_e , tada glodinta seka, vaizduojanti algebrinį ryšį tarp laiko eilučių x ir y , skamba taip:

$$s_k(R_i, R_e, \beta) = \frac{1}{R_i(2R_e + 1)} \sum_{j=k-R_e}^{k+R_e} \sum_{\delta=1}^{R_i} \|L_{\delta,j}^{(\beta)}\|, \quad (3)$$

čia $k = (1 + R_i + R_e), (2 + R_i + R_e), \dots, (n - R_i - R_e)$. Glodinimo parametrų optimizavimo problema yra suformuluota anksčiau pateiktame eksperimente visai asmenų grupei, $R_i = 3$, $R_e = 4$ ir $\beta = 1$. Šios parametrų vertės ir šiame darbe yra fiksuotos. Visi kiti skaičiavimai yra pagrįsti $s_k(3, 4, 1)$.

Mes iškeliame hipotezę, kad du iš eilės algebrinių santykių sumažėjimai tarp JT intervalo trukmės ir ST amplitudės veloergometrijos pratimo metu gali būti naudojami ankstyvam išeminės širdies ligos epizodų nustatymui.

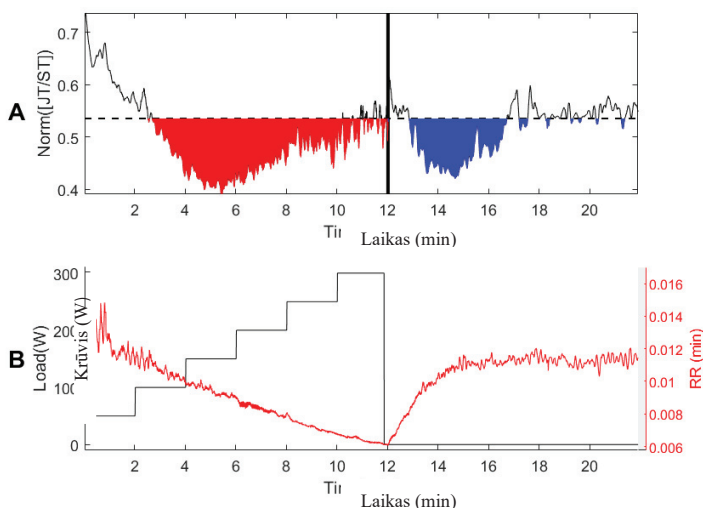
Siūlome šį algoritmą, kad būtų galima kiekybiškai apibūdinti du nuoseklius tarpparametrinės sąsajos sumažėjimus. Stebėjimo lange, pagrįstame veloergometrijos pratimo momento nutraukimu, randame vidutinę algebrinio ryšio tarp JT intervalo ilgio ir ST amplitudės vertę. Vidurkis yra būtinas norint sumažinti vietinį poveikį, kurį sukelia papildomas neišvengiamas triukšmas. Siūlome naudoti stebėjimo langus su 3 kartų žingsniais, kurių vidutinis spindulys yra aplink pratimo nutraukimo momentą.

$$\bar{S} = \frac{1}{7} \left[s_T(3, 4, 1) + \sum_{j=1}^3 (s_{T-j}(3, 4, 1) + s_{T+1}(3, 4, 1)) \right] \quad (4)$$

Toliau, užfiksuojame viršutinę ribą ties \bar{S} ir atskirai pažymėkite sritis žemiau \bar{S} ir JT / ST algebrinę sąsają skirtingomis spalvomis krūvio ir atkūrimo procesams.

JT / ST santykio dinamika per krūvio ir atsigavimo etapus iliustruojama ir aptariama sveikiems asmenims ir asmenims, kuriems įtariama išeminė širdies liga.

6A paveiksle raudona spalva pažymėtas visas algebrinių santykių funkcijos plotas pagal \bar{S} fizinio krūvio metu. 6A paveiksle mėlynai pažymėtas visas algebrinių santykių funkcijos plotas pagal \bar{S} atsigavimo proceso metu. Atkreipkite dėmesį, kad stora juoda vertikali linija žymi krūvio pabaigą (ir atsigavimo proceso pradžią), o plona juoda punktyrinė horizontali linija – skaitinė \bar{S} vertė 6A paveiksle.

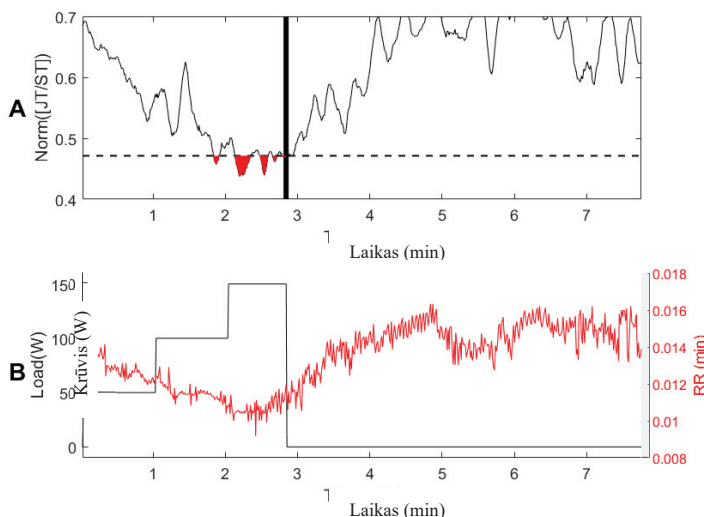


6 pav. JT / ST santykio dinamika krūvio metu ir atsigavimo procesai asmeniui Nr. 1. X ašis dalimis (A, B) rodo laiką (matuojamą minutėmis) nuo veloergometrijos pratimo pradžios. Kairioji y ašis (B) rodo krūvio galią vatais. Dešinioji y ašis (B) rodo RR intervalo kitimą min. Algebrinę JT / ST sąsają vaizduoja plona punktyrinė juoda linija A dalyje. Stora juoda vientisa vertikali linija A dalyje žymi krūvio pabaigą.

Galima pastebėti, kad JT / ST santykio kintamumas auga prieš nutraukiant krūvį. JT / ST santykis tampa labiau svyruojantis ir pratimo pabaigos momentu išauga iki lokalaus maksimumo ir taip sudaro pirmąją duobę krūvio proceso metu (raudona spalva pažymėta 6A paveiksle).

Veloergometrijos eksperimentų su sveikais žmonėmis rezultatai rodo, kad dvigubas nuoseklus JT / ST santykio sumažėjimas (raudona ir mėlyna duobės) gali būti naudojamas subtiliai apibūdinant širdies ir kraujagyslių sistemos saviorganizacijos procesus krūvio ir atsigavimo metu.

Asmuo Nr. 2 turėjo išemijos pasireiškimą miokarde ir pratimą galėjo tęsti mažiau nei 4 min. (7 pav.). Pirmasis algebrinio santykio sumažėjimas krūvio metu neturėjo pakankamai laiko išsivystyti (7A pav.). Atsigavimo proceso metu visiškai nėra mėlynos duobės. Tiesą sakant, JT / ST santykių trajektorija atsigavimo proceso metu primena chaotišką procesą. Sutrinka širdies ir kraujagyslių sistemos gebėjimas savarankiškai organizuotis, o situacija, akivaizdžiai, yra valdoma energetinių medžiagų trūkumu miokarde.



7 pav. Asmens Nr. 2 JT / ST santykio dinamika krūvio metu ir atsigavimo procesai. *X* ašis dalimis (A, B) rodo laiką (matuojamą minutėmis) nuo dviračio ergometrijos pratimo pradžios. Kairioji *y* ašis (B) rodo krūvio galią vatais. Dešinioji *y* ašis (B) rodo RR intervalo kitimą min. Algebrinę JT / ST sąsają vaizduoja plona punktyrinė juoda linija A dalyje. Stora juoda vientisa vertikali linija A dalyje žymi krūvio pabaigą.

Kiekvienas vertinamas parametras atspindi tik tam tikrą, specifinę fiziologinę žmogaus kūno funkcijos informaciją. Visos organų valdymo sistemų grandinės, kurios buvo įjungtos krūvio metu, atsigavimo proceso metu grįžta į pradinį lygį (sveikiems žmonėms). Tiesą sakant, minimalus visų stebėtų asmenų JT / ST santykio lygis buvo nuo 0,3 iki 0,5. Mes manome, kad žmogaus organizmui pasiekus šią ribą, ji nebegali nukristi žemiau, tada vyksta širdies ir kraujagyslių sistemos persitvarkymas. Repoliarizacijos proceso metu yra du galimi variantai – kompensaciniai mechanizmai sveikiems žmonėms yra įjungti, o asmenims, sergantiems išemine širdies liga, visiškai nesubalansuoti.

3.3. Žmogaus širdies ritmo sinchronizavimas su lokaliu Žemės magnetiniu lauku

Nustatyta, kad egzistuoja tiesioginis santykis tarp lokalaus Žemės magnetinio lauko ir žmonių širdies ir kraujagyslių sistemos. Keliame hipotezę, kad lokalus Žemės magnetinis laukas sinchronizuojasi ir turi įtaką žmogaus širdies ritmui. Stebėjome penkių valstybių grupes, kurios buvo atskirtos dideliu geografiniu atstumu, norėdami sužinoti, ar širdies ritmo variabilumo (ŠRV) sinchronizavimas su geomagnetiniu lauku vyksta visame pasaulyje.

2015 m. vasario 26 d. – kovo 13 d. 15 dienų trukmės tyrime dalyvavo 104 žmonės iš Kalifornijos, Lietuvos, Saudo Arabijos, Naujosios Zelandijos ir Anglijos. Globalios darnos (angl. *global coherence*) stebėjimo magnetometrai (McCraty ir kt., 2015) yra tose šalyse, todėl jų pasirinkimas buvo pagrįstas jų geografinė vieta. Tyrimų koordinatoriai kiekvienoje iš penkių vietovių iš viso įtraukė 104 savanorius.

ŠRV stebėjimas yra neinvazinis tyrimas, kuris atskleidžia žmogaus autonominės nervų sistemos dinaminę veiklą (Shaffer ir kt., 2014). Dalyviai turėjo 24 valandas per parą registruojamus ambulatorinius HRV įrašus dvi savaites, nuo 2015 m. vasario 26 d. iki kovo 12 d. Tyrimo pradžioje vietos koordinatoriai informavo kiekvieną dalyvį, kaip pritvirtinti, įjungti

ir sustabdyti ŠRV registratorius („Bodyguard2“, „Firstbeat Technologies Ltd.“, Jyvaskylä, Suomija).

Dalyviams taip pat buvo suteiktos instrukcijos, kaip užrašyti kasdienę veiklą, pvz., miego ir pabudimo laikotarpius. Modifikuotoje V5 (EKG normatyvai) padėtyje buvo naudojami „Ambu Blue Sensor L“ mikroporiniai vienkartiniai elektrodai. 1000 Hz imties dažniu ŠRV registratorius pagal elektrokardiogramą apskaičiavo intervalus tarp dviejų širdies susitraukimų (IBI – Inter Beat Intervals). RR intervalai (tapatūs IBI) buvo laikomi ŠRV registratoriaus atmintyje, kurie, tyrimo pabaigoje, buvo perkelti į duomenų rinkimo svetainę.

Programinis paketas DADiSP 6.7 buvo naudojamas ŠRV duomenims įvertinti, kai jie buvo atsisiųsti į duomenų rinkimo svetainę. Remiantis ŠRV darbo grupės (Novak ir kt., 1997) rekomendacijomis, visi ŠRV įrašai buvo padalyti į 5 minučių segmentus. Dėl skirtingų dalyvių skirtingų laiko juostų ŠRV duomenys buvo renkami 15 dienų, kad būtų gauti 14 pilnų dienų duomenys.

Magnetometrai (Zonge Engineering ANT-4) buvo naudojami rinkti duomenis apie lokalaus magnetinio lauko intensyvumą penkiose vietose. Kiekvienoje vietoje magnetometrą sudaro dvi, šiaurės–pietų ir rytų–vakarų ašyse išdėstytos antenos, registruojančios magnetinio lauko stiprumą (jautrumas 1 pT) dažnių diapazone (0,01–130 Hz) su plokščiu dažnio atsaku.

Širdies užrakinimo (angl. *Heart-lock-in*) procedūra. Kovo 5 d. Kiekviena grupė asmeniškai susitiko atitinkamose vietose 15 minučių trukmės „Heart-Lock-In“(HLI) sesijos metu. HLI technikos požiūriu siekiama padidinti žmogaus sugebėjimą išlaikyti nuoširdžias laimingas emocijas (McCraty, R ir kt., 2006; McCraty ir kt., 2016; p. 126). Buvo realizuotas grupių susijungimas per „Skype“ skambutį, kad grupės galėtų jaustis labiau susijusios. HLI eigos žingsniai buvo garsiai perskaityti per kompiuterio garsiakalbius, kad visi kambaryje esantys žmonės juos girdėtų:

„1 žingsnis: susikoncentruoti ties širdies sritimi. Įsivaizduoti, kad jūsų kvėpavimas eina ir išeina iš krūtinės ar širdies, šiek tiek lėtesnis ir gilesnis nei įprasta.

2 žingsnis: inicijuoti ir palaikyti regeneruojančias emocijas, tokias kaip dėkingumas, rūpestis ar užuojauta.

3 žingsnis: pasidalinti tuo atgaivinančiu pojūčiu su kitais.“

Ši technika paprastai siejama su ramybės, harmonijos ir vidinės šilumos jausmais ir buvo įrodyta, kad tai yra patikimas širdies ritmo darnos stiprinimo būdas (McCraty ir Tomasino, 2006). Tai taip pat puikus būdas išsklaidyti sukauptą stresą ir nemalonius jausmus.

Lokalaus magnetinio lauko galios apskaičiavimas. Pagrindinė tyrimo dalis buvo apskaičiuoti magnetinio lauko intensyvumo spektrogramą vienas po kito einantiems sekundžių intervalams, nustatyti spektro amplitudę ir susumuoti spektrinės galios vertes dažnių juostoje tarp 0,2 ir 3,5 Hz (Timofejeva ir kt., 2017; McCraty ir kt., 2017; Alabdulgader ir kt., 2018).

Po to buvo naudojamas „Hampel“ filtras, kuris pašalino žaibo, žmogaus sukurtų šaltinių ir kitų veiksmų keliamą triukšmą iš magnetinio lauko spektrinės galios laiko eilutės kiekvienoje vietoje (Pearson ir kt., 2015; Hampel, 1971).

Dalyvių HRV ir Žemės magnetinio lauko sinchronizavimas. Sinchronizacijos laipsnis tarp grupių ŠRV ir lokalaus magnetinio lauko spektrinės galios buvo nustatytas naudojant metodus, paskelbtus straipsnyje (Timofejeva ir kt., 2017). Trumpas modifikuoto metodo aprašymas pateiktas toliau.

Imkime dvi sinchroniškai atrinktas duomenų eilutes kaip pavyzdį $RR = (RR_1, \dots, RR_n)$ ir $M = (M_1, \dots, M_n)$, proporcingus dalyvio ŠRV (RR) ir lokalaus magnetinio lauko (M) spektrinei galiai.

RR ir M duomenų signalai yra suskirstyti į $T5$ - min stebėjimo langus, o kiekvienam stebėjimo langui sukonstruojamos tinkamos laiko vėlinimo vertės ŠRV laiko eilutėms ($\tau_*^{(RR)} = (\tau_{*1}^{(RR)}, \dots, \tau_{*T}^{(RR)})$) ir magnetinio lauko spektrinės galios duomenų signalui ($\tau_*^{(M)} = (\tau_{*1}^{(M)}, \dots, \tau_{*T}^{(M)})$).

Norint rasti vidutinius ŠRV ($\bar{\tau}_*^{(RR)}$) ir magnetinio lauko duomenų M ($\bar{\tau}_*^{(M)}$), laiko vėlinimo pokyčius, gauti idealūs laiko vėlinimo vektoriai išlyginami naudojant slenkančio vidurkio algoritmą. Slenkantis vidurkis apskaičiuojamas naudojant 20 duomenų taškų stebėjimo langą.

Pearsono koreliacijos $C^{RR,M} = \rho(\bar{\tau}_*^{(RR)}, \bar{\tau}_*^{(M)})$ apskaičiuojamas naudojant optimalius vidurkintus laiko vėlinimo vektorius. Gauta reikšmė $C^{RR,M}$ žymi analizuojamos ŠRV ir magnetinio lauko spektro galios signalų sinchronizacijos laipsnį. Natūralu, kad didesnė $C^{RR,M}$ reikšmė rodo didesnę sinchronizacijos laipsnį ir atvirkščiai ($C^{RR,M} \in [-1,1]$).

Tegul $\{RR^{(k)} = RR_1^{(k)}, \dots, RR_n^{(k)}, k = 1, \dots, K\}$ yra HRV duomenų signalų rinkinys, kur $\{RR^{(k)}\}$ atitinka k -tąjį dalyvį iš vienos iš nagrinėjamų šalių. Vidutinis koreliacijos koeficientas $C^{(RR^{(1,\dots,K)}, M)} = \frac{1}{K} \sum_{k=1}^K C^{(RR^{(k)}, M)}$, naudojami apskaičiuojant vidutinį kiekvienos grupės ŠRV ir atitinkamo magnetinio lauko spektrinės galios signalo sinchronizavimą.

Norint įvertinti gautų rezultatų statistinį reikšmingumą, tolesniame tyrime atliekami išvardijami statistiniai testai. Pearsono koreliacijos reikšmingumo testas naudojamas statistiniam sinchronizacijos tarp dalyvių ŠRV ir Žemės magnetinio lauko reikšmingumui, gautam taikant ankstesniame poskyryje minimą metodą, analizuoti (Nulinė hipotezė ($H_0: C^{(RR^{(1,\dots,K)}, M)} = 0$). Naudojant „Pakartotinių matavimų“ metodą, atliekami keli to paties kintamojo matavimai tiems patiems dalyviams skirtinguose kontekstuose arba du ar daugiau kartų. Sferiškumo prielaida buvo išbandyta naudojant Mauchly sferiškumo testą, o rezultatų lentelėse buvo pastebėtos visos klaidos kartu su jų taisymo technika. Bonferroni testas buvo naudojamas norint pakoreguoti pastebėtą reikšmingumo lygį atsižvelgiant į tai, kad buvo atlikti keli palyginimai, kai buvo naudojami *post hoc* daugkartiniai palyginimo testai. Taip pat buvo naudojamas pakartotinių matavimų ANOVA, kad peržiūrėtų vidutinių lokalaus Žemės magnetinio lauko (LŽML) ir ŠRV koreliacijų pokyčius laikui bėgant šiame tyrime. Jis taip pat buvo naudojamas norint sužinoti, ar nebuvo širdies ritmo suderinamumo ir širdies ritmo sinchronizavimo skirtumų prieš heart-lock-in technikos taikymą, jos metu ir po jos.

LŽML-ŠRV koreliacijų skirtumų statistiniam reikšmingumui tirti buvo naudojama pakartotinė dispersijos matavimų analizė. ANOVA nagrinėja vidutinį tiriamųjų skirtumą per dešimt eksperimento dienų (vasario 28 d. – kovo 11 d.).

Mes įvertinome LŽML-ŠRV koreliacijos koeficientus visiems dalyviams per 11 dienų tyrimą, kad nustatytume, ar jie skiriasi pagal vietą, žinodami, kad LMFL skiriasi pagal regioną. Pirmoje lentelėje parodyta, kad kiekvienos grupės dienomis buvo reikšmingų vidutinių LŽML-ŠRV koreliacijų skirtumų. Antroje lentelėje parodyti pakartotinių matavimų rezultatai. Norint iširti LŽML-ŠRV koreliacijos skirtumus, ANOVA testas buvo atliekamas atskirai kiekvienai grupei kiekvienoje vietoje. Šioje lentelėje pamatysite, kad kiekvienos grupės vidutinė LŽML-ŠRV koreliacija kiekvieną dieną labai skiriasi.

1 lentelė. Kiekvienos grupės vidutinė LŽML-ŠRV koreliacija tyrimo dienomis

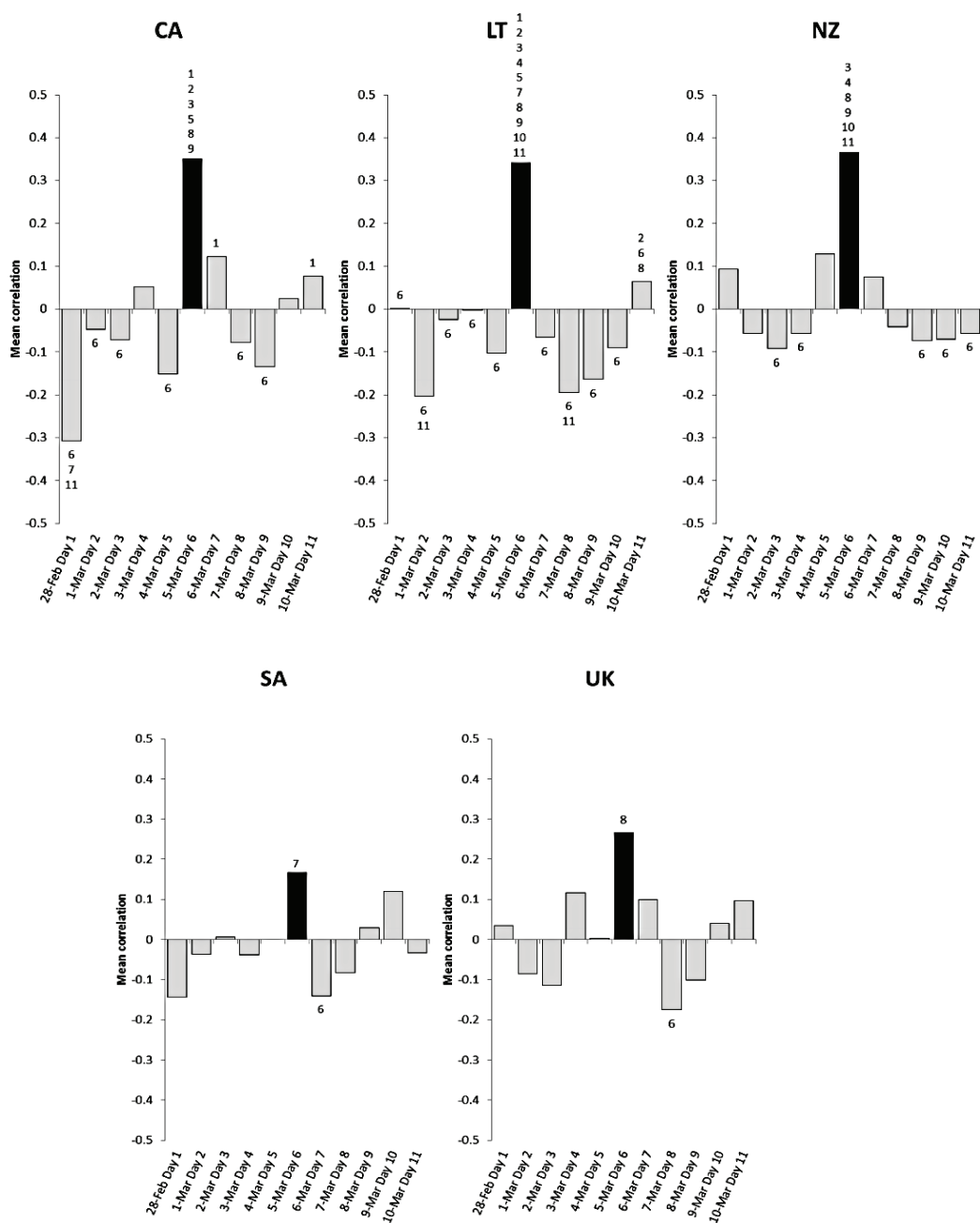
	<i>N</i>	Vid. kv.	df	F	<i>p</i> <	Dalinis η^2 koeficientas
Kalifornija	17	0,50	10	8,46	0,001	0,35
Lietuva	19	0,44	10	9,26	0,001	0,34
Naujoji Zelandija	21	0,40	10	6,22	0,001	0,24
Saudo Arabija	19	0,18	10	2,62	0,01	0,13
Didžioji Britanija	11	0,18	10	2,88	0,01	0,22

Statistinis vidutinio sinchronizavimo tarp dalyvių LŽML ir ŠRV aktyvumo reikšmingumas buvo nustatytas naudojant Pearsono koreliacijos reikšmingumo testą. 2 lentelėje pateikiami testo rezultatai 6 dieną (HLI dieną) visų penkių grupių vidutinė LŽML-ŠRV sinchronizacija iš esmės skyrėsi nuo nulio.

2 lentelė. Koreliacijos koeficiento statistinio reikšmingumo testo rezultatai (* $p < 0,05$, ** $p < 0,01$, *** $p < 0,001$). Vidutinė LMF-ŠRV sinchronizacija 6-tą dieną (HLI dieną) visoms penkioms grupėms reikšmingai skyrėsi nuo nulio.

Diena	Kalifornija Koreliacija <i>p</i> -reikšmė	Lietuva Koreliacija <i>p</i> -reikšmė	Naujoji Zelandija Koreliacija <i>p</i> -reikšmė	Saudo Arabija Koreliacija <i>p</i> -reikšmė	Didžioji Britanija Koreliacija <i>p</i> -reikšmė
Vasario 28	-0,297 0,000***	0,001 0,983	0,094 0,114	-0,114 0,054	0,042 0,481
Kovo 1	0,056 0,342	-0,214 0,000***	-0,056 0,345	-0,033 0,574	-0,096 0,106
Kovo 2	-0,068 0,251	-0,051 0,391	-0,092 0,120	0,017 0,769	-0,125 0,034*
Kovo 3	0,058 0,329	-0,004 0,952	-0,056 0,348	-0,044 0,455	0,128 0,031*
Kovo 4	-0,139 0,019*	-0,096 0,104	0,128 0,031*	0,005 0,928	0,005 0,928
Kovo 5	0,335 0,000***	0,320 0,000***	0,366 0,000***	0,183 0,002**	0,254 0,000***
Kovo 6	0,115 0,053	-0,074 0,212	0,075 0,205	-0,137 0,020*	0,090 0,130
Kovo 7	-0,070 0,236	-0,201 0,001***	-0,041 0,495	-0,083 0,161	-0,184 0,002**
Kovo 8	-0,127 0,031*	-0,146 0,013*	-0,073 0,220	0,045 0,446	-0,138 0,019*
Kovo 9	0,017 0,771	-0,101 0,088	-0,071 0,232	0,114 0,053	0,054 0,364
Kovo 10	0,088 0,139	0,047 0,430	-0,056 0,344	-0,043 0,469	0,086 0,148

8 paveiksle parodyta, kaip 6 diena (HLI) Lietuvos grupėje tyrimo laikotarpiu reikšmingai skyrėsi nuo visų kitų dienų. Vienuolikta diena skyrėsi nuo ankstesnių trijų dienų (įskaitant 6 dieną). Kalbant apie reikšmingus dienų skirtumus, Kalifornijos ir Naujosios Zelandijos grupės finišavo atitinkamai antroje ir trečioje vietose, o HLI diena (6 diena) gerokai skyrėsi nuo šešių kitų dienų.



8 pav. Vidutinė LŽML-ŠRV koreliacija pagal dieną ir grupę. 6 diena, kai visos grupės, dalyvavusios 15 minučių trukmės „Heart-Lock-In“ meditacijoje vienu metu, yra tamsios spalvos. Porų svarbą rodo dienos žymekliai virš kiekvienos juostos. Pavyzdžiui, lietuvių grupei 6 diena (HLI diena) buvo gerokai kitokia nei likusio tyrimo laikotarpio.

HLI diena buvo vienintelė diena, kai visos grupės ŠRV buvo teigiamai koreliuojamos su LŽML, o visų grupių ŠRV ir LŽML sinchronizacija buvo žymiai didesnė nei daugeliu kitų dienų. Buvo pastebėti asmenys, kurių jautrumas žemės magnetinio lauko pokyčiams yra labai skirtingas, ir jie gali reaguoti į to paties aplinkos kintamojo pokyčius įvairiais būdais (Alabdulgade ir kt., 2015). Kiti aplinkos veiksniai, be jokios abejonės, daro įtaką ŠRV. Tačiau verta paminėti, kad visi tiriamieji visą 11 dienų eksperimentą liko tame pačiame geografiniame regione.

Dalyvių ŠRV sinchronizacija su lokalaus magnetinio lauko aktyvumu buvo matuojama kiekvieną dieną 11 dienų laikotarpiu, apimant 5 dienų laikotarpį prieš 15 minučių meditaciją, jos dieną ir 5 dienas po HLI meditacijos. Meditacijos diena buvo vienintelė diena, kai visos grupės ŠRV teigiamai koreliavo su lokalaus magnetinio lauko aktyvumu, o sinchronizacija tarp dalyvių ŠRV ir lokalaus magnetinio lauko aktyvumo buvo žymiai didesnė nei kitomis dienomis. Remiantis statistinio tyrimo išvadomis, galima teigti, kad „Heart-Lock-In“ technika statistiškai pagerina lokalaus žemės magnetinio lauko ir širdies ritmo variabilumo darną.

Buvo nustatyti specifiniai ŠRV ir lokalaus magnetinio lauko elgesio sinchronizavimo reiškiniai, taip pat įvertintas ŠRV darnos poveikis sinchronizacijai tarpusavyje ir su Žemės magnetiniu lauku įvairiose žmonių grupėse.

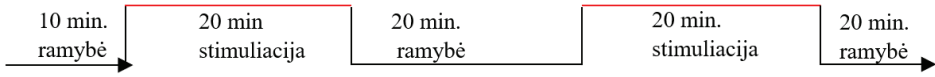
3.4. Širdies ir kraujagyslių sistemos dinamikos vizualizacija atliekant elektrinę ausies ausies klajoklio nervo stimuliaciją

Klajoklis nervas (KN) yra ilgiausias kaukolės nervas žmogaus kūne, reguliuojantis įvairias organizmo sistemas (Yuan ir kt., 2016). Dėl savo didelės įtakos daugeliui sistemų ir svarbaus vaidmens palaikant homeostazę, tyrėjai jau seniai domisi KN aktyvavimu, kad būtų galima kontroliuoti susietų organų funkcijas (Yuan ir kt., 2016). Vienintelė kūno vieta, kur KN turi savo periferinę šaką, yra išorinė ausis. Ausies klajoklio nervo stimuliacija (aKNS) gali įtakoti tiek autonominę nervų sistemą (ANS), tiek centrinę nervų sistemą (CNS). ANS susidedanti iš simpatinių ir parasimpatinių šakų, reguliuoja kardiovaskulinių, kvėpavimo ir imunologinių funkcinis sisteminius veiksniai, kad išlaikytų juos homeostatiniuose ribose, todėl galima tikėtis, kad aKNS poveikis organizmui bus sisteminis. Integralaus stebėjimo metodai reikalingi registruojant, patvirtinant ir optimizuojant ausies KNS sukeltą sisteminių poveikį. Čia EKG yra ypač svarbi.

EKG parametrų sąsajos skiriasi atsižvelgiant į įvairias fiziologines ir patologines priežastis (Malik ir kt., 2002). Įvertindami žmogaus funkcinę būseną klajoklio nervo stimuliacijos metu, naudojome integralųjį sveikatos vertinimo modelį. Šis modelis parodytas kartu su trumpalaikio barorefleksinio grįžtamojo ryšio kilpos atsako modeliu (Šiaučiūnaitė ir kt., 2021).

Mūsų tyrimą sudarė 4 pavieniai atvejai (du vyrai ir dvi moterys), kurių amžius buvo $27,8 \pm 2,22$ metai. Jie buvo įvertinti keturis kartus, du verum ir du placebo eksperimentai. Naudojant „Kaunas-Krūvis“ EKG analizės sistemą, 25 širdies parametrai ir jų tarpusavio sąsajos buvo įvertintos kiekvienam širdies ciklui. Eksperimentas prasidėjo pradine 10 minučių be KNS registravimo faze (juoda linija 9 pav.). Po to sekė 20 minučių verum fazė su KNS (raudona linija), poilsio fazė – 20 minučių be KNS (juoda linija), kita 20 minučių stimuliacijos

fazė (raudona linija) ir 20 minučių atsigavimo fazė (juoda linija). Buvo užregistruota ir iš viso įvertinta virš 5000 širdies ciklų.



9 pav. Eksperimento laiko matavimų intervalų protokolai

Keturi adatiniai elektrodai buvo įdėti į inervuotas ausies dalis, į / aplink cymba conchae regioną, kad būtų atlikta perkutaninė ausies KNS. Stimuliavimo seka susidarė iš kintančio poliariskumo vienfazių impulsų, kurie buvo kartojami kas 1 sekundė (amplitudė 4V, impulso trukmė 1ms).

Vektoriai $x = (x_1, x_2, \dots, x_n)$ ir $y = (y_1, y_2, \dots, y_n)$ atspindi sinchroninius matavimo duomenis, atstovaujančius dviem skirtingiems širdies intervalams; kur n – eksperimento metu užfiksuotas bendras širdies susitraukimų skaičius. Algebrinis santykis tarp laiko eilučių x ir y rekonstruojamas naudojant (Žiaukas ir kt., 2017) pateiktą algoritmą. Šį algoritmą sudaro trys pagrindinės dalys.

1 žingsnis. Šeši elementai $x_{k-\delta}, x_k, x_{k+\delta}, y_{k-\delta}, y_k, y_{k+\delta}$ yra susieti su dviejų matmenų tobulu Lagranžo skirtumų matrica (Žiaukas ir kt., 2017), kur δ yra laiko skirtumas; $k = (1 + \delta), (2 + \delta), \dots, (n - \delta)$. Tobulosios Lagranžo skirtumų matricos struktūra yra:

$$L_{\delta,k} = \begin{bmatrix} x_k & x_{k+\delta} - y_{k+\delta} \\ x_{k-\delta} - y_{k-\delta} & y_k \end{bmatrix} \quad (5)$$

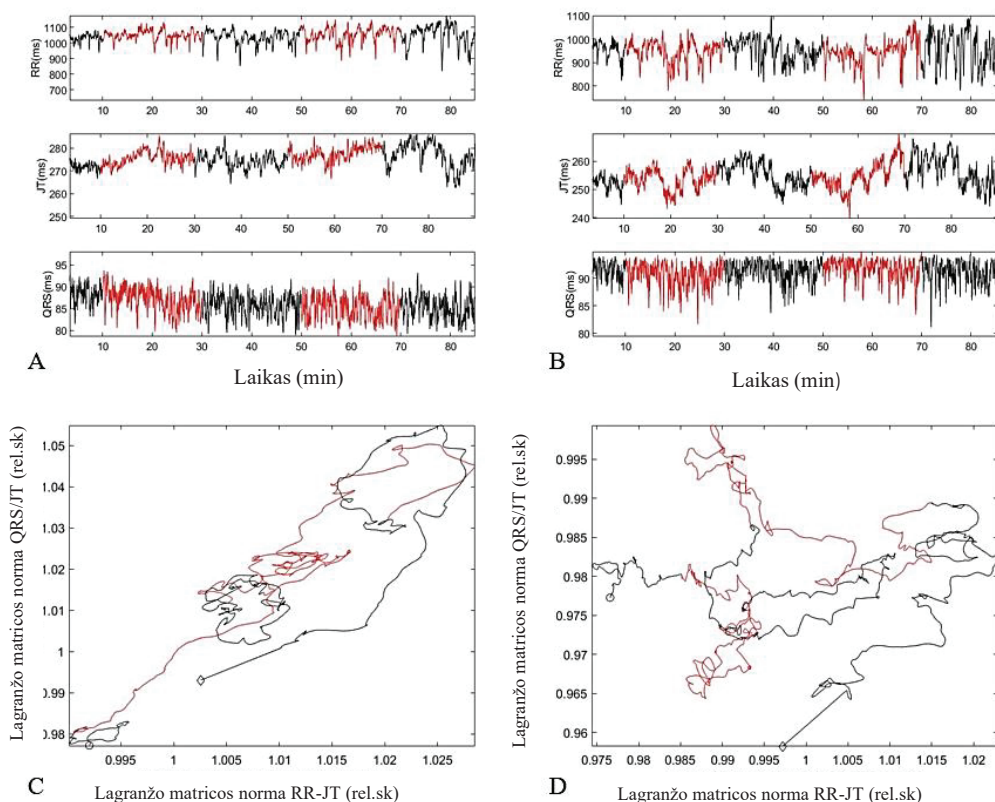
2 žingsnis. Kiekviena matrica $L_{\delta,k}$ transformuojama į skaliarinę reikšmę $s_{\delta,k} = \max(|\lambda_1|, |\lambda_2|)$, kur λ_1 ir λ_2 yra dvi $L_{\delta,k}$ tikrinės reikšmės (Saunorienė ir kt., 2019).

3 žingsnis. Galiausiai, sukurta maksimalių nuosavų verčių skaliarinė seka yra išlyginta viduje ir išorėje. Jei vidinis išlyginimo spindulys yra R_i , o išorinio išlyginimo spindulys yra R_e , išlyginta seka, atspindinti algebrinį ryšį tarp laiko eilučių x ir y :

$$\bar{s}_k(R_i, R_e) = \frac{1}{R_i(2R_e + 1)} \sum_{j=k-R_e}^{k+R_e} \sum_{\delta=1}^{R_i} s_{\delta,j} \quad (6)$$

kur $k = (1 + R_i + R_e), (2 + R_i + R_e), \dots, (n - R_i - R_e)$. Gerai parinktų parametrų optimizavimo problema yra suformuluota (Žiaukas ir kt., 2017) visai asmenų grupei, kur $R_i = 3$ ir $R_e = 4$. Šios išlyginimo parametrų vertės yra fiksuotos. Visa tolesnė analizė pagrįsta $\bar{s}_k(3,4)$.

Siekiant apibūdinti atraktorių (ir išmatuoti jų stabilumą), fazinėje plokštumoje vizualizuojami klajoklio nervo stimuliacijos dinaminiai procesai. Žemiau pateiktuose grafikuose pavaizduota visa klajoklio nervo stimuliacijos eksperimento dinamika.



10 pav. A – RR intervalo, JT intervalo ir QRS trukmės parametrų dinamika eksperimento metu (stimuliacija). B – RR intervalo, JT intervalo ir QRS trukmės parametrų dinamika eksperimento metu (placebas). C – JT / QRS ir RR / JT fazinė plokštuma stimuliacijos metu. D – RR / JT ir JT / QRS Lagranžo matricių skirtumų sąsajų normos placebo metu. F – fazinė plokštuma JT / QRS ir RR / JT normoms placebo metu.

Kai kūnas atsipalaiduoja, kreivė juda į viršutinį dešininį kampą (10B pav.). Tiek JT-QRS, tiek RR-JT santykių vertės didėja (10B pav.). Po pirmosios stimuliacijos juodos spalvos kreivė nustoja kilti (ramybė po pirmosios stimuliacijos), daro kilpą, cirkuliuojančią vienoje vietoje, tada raudona kreivė – antroji stimuliacijos fazė, vėl kyla. Tai reiškia dviejų sistemų nepriklausomumą, padidėja parametrų sudėtingumas, tada vėl atsigauant – priverčiant kilpą grįžti į pradinę kūno būseną. Visai kitas elgesys rodo stimuliacijos palyginimą su placebo eksperimentu. Nėra aiškių proceso dinamikos pokyčių, nedideli tik pirminės kūno būsenos svyravimai. Nors žmogaus kūno reakcija į bet koki dirgiklį gali būti labai skirtinga ir unikali, tačiau naudodamiesi vizualizavimo technika mes galime sėkmingai stebėti visą klijoklio nervo stimuliacijos procesą dviem skirtingais žmogaus organizmo fraktaliniais lygiais.

IV. IŠVADOS

1. Įrodyta, kad anaerobinį slenkstį galima nustatyti naudojant matematinius modelius ir algoritmus, naudojant tik algebrinį ryšį tarp RR ir DQRS širdies intervalų (kitų standartinių metodų, pagrįstų laktato ar iškvepiamųjų dujų koncentracijos matavimu, tam nereikia).
2. Remiantis algebriniu ryšiu tarp JT ir ST širdies parametru, galima nustatyti ankstyvą išemijos epizodų atsiradimą širdyje.
3. Ryšių tarp RR / DQRS ir RR / JT širdies intervalų vizualizavimas fazinėje plokštumoje leidžia unikaliai pažvelgti į sudėtingus širdies ir kraujagyslių sistemos saviorganizacijos procesus elektrinės ausies vaguso nervo stimuliacijos metu.
4. Naujas sinchronizacijos aptikimo algoritmas leido aptikti žmogaus širdies ritmo variabilumo (ŠRV) ir lokalaus Žemės magnetinio lauko (LŽML) tarpusavio ryšius. Tai padėjo patvirtinti teigiamą „Heart-Lock-In“ technikos poveikį LŽML ir ŠRV suderinamumui.

LITERATŪROS SĄRAŠAS

1. Alabdulgader, A.; McCraty, R.; Atkinson, M.; Dobyns, Y.; Vainoras, A.; Ragulskis, M.; Stolc, V. Long-term study of heart rate variability responses to changes in the solar and geomagnetic environment. *Sci. Rep.* 2018, 8, 1–14. [CrossRef] [PubMed]
2. Ballarin E, Borsetto C, Cellini M, Patracchini M, Vitiello P, Ziglio PG, et al. Adaptation of the “Conconi test” to children and adolescents. *Int J Sports Med.* 1989; 10:334–338. <https://doi.org/10.1055/s-2007-1024924> PMID: 2599720
3. BIALEK, William. *Biophysics: searching for principles*. Princeton University Press, 2012.
4. Conconi F, Ferrari M, Ziglio PG, Droghetti P, Codeca L. Determination of the anaerobic threshold by a noninvasive field test in runners. *J Appl Physiol.* 1982; 52:862–873. <https://doi.org/10.1152/jappl.1982.52.4.869>
5. Elgendi M On the Analysis of Fingertip Photoplethysmogram Signals. *Curr. Cardiol. Rev* 8, 14–25 (2012). [PubMed: 22845812]
6. FERREIRA, B. B. et al. Chaos control applied to heart rhythm dynamics. *Chaos, Solitons & Fractals.* 2011, 44(8), 587–599. ISSN: 0960-0779.
7. Gierałowski J, Żebrowski JJ & Baranowski R Multiscale multifractal analysis of heart rate variability recordings with a large number of occurrences of arrhythmia. *Phys. Rev. E* 85, 021915 (2012).
8. Goncalves H, Pinto P, Silva M, Ayres-de-Campos D & Bernardes J Electrocardiography versus photoplethysmography in assessment of maternal heart rate variability during labor. *Springerplus* 5, 1079 (2016). [PubMed: 27462527]
9. Householder, Alston S. (1975), *The theory of matrices in numerical analysis*, New York, NY: Dover Publications, MR 0378371
10. Yuan H, Silberstein SD. Vagus nerve and vagus nerve stimulation, a comprehensive review: part I. *Headache* (2016) 56(1):71–8. [10.1111/head.12647](https://doi.org/10.1111/head.12647)
11. KARAGUEUZIAN, H. S. et al. Bifurcation theory and cardiac arrhythmias. *American journal of cardiovascular disease.* 2013, 3(1), 1.
12. Kim H. S., Eykholt R., Salas J. D., Nonlinear dynamics, delay times, and embedding windows. *Physica D*, 1999, 127, p. 48–60.
13. Lin DC & Sharif A Common multifractality in the heart rate variability and brain activity of healthy humans. *Chaos Interdiscip. J. Nonlinear Sci* 20, 023121 (2010).

14. Mayra O., Ahola T., Leiviska K., Time delay estimation and variable grouping using genetic algorithm, Control Engineering Laboratory ,2006, Report A no. 32.
15. Malik M, Färholm P, Batchvarov V, Hnatkova K, Camm AJ. Relation between QT and RR intervals is highly individual among healthy subjects: implications for heart rate correction of the QT interval. *Heart*. 2002;87(3):220–228. pmid:11847158
16. Mandel Y et al. Human embryonic and induced pluripotent stem cell-derived cardiomyocytes exhibit beat rate variability and power-law behavior. *Circulation* 125, 883–93 (2012). [PubMed:22261196]
17. McArdle WD, Katch FI, Katch VL. *Essentials of exercise physiology*. 2nd ed. Philadelphia, PA: Lippincott Williams & Wilkins, 2000.
18. McCraty R, Atkinson M, Tomasino D, Bradley RT. *The coherent heart: heart-brain interactions, psychophysiological coherence, and the emergence of system-wide order*. Boulder Creek, CA: Institute of Heartmath; 2009.
19. McCraty, R.; Deyhle, A. The global coherence initiative: Investigating the dynamic relationship between people and earth's energetic systems. *Bioelectromagn. Subtle Energy Med*. 2015, 2, 411–425.
20. McCraty, R.; Atkinson, M.; Stolc, V.; Alabdulgader, A.A.; Vainoras, A.; Ragulskis, M. Synchronization of human autonomic nervous system rhythms with geomagnetic activity in human subjects. *Int. J. Environ. Res. Public Health* 2017, 14, 770. [CrossRef] [PubMed]
21. McCraty, R.; Moor, S.; Goelitz, J.; Lance, S.W. *Transforming Stress for Teens: The Heartmath Solution for Staying Cool under Pressure; Instant Help Books, an Imprint of New Harbinger Publications, Inc.: Oakland, CA, USA*, 2016.
22. McCraty, R.; Tomasino, D. Emotional Stress, Positive Emotions, and Psychophysiological Coherence. In *Stress in Health and Disease*; Wiley-VCH: Hoboken, NJ, USA, 2006.
23. Ning, et al. Application of parallel RBF network on iterative prediction of chaotic time series. In: 2010 International Workshop on Chaos-Fractal Theories and Applications. IEEE, 2010. p. 341-345.
24. Porta, A., Di Rienzo, M., Wessel, N., & Kurths, J. (2009). Addressing the complexity of cardiovascular regulation.
25. QU, Z. Chaos in the genesis and maintenance of cardiac arrhythmias. *Progress in Biophysics and Molecular Biology*. 2011, 105(3), 247–257. ISSN: 0079-6107. 149.
26. QU, Z. et al. Nonlinear and stochastic dynamics in the heart. *Physics Reports*. 2014, 543(2), 61–162. ISSN: 0370-1573
27. Quarteroni A, Fornaggia L, Veneziani A.. *Complex Systems in Biomedicine*. Springer, 2006.
28. Saunoriene, L.; Siauciunaite, V.; Vainoras, A.; Bertasiute, V.; Navickas, Z.; Ragulskis, M. The characterization of the transit through the anaerobic threshold based on relationships between RR and QRS cardiac intervals. *PLoS ONE* 2019, 14, e0216938.
29. Segerstrom SC, Nes LS. Heart rate variability reflects self-regulatory strength, effort, and fatigue. *Psychol Sci*. 2007;18(3):275–81.
30. Shaffer F, McCraty R, Zerr CL. A healthy heart is not a metronome: an integrative review of the heart's anatomy and heart rate variability. *Front Psychol*. 2014;5: 1040.
31. Sharma V, Deterministic chaos and fractal complexity in the dynamics of cardiovascular behavior:perspectives on a new frontier. *Open Cardiovasc Med J* 3, 110–23 (2009). [PubMed: 19812706]

32. Šiaučiūnaitė, V., Kaniušas, E., Kampusch, S., Szeles, J. C., & Vainoras, A. (2018, September). Auricular vagus nerve stimulation affects fractality of the human body as resolved by advanced ECG. In 2018 EMF-Med 1st World Conference on Biomedical Applications of Electromagnetic Fields (EMF-Med) (pp. 1-2). IEEE.
33. Šiaučiūnaitė, V., Ragulskis, M., Vainoras, A., Dabiri, B., & Kaniušas, E. (2021). Visualization of Complex Processes in Cardiovascular System during Electrical Auricular Vagus Nerve Stimulation. *Diagnostics*, 11(12), 2190.
34. Takens F., Detecting strange attractors in turbulence, *Lecture Notes in Mathematic*, 1980, 898, p. 366-381
35. Tao D., Hongfei X., Chaotic Time Series Prediction Based on Radial Basis Function Network, Eighth ACIS International Conference, 2007.
36. Timofejeva, I.; McCraty, R.; Atkinson, M.; Joffe, R.; Vainoras, A.; Alabdulgader, A.A.; Ragulskis, M. Identification of a group's physiological synchronization with earth's magnetic field. *Int. J. Environ. Res. Public Health* 2017, 14, 998. [CrossRef]
37. Uzal L.C., Grinblat G.L., Verder P. F., Optimal reconstruction of dynamical systems: A noise amplification approach, *Physical Review E* 84, 2011. Vainoras A, Gargasas L, Ruseckas R, Miskinis V, Jurkoniene R, Schwela H, et al. Computerized exercise electrocardiogram analysis system "Kaunas-Load". In: Bacharova L, Macfarlane PW, editors. *Electrocardiology'97: Proceedings of the XXIV International Congress on Electrocardiology*; 1997 June 24– 28; Bratislava, Slovak Republic. Singapore, World Scientific; 1998. p.253-256
38. Žiaukas P, Alabdulgader A, Vainoras A, Navickas Z, Ragulskis M. New approach for visualization of relationships between RR and JT intervals. *Plos One*. 2017; 12(4):0174279. <https://doi.org/10.1371/journal.pone.0174279>

CURRICULUM VITAE

Personal information:

Date of Birth: 15 May, 1991.

Place of Birth: Kaunas.

Education:

2010–2014 Bachelor of Science Degree in Rehabilitation and professional qualification in Physical Therapy, Faculty of Nursing, Lithuanian University of Health Sciences

2014–2016 Master of Science Degree in Physical Medicine and Rehabilitation, Faculty of Nursing, Lithuanian University of Health Sciences

2017–2021 Doctoral Studies in Physical Sciences, Informatics (09P), Department of Mathematical Modeling, Faculty of Mathematics and Natural Sciences, Kaunas University of Technology.

Professional experience:

2019–2021 Junior Researcher in the Department of Mathematical Modeling, Faculty of Mathematics and Natural Sciences, Kaunas University of Technology.

2019–2020 Invited lecturer in the Institute of Mechatronics, Faculty of Mechanical Engineering and Design, Kaunas University of Technology.

2021–present Lecturer in the Institute of Mechatronics, Faculty of Mechanical Engineering and Design, Kaunas University of Technology.

Research interests:

Application of nonlinear dynamics methods in cardiosignal analysis.

LIST OF PUBLICATIONS AND CONFERENCES

Publications in Journals of the Institute of Scientific Information (ISI):

1. Saunoriene, L., Šiauciūnaitė, V., Vainoras, A., Bertasiute, V., Navickas, Z., and Ragulskis, M. (2019). The characterization of the transit through the anaerobic threshold based on relationships between RR and QRS cardiac intervals. *PloS one*, 14(5), e0216938.
2. Timofejeva, I., McCraty, R., Atkinson, M., Alabdulgader, A. A., Vainoras, A., Landauskas, M., Šiauciūnaitė, V., and Ragulskis, M. (2021). Global study of human heart rhythm synchronization with the Earth's time varying magnetic field. *Applied Sciences*, 11(7), 2935.
3. Šiauciūnaitė, V., Vainoras, A., Navickas, Z., and Ragulskis, M. (2021). Detection of ischemic episodes based on two consecutive declines in the JT/ST algebraic relationship. *Applied Sciences*, 11(11), 4805.
4. Šiauciūnaitė, V., Ragulskis, M., Vainoras, A., Dabiri, B., and Kaniusas, E. (2021). Visualization of complex processes in cardiovascular system during electrical auricular vagus nerve stimulation. *Diagnostics*, 11(12), 2190.

Publications in peer-reviewed journals and conferences:

1. Šiauciūnaitė, V., Landauskas, M., Vainoras, A., and Ragulskis, M. K. (2017). Evaluation and analysis of the power of local geomagnetic field. In *9th International Workshop "Data analysis methods for software systems" – DAMSS: Druskininkai, Lithuania, November 30-December 2, 2017/Lithuanian Computer Society. Vilnius University. Institute of Data Science and Digital Technologies. Lithuanian Academy of Sciences; [compiled by Jolita Bernatavičienė]. Vilnius: Vilnius University Institute of Data Science and Digital Technologies, 2017.*
2. Šiauciūnaitė, V., Kaniusas, E., Kampusch, S., Szeles, J. C., and Vainoras, A. (2018, September). Auricular vagus nerve stimulation affects fractality of the human body as resolved by advanced ECG. In *2018 EMF-Med 1st World Conference on Biomedical Applications of Electromagnetic Fields (EMF-Med)* (pp. 1–2). IEEE.
3. Vainoras, A., Kaniušas, E., and Šiauciūnaitė, V. (2019). Electrocardiologic changes during auricular vagus nerve stimulation in humans. In *King of Organs 2019–The 5th International Conference for Advanced Cardiac and Heart Transplant "Heart Sciences from Genes to Galaxies": March 24–27, 2019, Kingdom of Saudi Arabia: conference abstracts/organized by the Prince Sultan Heart Center in Al-Ahsa, in collaboration with the Cardiology Center at the Hospital La Salpetriere in Paris. European Heart Association and the Saudi Heart Association.*
4. Žiubrytė, G., Šiauciūnaitė, V., Jaruševičius, G., and McCraty, R. (2018). Local earth magnetic field and ischemic heart disease: peculiarities of interconnection. *Cardiovascular Disorders and Medicine*, 3(4), 1–3.
5. Timofejeva, I., Alabdulgader, A., Vainoras, A., McCraty, R., Atkinson, M., Šiauciūnaitė, V., and Ragulskis, M. (2021). The variation of geometrical

shapes of reconstructed attractors of HRV data before, during and after the Heart Lock-In® experiment. *Cardiology and vascular research*. Wilmington, Del.: SciVision Publishers LLC, 2021, vol. 5, no. 1.

ACKNOWLEDGEMENTS

Words cannot express my gratitude to my professors and doctoral committee for their patience and valuable feedback. I could not have completed this journey without the knowledge and expertise provided by my supervisor Prof. Dr. Minvydas Ragulskis and scientific advisor Prof. Dr. Alfonsas Vainoras.

I cannot begin to express my thanks to my dissertation reviewers: Assoc. Prof. Dr. Paulius Palevicius, Prof. Dr. Daiva Petrusėviciene, Prof. Gintaras Palubeckis and Assoc. Prof. Dr. Kristina Poskuvienė, for their valuable and constructive comments and help in improving this dissertation.

Many thanks are sent to the colleagues from the Department of Mathematical Modeling for pleasant communication, assistance, and advice in cases of uncertainties during the studies.

I very much appreciate the Doctoral School administration staff and editors for assistance and guidance during the study process.

I would like to extend my sincere thanks to Prof. Dr. Eugenijus Kaniusas and his entire team for the warm welcome, extensive knowledge, and support during the ERASMUS exchange program at the Vienna University of Technology (TUWien).

Finally, I would be remiss if I did not mention my dearest family and friends, especially my parents. Throughout the process, their faith in me has kept my spirit and motivation high.

UDK 517.957+616.12-073.7+612.1] (043.3)

SL 344. 2022-06-14, 15,75 leidyb. apsk. l. Tiražas 14 egz. Užsakymas 111.
Išleido Kauno technologijos universitetas, K. Donelaičio g. 73, 44249 Kaunas
Spausdino leidyklos „Technologija“ spaustuvė, Studentų g. 54, 51424 Kaunas

